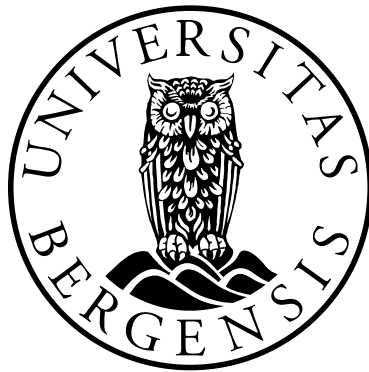


# **Bioactive copolymer scaffolds for bone tissue engineering**

Efficacy and host response

**Salwa Mustafa Nourelhuda Suliman**



Dissertation for the degree of philosophiae doctor (PhD)  
at the University of Bergen

2015

Dissertation date: 11th December

© Salwa Suliman

The material in this publication is protected by copyright law.

Year: 2015

Title: Bioactive Copolymer Scaffolds for Bone Tissue Engineering  
Efficacy and host response

Author: Salwa Suliman

Print: AIT OSLO AS / University of Bergen

## **Dedication:**

**This thesis is lovingly dedicated to my parents and siblings**

”ربما ننفق كل العمر كي نثقب ثغرة.. ليمر النور للأجيال مرة“ - امل دنقل

“Sometimes we may spend a whole lifetime digging a tiny hole, so that  
light may pass to the coming generations if just for once”

Amal Doqol (1940-1983)



# TABLE OF CONTENTS

<b>SCIENTIFIC ENVIRONMENT .....</b>	<b>vi</b>
<b>SUMMARY .....</b>	<b>vii</b>
<b>LIST OF PUBLICATIONS .....</b>	<b>ix</b>
<b>ABBREVIATIONS .....</b>	<b>xi</b>
<b>LIST OF FIGURES AND TABLES.....</b>	<b>xiii</b>
<b>1. INTRODUCTION.....</b>	<b>1</b>
1.1 BONE TISSUE ENGINEERING.....	1
1.2 SCAFFOLDS IN BONE TISSUE ENGINEERING.....	2
1.2.1 Inspired by nature.....	2
1.2.2 Designing and fabricating scaffolds.....	3
1.2.3 Materials used in fabricating BTE scaffolds.....	4
1.3 BIOACTIVE SIGNALLING MOLECULES IN BONE HEALING .....	8
1.3.1 Bone Morphogenetic Protein 2 .....	10
1.4 CLINICAL IMPLICATIONS OF BMP-2 DELIVERY - <i>Status Quo</i> .....	12
1.5 STRATEGIES FOR A CONTROLLED BMP-2 DELIVERY- <i>Quo Vadis</i> .....	15
1.5.1 Physical mixtures/entrapment .....	16
1.5.2 Chemical immobilisation .....	20
1.5.3 On-demand delivery and hybrids .....	21
1.6 CONSIDERATIONS FOR A SCAFFOLD DELIVERING BMP-2 .....	23
1.6.1 Osteoinductivity .....	23
1.6.2 Host response and degradability of implanted scaffolds .....	24
1.7 RATIONALE.....	30
<b>2. AIMS .....</b>	<b>31</b>
<b>3. METHODOLOGICAL CONSIDERATIONS.....</b>	<b>32</b>
3.1 THE CHOICE OF METHODS .....	32
3.2 SCAFFOLD FABRICATION .....	34
3.2.1 Scaffold functionalisation and BMP-2 immobilisation .....	35
3.3 CELL SOURCE AND MAINTAINENCE .....	36
3.3.1 Cell culture.....	36

3.4 QUANTIFYING THE RELEASE OF BMP-2 FROM SCAFFOLDS .....	39
3.4.1 Optimising the use of MS as a method for assessing release of BMP-2 ....	41
3.5 INVESTIGATING OSTEOINDUCTIVITY AND HOST RESPONSE .....	43
3.5.1 <i>In vitro</i> experiments .....	43
3.5.2 <i>In vivo</i> experiments .....	44
3.6 CHEMICAL ANALYSIS OF DEGRADING SCAFFOLDS .....	46
3.7 NON-INVASIVE MICROENVIRONMENTALLY-INDUCED ORAL CARCINOGENESIS: AN <i>IN VIVO</i> BLI MODEL.....	47
3.7.1 <i>In vivo</i> experiments .....	47
3.8 FUNCTIONAL <i>IN VITRO</i> TUMORIGENICTIY ASSAYS .....	49
3.8.1 <i>In vitro</i> assays.....	49
3.9 STATISTICAL ANALYSIS.....	53
3.10 ETHICAL STATEMENT .....	54
<b>4. MAIN RESULTS AND GENERAL DISCUSSION .....</b>	<b>55</b>
4.1 OSTEOINDUCTIVITY .....	55
4.1.1 Osteogenic potential of a controlled, sustained release of BMP-2 .....	55
4.1.2 Effects of nanodiamond particles on the scaffold’s osteogenic potential ...	59
4.1.3 Importance of a controlled release of BMP-2 in low amounts .....	61
4.2 DEGRADABILITY .....	63
4.2.1 Degradation of functionalised poly(LLA-co-CL) scaffolds .....	63
4.3 HOST RESPONSE.....	64
4.3.1 Inflammatory response.....	64
4.3.2 Persistence of nanodiamond particles at the implantation site .....	68
4.3.3 Tumorigenicity.....	69
<b>5. CONCLUDING REMARKS .....</b>	<b>81</b>
<b>6. FUTURE PERSPECTIVES.....</b>	<b>83</b>
<b>ACKNOWLEDGEMENTS .....</b>	<b>85</b>
<b>BIBLIOGRAPHY .....</b>	<b>88</b>
<b>ORIGINAL PAPERS .....</b>	<b>104</b>

## **SCIENTIFIC ENVIRONMENT**

The work comprising this thesis was conducted at The Faculty of Medicine and Dentistry, University of Bergen, over the course of four years (2011-2015). Experiments were mainly undertaken at the Department of Clinical Dentistry - Center for Clinical Dental Research and the Department of Clinical Medicine - Gade Laboratory for Pathology. The SRM work was carried out in collaboration with the Proteomics Unit (PROBE). The luciferase transduction experiments were carried out in collaboration with the Department of Clinical Science, Hematology Section. The animal experiments were conducted at The Laboratory Animal Facility, Department of Clinical Medicine. Within the frame of the FP7 EU project (242175-VascuBone), the scaffolds were fabricated in collaboration with The Fibre and Polymer Department, KTH The Royal Institute of Technology, Stockholm. The production of nanodiamond particles, functionalisation and subsequent modification on polymer scaffolds was done at The University of Wuerzburg, Germany and Diacoating, Innsbruck, Austria. The production of the microsphere modified scaffolds was done in collaboration with the Department of Cranio-Maxillofacial and Oral Surgery, Medical University of Innsbruck, Innsbruck, Austria.

The principle supervisor of the project was Professor Kamal Mustafa. The co-supervisors were Professor Daniela Elena Costea, Professor Anne Christine Johannessen and Dr. Ying Xue.

## SUMMARY

Current research focuses on developing a novel bone-inducing scaffold that could deliver controlled osteogenic growth factors. Several aspects, in particular those influencing the efficacy of such bioactive scaffolds, such as release kinetics of the growth factor, biocompatibility and biodegradability, need further study.

The aim of this thesis was to determine a mode of bone morphogenetic protein-2 (BMP-2) delivery from copolymer scaffolds that reduce the dose to improve clinical safety while retaining efficacy. A low dose of 1 µg BMP-2 was immobilised via four different functionalising techniques on recently developed poly(LLA-co-CL) scaffolds. Sustained release of low levels was seen from BMP-2 physisorbed on nanodiamond modified scaffolds (nDP-PHY) for up to 70 days *in vitro* compared to that from scaffolds modified with microspheres containing BMP-2 (MICS) and unmodified scaffolds with physisorbed BMP-2 (PHY). No release was detected from BMP-2 covalently bound to nanodiamond modified scaffolds. nDP-PHY, MICS and PHY scaffolds promoted bone regeneration in a rat mandible critical-sized defect after 4 weeks, however, nDP-PHY and MICS scaffolds demonstrated osteogenic potential *in vivo* as well as in mesenchymal stem/stromal cell (MSC) cultures.

Poly(LLA-co-CL) scaffolds modified with nanodiamond (nDP) and nDP with physisorbed BMP-2 were then evaluated through *in vivo* degradation, host tissue response and tumorigenic potential. Modified scaffolds degraded faster than unmodified scaffolds. Gene expression of proinflammatory, osteogenic and angiogenic markers were upregulated in the nDP and nDP-PHY scaffolds with ectopic bone seen at week 8 only from the latter. Inflammatory cells, foreign body giant cells and fibrous capsule tissue were significantly reduced around the modified scaffolds. Tissue regeneration markers were most highly expressed in the modified groups. Interestingly, nanodiamond particles were found in the implantation site after 27 weeks when 90% of the scaffolds had degraded.

To evaluate the tumorigenic potential of the functionalised scaffolds *in vivo*, a sensitive and non-invasive model using xenotransplantation of early neoplastic oral keratinocytes transfected to express luciferase (DOK<sup>Luc</sup>) together with carcinoma associated fibroblasts (CAF) for monitoring microenvironmentally-induced carcinogenesis was developed. nDP scaffolds without BMP-2 reduced the bioluminescence intensity of positive control tumours formed by DOK<sup>Luc</sup>+CAF *in vivo*. When cultured *in vitro* as 3D organotypic models of neoplastic oral mucosa, DOK<sup>Luc</sup> previously cultured on nDP scaffolds demonstrated reduced tumorigenic potential compared to DOK<sup>Luc</sup> from nDP-PHY and unmodified scaffolds. nDP-PHY scaffolds showed enhanced tumorigenic potential *in vivo* and *in vitro*.

These results suggest a role played by nanodiamonds in reducing tumorigenic potential of DOK<sup>Luc</sup> and also raises concerns for the therapeutic use of BMP-2 for the reconstruction of bone defects in oral cancer patients. This thesis also highlights that the mode of binding BMP-2 to a scaffold has a significant effect on its osteogenic potential. Furthermore, the efficacy of delivering low, sustained amounts of BMP-2 is emphasised and the modality of nDP-PHY is shown to provide a promising bioactive scaffold for bone tissue engineering.

## LIST OF PUBLICATIONS

The thesis is based on the following papers and will be referred to according to their Roman numbers:

- I. **Suliman S**, Xing Z, Wu X, Xue Y, Pedersen TO, Sun Y, Døskeland AP, Nickel J, Waag T, Lygre H, Finne-Wistrand A, Steinmüller-Nethl D, Krueger A, Mustafa K. Release and bioactivity of bone morphogenetic protein-2 are affected by scaffold binding techniques *in vitro* and *in vivo*. ***J Control Release***. **2015;197:148–157**.
- II. **Suliman S**, Sun Y, Pedersen TO, Xue Y, Nickel J, Waag T, Finne-Wistrand A, Steinmüller-Nethl D, Krueger A, Costea DE, Mustafa K. *In vivo* host response and degradation of copolymer scaffolds functionalised with nanodiamonds and bone morphogenetic protein 2. *Submitted Manuscript*.
- III. **Suliman S**, Parajuli H, Sun Y, Johannessen AC, Finne-Wistrand A, McCormack E, Mustafa K, Costea DE. Establishment of a bioluminescence model for microenvironmentally induced oral carcinogenesis with implications for screening bioengineered scaffolds. ***Head and Neck***. **2015 doi: 10.1002/hed.24187(Epub ahead of print)**.
- IV. **Suliman S**, Mustafa K, Krueger A, Steinmüller-Nethl D, Finne-Wistrand A, Osdal T, Hamza AO, Sun Y, Parajuli H, Waag T, Nickel J, Johannessen AC, McCormack E, Costea DE. Nanodiamond modified copolymer scaffolds decrease tumour progression of early neoplastic oral keratinocytes. *Submitted Manuscript*.

Paper I and III are reprinted with permission from the publishers. All rights reserved.

The author has also contributed to the following work during the course of the PhD period, not included in this thesis:

- I. Costea DE, Hills A, Osman AH, Thurlow J, Kalna G, Huang X, Murillo CP, Parajuli H, **Suliman S**, Kulasekara KK, Johannessen AC, Partridge M. Identification of two distinct carcinoma-associated fibroblast subtypes with differential tumor-promoting abilities in oral squamous cell carcinoma. *Cancer Res.* 2013;73(13):3888-901.
- II. **Suliman S**, Wu X, Sun Y, Pedersen TO, Xue Y, Waag T, Nickel J, Finne-Wistrand A, Steinmüller-Nethl D, Krueger A, Mustafa K. Effect of chemical or physical functionalising of BMP-2 on its osteogenic potential: an *in vivo* ectopic model. *Manuscript*.
- III. **Suliman S**, Vindenes H, Hellem S, Mustafa K, Idris SB. Osteogenic potential of adipose stem cells seeded onto biphasic calcium phosphate scaffolds as compared to bone marrow stem cells: an *in vivo* ectopic model. *Manuscript*.
- IV. Parajuli H, Sapkota D, Rajthala S, Virlan J, Lu N, Osman T, **Suliman S**, McCormack E, Neppelberg E, Lybak S, Liavaag PG, Johannessen AC, Gullberg D, Costea DE. Silencing expression of integrin  $\alpha 11$  in carcinoma associated fibroblasts reduce tumour growth and invasion of oral neoplastic cells. *Manuscript*.

## ABBREVIATIONS

ALP	Alkaline phosphatase
ANGPT	Angiopoietin
BLI	Bioluminescence imaging
BMPR1A	Bone morphogenetic protein receptor, type IA
BTE	Bone tissue engineering
CAF	Carcinoma associated fibroblast
CaP	Calcium phosphate
DOK <sup>Luc</sup>	Early neoplastic dysplastic keratinocyte (luciferase transduced)
DOK <sup>WT</sup>	Early neoplastic dysplastic keratinocyte (wild type)
$\epsilon$ -CL	$\epsilon$ -caprolactone
ECM	Extracellular matrix
E-coli	Escherichia coli
EGFR	Epithelial growth factor receptor
EMT	Epithelial mesenchymal transition
FBGC	Foreign body giant cell
FBR	Foreign body response
FGF	Fibroblast growth factor
HA	Hydroxyapatite
HOB	Human osteoblast
IGF	Insulin-like growth factor
IL	Interleukin
Ki67	MKI67, proliferation marker
LC	Liquid chromatography
LLA	L-lactide
Micro-CT	Micro-computed tomography
MICS	Poly(LLA-co-CL) scaffolds modified with BMP-2 entrapped microspheres
MMP	Matrix metalloproteinase
M <sub>n</sub>	Number average molecular weight

MRI	Magnetic resonance imaging
mRNA	Messenger ribonucleic acid
MS	Mass spectrometry
MSC	Mesenchymal stromal/stem cell
nDP	Nanodiamond particle
nDP-COV	Poly(LLA-co-CL) scaffolds modified with nDP and covalently linked BMP-2
nDP-PHY	Poly(LLA-co-CL) scaffold modified with nDP and physisorbed BMP-2
NSG	Non-obese diabetic severe combined immunodeficient IL2rynull mouse
O-NCD	Oxygen-terminated nanocrystalline diamond
OSCC	Oral squamous cell carcinoma
PCL	Polycaprolactone
PDGF	Platelet derived growth factor
PEG	Polyethylene glycol
PHY	Unmodified poly(LLA-co-CL) scaffold with physisorbed BMP-2
PLGA	Poly(lactic-co-glycolic acid)
Q	Quadrupole
RGD	Arginine glycine-aspartic acid
rhBMP-2	Recombinant bone morphogenetic protein 2
ROS	Reactive oxygen species
RUNX2	Runt-related transcription factor 2
SIS	Stable isotope-labelled internal standard
SRM	Selected reaction monitoring
TGF- $\beta$	Transforming growth factor beta
TNF- $\alpha$	Tumour necrosis factor alpha
VEGF	Vascular endothelial growth factor
$\beta$ -TCP	Beta-tricalcium phosphate

# LIST OF FIGURES AND TABLES

## Chapter 1

Figure 1.1 Basic triad of bone tissue engineering construct.....	2
Figure 1.2 Bioactive molecules involved in bone healing.....	9
Figure 1.3 Bone morphogenetic protein 2 canonical signalling cascade.....	12
Figure 1.4 Strategies for a controlled scaffold-based release of BMP-2.....	16
Figure 1.5 Nanodiamond particles.....	19
Figure 1.6 Foreign body reaction to a degradable scaffold.....	26
Table 1.1 Scaffolds designed to deliver growth factors.....	23

## Chapter 3

Figure 3.1 Schematic summary of the study designs used in the four studies.....	33
Figure 3.2 Schematic workflow of SRM-based proteomic experiment.....	41
Figure 3.3 SRM standard curves generated.....	43
Figure 3.4 Animal procedures to evaluate osteoinductivity and host response.....	45
Figure 3.5 <i>In vivo</i> cell inoculation and optical imaging.....	48
Figure 3.6 <i>In vitro</i> functional tumorigenicity assays.....	52
Table 3.1 Immunostaining of tumour xenotransplants.....	49
Table 3.2 Immunostaining of 3D-OT.....	53

## Chapter 4

Figure 4.1 Release profile of BMP-2 from different scaffolds.....	56
Figure 4.2 Results of migration assays.....	75

# 1. INTRODUCTION

## 1.1 BONE TISSUE ENGINEERING

Bone serves as a mechanical support, a site for muscle attachment, a barrier protecting vital organs and a storage for ions (1). It is the second most commonly transplanted tissue after blood (2). Despite the bone's capacity for self-repair, grafts are used to heal defects such as non-union fractures, critical-size defects caused by injury or tumour resection, chronic conditions such as congenital malformations or sometimes to create a base for dental implants (2). Autogenous bone grafts (autografts) are considered the 'gold standard' since they hold strong biological properties of osteogenesis, osteoconduction and osteoinduction relevant to bone healing and homeostasis. Nevertheless, their limitations include inadequate availability, donor site morbidity and supporting tissue injuries (3). As an alternative, allogeneic bone (allografts) and xenogenic bone (xenografts) from humans and animals respectively are used, but they carry the risk of disease transmission, rejection and impaired osteoinductivity due to the pre-transplantation processing (3).

The increasing emphasis on quality of life in healthcare led biologists, engineers, chemists and biomaterial scientists to assemble and propose the field of tissue engineering or regenerative medicine in an attempt to surpass conventional treatments and discover methods for providing custom-made body parts. It was proposed that the means could be found to allow the body to harness restoration of configuration and function of the injured tissue to a state that is biologically and functionally like the native tissue prior to injury (4). Bone tissue engineering (BTE) typically involves presenting *physical and/or bioactive signalling molecules* to transplanted *cells* in a *3 dimensional (3D) scaffold* or to the host cells which are capable of responding to these signals and forming new, functional bone tissue that can integrate with surrounding host tissue (**Fig. 1.1**). Bioactive signalling molecules can be in the form of soluble biochemical factors, such as growth factors, genetic material, drugs and small molecules, and they can be delivered from a 3D scaffold with control of both time and space (5, 6).

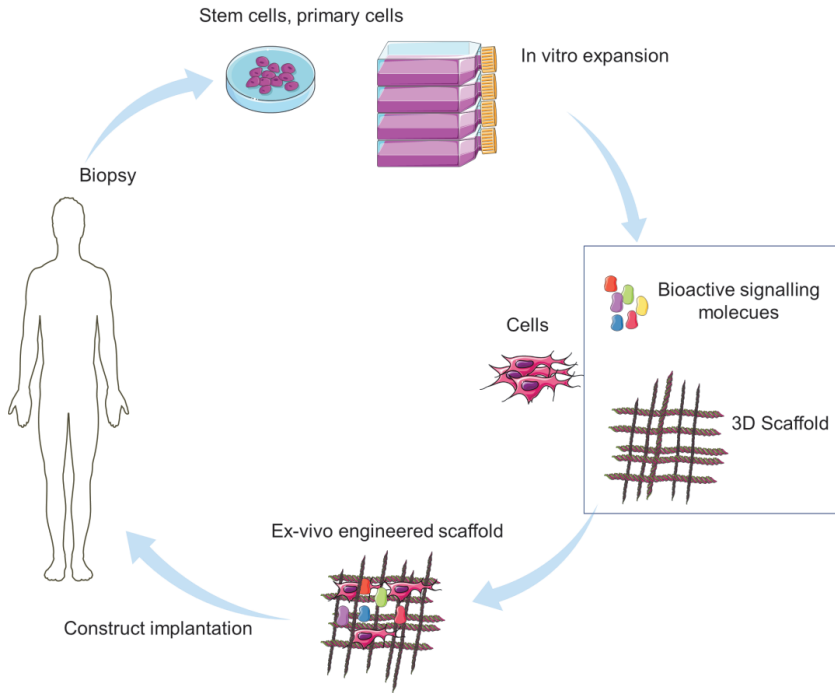


**Figure 1.1 Basic triad of bone tissue engineering construct.** Inspired by the basic compositional elements of bone and recapitulating autografts, which provide osteogenic cells, osteoinductive growth factors, and an osteoconductive scaffold/carrier, which are all essential for bone regeneration. Bioactive signalling molecules and 3D scaffolds are the focus of this thesis. Figure inspired from (4, 5).

## 1.2 SCAFFOLDS IN BONE TISSUE ENGINEERING

### 1.2.1 Inspired by nature

The scaffolds used in BTE are generally meant to provide provisional substitutes for the skeletal extracellular matrix (ECM) (7). They provide a 3D physical/mechanical temporary support combined with specific signalling molecules to assist cells implanted with it or cells from the vicinity to produce their own ECM microenvironment (8). The ECM is organised in a structural manner that controls processes of morphogenesis such as adhesion, migration, proliferation, differentiation, and signal transmission to cell membrane receptors that eventually affect genetic expressions (9). ECM in human skeletal tissue is composed mainly of water, collagen

and proteoglycans containing glycosaminoglycan, attached to a main protein via a tetra-saccharide linkage (8). Another vital role of ECM is as a reservoir for growth factors or their precursors in addition to presenting many adhesion molecules with a signalling function (10). These growth factors are stored locally in an insoluble/non-active form via low affinity binding with ECM molecules that protects them from degradation. They can be liberated in response to physiological need, for example bone repair after injury (10). ECM proteins such as fibrin, collagen, fibronectin and vitronectin can also bind to a number of growth factors either indirectly via their heparin-binding domains or more directly via their growth factor-binding domains (11). Therefore, it is important that these interactions between cell surface receptors and the ECM characteristics are mimicked to guide the design of a *bioactive scaffold-cell interaction*.

### **1.2.2 Designing and fabricating scaffolds**

When designing a scaffold for bone tissue, several complex parameters need to be considered. These include material composition, porous architecture, mechanics, surface properties, degradation properties and by-products, together with the composition of any added biological components that affect its bioactivity (7, 12). To mimic ECM and modulate osteogenesis, the geometrics of porosity and pore size are important (13). Although the pore size for BTE scaffolds is controversial, it has generally been found that there is a minimum requirement of around 100  $\mu\text{m}$  for adhesion and migration of cells and more than 300  $\mu\text{m}$  are recommended for bone matrix ingrowth and neovascularization to promote osteogenesis (14). Porosity of around 90% and interconnectivity of almost 100% is necessary to facilitate nutrient and waste passage and to provide interlocking with the surrounding tissue (13). Also important are the mechanical, degradation and biocompatibility properties, which are inter-related. A scaffold should express adequate mechanical properties, as close as possible to the replaced tissue, and prevent stress shielding (7). The scaffold degradation rates should be tailored to correspond to the bone regeneration timeframe *in vivo* allowing load transfer gradually; and as it degrades, the selected materials should not elicit any by-products causing adverse responses (7). In general these

parameters promote the osteoconductivity of the scaffold, allowing the bone cells to adhere, proliferate, and form extracellular matrix on its surface and pores (15).

To tune the architecture of a scaffold, the choice of fabrication technique is essential. Several technologies have been and are being developed to provide state-of-the-art fabrication of 3D porous degradable scaffolds. One commonly used conventional method is particulate leaching, where a polymer solution is added over granular porogens which are leached out once the polymer has solidified (16). Drawbacks of this method include lack of reproducibility and preciseness in architecture; however, it is inexpensive and easy production makes it a popular method. Foaming techniques are an alternative, in which gas bubbles are produced by expansion of carbon dioxide (17). Nonwoven constructs may be produced by electrospinning giving fibrous polymer scaffolds (18). Emulsion freeze drying and thermally induced phase separation has also been studied to provide scaffolds with high porosity and interconnectivity (19). During the last decade, rapid prototyping or solid free form fabrication methods have emerged with the introduction of computerised technologies facilitating layer by layer plotting design of scaffolds (20). Bone defects can be captured by magnetic resonance imaging (MRI) or micro-computed tomography (micro-CT), reconstructed using computer-aided design manufacturing and then based on the printing strategy: solid free form fabrication scaffolds can be produced either via laser-bed stereolithography, selective laser sintering, extrusion based fused deposition modelling (21) or 3D printing (22). Some of these advanced options require more specific material than the simpler techniques, but they bring us forward towards personalised treatment.

### **1.2.3 Materials used in fabricating BTE scaffolds**

A variety of materials have been investigated to fabricate BTE scaffolds with the aim of identifying the most appropriate physical, chemical and biological properties to encourage bone production (12). These materials can be generally considered either degradable or non-degradable, either organic or inorganic, either natural or synthetic. They include metals, ceramics, polymers and their composites/combinations are now

emerging (12). Titanium and tantalum are the most commonly used metals to produce porous scaffolds exhibiting biocompatibility together with a mechanical stiffness close to bone, promoting enhanced osteoconduction, calcium deposition and bone formation *in vivo* (23). However, lack of degradation, corrosion, ionic leaching and costly processing limits their applications (23, 24).

Bone is composed of an inorganic portion of hydroxyapatite (HA) and calcium phosphates (CaP), thus ceramic scaffolds are characterised with comparable crystallinity to bone mineral components making them biocompatible and bioactive (25). Co-culturing MSC and endothelial cells for pre-vascularisation attempts in porous beta-tricalcium phosphate ( $\beta$ -TCP) have also shown success in large segmental defects in rabbits (26). Furthermore, in a recent prospective clinical study bone defects caused by bone tumours were treated with biphasic CaP granules consisting of 60% HA and 40%  $\beta$ -TCP, in combination with a fibrin matrix (27). Of the patients with a mean defect size of 11.8 cm<sup>3</sup>, 98% showed complete bone healing after approximately 2 years (27). In general, CaP granules have been restricted to small bone defects, however changing physicochemical compositions and structural features displayed osteoinductivity equivalent to autologous bone grafts in a sheep critical sized defect (28). Clinical applications of ceramic scaffolds are limited due to their inherent brittleness and difficulty of shaping as well as a slow degradation rate (25).

Polymers are categorised into either natural or synthetic and they can be shaped into different scaffold types in addition to 3D porous solids, ranging from gels to fibres. The common natural materials used in bone regeneration are polysaccharide derivatives such as alginate, chitosan, hyaluronic acid and protein derivatives such as collagen, fibrin and silk (12). They can be biologically recognised, which supports cellular response. Collagen type I is the main organic component of bone ECM, which made it the most studied natural polymer in BTE scaffolds playing a role in cell adhesion, growth and differentiation (29). Drawbacks such as the possibility of pathogenic contamination, lack of control over mechanical properties, degradability and production stability are presented in this group (30).

### 1.2.3.1 Synthetic polymers

Drawbacks from natural polymers encouraged the development of synthetic polymers that have shown capacity as scaffold materials for BTE. This is due to their reproducibility in large scale in addition to the ease of tuning their chemical, physical, mechanical and degradation properties (31). Commonly studied synthetic polymers for potential scaffolding applications include aliphatic polymers, poly(carbonates), poly(propylene fumarates), and poly(anhydrides) (32-35).

The research presented in this thesis utilised degradable aliphatic polyesters/polymers, a group of synthetic polymers that contain the ester functional group in the main chain. Aliphatic polyesters synthesised from monomers such as L-lactide (LLA),  $\epsilon$ -caprolactone ( $\epsilon$ -CL) and glycolide forming homopolymers or copolymers are the most commonly used aliphatic polyesters for BTE applications (18, 35, 36). These degrade by non-enzymatic hydrolysis (37) and their degradation products can be removed by natural metabolic pathways. Certain devices for other applications based on these polymers, regulated by the US Food and Drug Administration (FDA), have been approved after clinical trials and patented (35, 38, 39). Nonetheless, they have important shortcomings such as lack of biological cues and hydrophobicity that causing poor wetting and affects cellular adherence (40).

Amalgamating different polyesters and tuning the molar ratios or polymer molecular weights have been used to produce a copolymer with customised properties (41, 42). Mixing poly(LLA) and poly(caprolactone triol) for example was used to produce membranes and *in vitro* results with osteoblasts showed that this modifies its mechanical, thermal, and biological properties, i.e. improved cellular migration, attachment, proliferation and matrix production (43). A recently developed copolymer matrix yielded porous scaffolds composed of 75% poly(LLA) and 25%  $\epsilon$ -CL or 1,5-dioxepan-2-one (DXO). The poly(LLA-co-CL) and poly(LLA-co-DXO) scaffolds were produced by random ring opening polymerisation (16) and the former is the copolymer scaffold used in this thesis. These copolymer scaffolds were evaluated and compared *in vitro* to the poly(LLA) scaffolds using MSC (16, 44) and human osteoblast (HOB) (45). Cellular responses demonstrated the MSC to spread and

proliferate better on copolymers compared to poly(LLA) after 1 and 7 days and also exhibited differentiation potential towards an osteogenic lineage (44). Furthermore, the same trend was also seen with HOB, where surface analysis disclosed improved attachment, spreading and growth of the cells into the pores of the copolymer scaffolds compared to the PLLA, which induced higher collagen type I and osteocalcin production (45). Poly(LLA-co-DXO) scaffolds also showed enhanced bone regeneration and suitability for BTE when cultured with a mix of MSC and endothelial cells and then implanted in a rat calvaria defect model (46).

Thus, while these synthetic copolymers have exhibited excellent osteoconductive qualities, they lack biological recognition on the material surface that renders them less bioactive than natural polymers or ceramics. In an effort to overcome this drawback, hybrid or composite scaffolds were produced that were modified with ceramics or natural polymers or both (47). These showed variable advantages from good biocompatibility and improved mechanical properties (48) as well as osteoblastic lineage cell responses due to increased wettability accompanied with improved bone formation in a mouse calvarial model (49).

In addition to mixing different materials, other modification strategies have also employed to functionalise scaffolds, specifically synthetic polymers that render more representative of native ECM. These modifications may be categorised as morphological, chemical or biological (40, 50). Surface topography modifications providing micro- to nano-meter scale architecture resembles the physical arrangement of components in the ECM. For example, silica nanoparticles have been applied onto the fibre surface of 3D polycaprolactone (PCL) fibrous scaffold and were found to improve the fibre wettability and surface roughness thus enhancing osteoblastic attachment and differentiation (51). Carbon-derived nanodiamond particles (nDP) have been employed on poly(LLA-co-CL) scaffolds improving mechanical properties (52, 53) and biological influences due to enhanced hydrophilicity that promoted cellular attachment and differentiation leading to bone formation in a critical defect (54). Furthermore, the addition of functional chemical groups by grafting, radiation, plasma treatments, or alkali treatments to the polymer has been shown to increase the

hydrophilicity of the scaffold, promoting cellular attachment and diffusion of nutrients (50). These functionalisation modalities also offer opportunities to tether bioactive signals (50). Alternatively, incorporation of biomolecules meant to mimic ECM, such as growth factors, adhesion proteins or bioactive peptide motifs into the scaffold's surface promotes integrin-mediated cellular responses (55). Therefore, in an attempt to make synthetic scaffolds osteoinductive, researchers have developed *bioactive scaffolds* delivering signalling cues which stimulate cells and initiate repair by actively participating in bone tissue regeneration (15).

The research in this thesis is focused on functionalising synthetic copolymer scaffolds to deliver growth factors for BTE.

### **1.3 BIOACTIVE SIGNALLING MOLECULES IN BONE HEALING**

The mechanism of bone regeneration after injury is complex and it follows the natural embryonic skeletogenesis in addition to normal responses to tissue injury. Bone healing may occur through intramembranous or endochondral ossification or a combination of both (56). It involves several phases: such as inflammation, reparative and finally remodelling. This complex regenerative process involves multiple cell types in the microenvironment, including inflammatory cells, osteoprogenitor and differentiated osteogenic cells, endothelial cells, and fibroblasts. The cells produce and release bioactive signalling molecules that facilitate coordinated biological actions (**Fig. 1.2**). The secreted bioactive molecules are usually characterised under the following groups; (a) proinflammatory cytokines, (b) growth factors (c) metalloproteinases (d) vascular promoting factors (57).

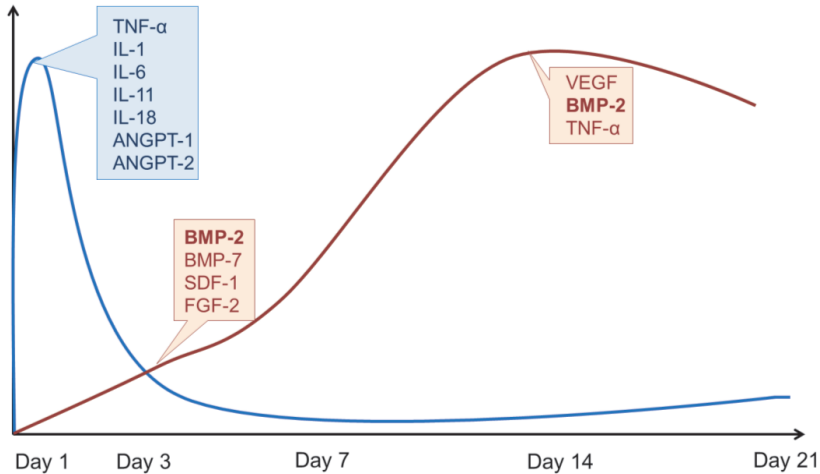


**Figure 1.2 Bioactive molecules involved in bone healing.** The relative levels of some of the significant bioactive molecules involved in bone regeneration process and the ability to recapitulate and manipulate those signalling processes on a similar spatiotemporal scale could provide control over the regenerative process. SDF-1 is stromal cell-derived factor 1. Figure adapted and modified from (58).

When a bone is injured, the haematoma formed stimulates inflammatory cytokines to initiate the regenerative cascade. Inflammatory cells secrete mainly interleukins (IL) (IL-1 and IL-6) and tumour necrosis factor alpha (TNF- $\alpha$ ) during the first 24 hours, which recruit other inflammatory cells as well as MSC before declining after the acute inflammatory phase (59). Simultaneously, the release of growth factors initiates the reparative phase, several growth factors are expressed during the different phases. Among them, the most significant are the superfamily of transforming growth factor beta (TGF- $\beta$ ), which also includes the bone morphogenetic proteins (BMP), followed by the fibroblast growth factor (FGF), platelet-derived growth factor (PDGF), vascular endothelial growth factor (VEGF) and insulin-like growth factor (IGF) (60). Platelets at the site of the defect release PDGF and TGF- $\beta$  starting the repair cascade. They stimulate bone repair by recruiting and expanding the osteoprogenitor cells (61). Consequently, BMP expressed in bone matrix and from recruited MSC promote their differentiation into chondrocytes and osteoblasts. These MSC secrete growth factors,

such as IGF and FGF which play important roles in enhancing vascularity (62). Secreted angiogenic growth factors such as VEGF and angiopoietins 1/2 (ANGPT 1/2) regulate the vascular supply which plays a critical role in maintaining bone homeostasis (63). VEGF was found to work synergistically with BMP enhancing the recruitment and differentiation of MSC (64). Matrix metalloproteinases (MMP) degrade cartilage and shape bone to allow infiltration of blood vessels in the final phases of ossification and the remodelling (57).

### **1.3.1 Bone Morphogenetic Protein 2**

Over the past several decades, the growth factors most studied as therapeutic agents to enhance bone repair are the BMPs. In 1965 Marshall R. Urist made a pioneering discovery through the implantation of de-mineralised bone matrix, which was found to induce bone formation in heterotopic sites (65). This phenomenon shed light on bone BMP, a group of proteins with osteoinductive potential (66). Scientists today suggest describing them as ‘body morphogenetic proteins’ due to their versatile involvement in several developmental processes (67). Currently there are around 20 identified human BMPs and they are involved in skeletal development and the physiological process during embryogenesis of tissues as teeth, brain, heart, lung, kidney, spleen and liver, in addition to glucose homeostasis and modulation of iron homeostasis (68). BMPs are synthesised by osteoprogenitor cells as well as differentiated osteoblasts and chondrocytes and were also localised in megakaryocytes and platelets (69). Except for BMP-1, the BMPs belong to the multifunctional TGF-  $\beta$  family. The structure of the primary amino acid sequence homology stratifies BMPs into four groups: BMP-2/4, BMP-5/6/7/8a/8b, BMP-9/10 and BMP-12/13/14 (70). During early studies, recombinant adenoviruses expressing fourteen human BMPs were constructed to infect pluripotent mesenchymal progenitor cells, preosteoblastic cells, and osteoblastic cells. Results of these studies suggested differences among their osteogenic potentials, but BMP-2, -4, -6, -7 and -9 were most able to induce osteogenic factors as well as matrix mineralisation (71). BMP-2 and BMP-7 are the ones used in clinical applications (72).

BMP-2 is initially synthesised as a pro-protein with 453 amino acids before it is glycosylated and broken down by enzymes to produce the mature, biologically active BMP-2 which is a homodimer of two subunits, each consisting of 114 C-terminal amino acids (73). Each monomer has a molecular weight of approximately 16 kilo Dalton and contains six additional cysteine residues, which are involved in three intra-chain disulphide linkages (73). BMP-2 contains a heparin binding domain in an N-terminal region that enables interactions with ECM elements (73). Murine studies inhibiting the expression of BMP-2 demonstrated the role played by this protein in morphogenetic regulation of post-natal osteoprogenitor differentiation. In the same study, the addition of BMP-2 to osteoprogenitor cells liberated runt-related transcription factor 2 (RUNX2) and osterix expression with observed mineral deposits (74). *In vitro* studies showed the exogenous addition of recombinant (rh)BMP-2 to human adipose-derived stromal cells (75) or MSC (76) augments their osteogenic potential.

It has been reported that mice lacking the ability to produce BMP-2 in their limb bones have experienced spontaneous fractures with impaired healing capabilities and lack of callus formation (77). *In vivo* gene modified mouse investigations revealed the initiation of the osteogenic and chondrogenic differentiation of periosteal progenitors during repair in cortical periosteum-mediated repair to be controlled by endogenous BMP-2 (78). A study examining the fate of injected labelled MSC in nude mice, demonstrated their chemotactic homing towards the carrier of BMP-2 and their differentiation into osteogenic cells (64). The multifaceted roles of BMP-2 were also demonstrated in dentin formation and pulp vascularisation (79). Following the secretion of the active form of BMP-2 from cells, osteogenesis is initiated by the binding of BMP-2 to serine/threonine kinase BMP type I and type II receptors. It follows an osteodifferentiation canonical (Smad) signalling pathway (see **Fig. 1.3**) and a non-canonical (p38 MAPK) signalling pathway (72).

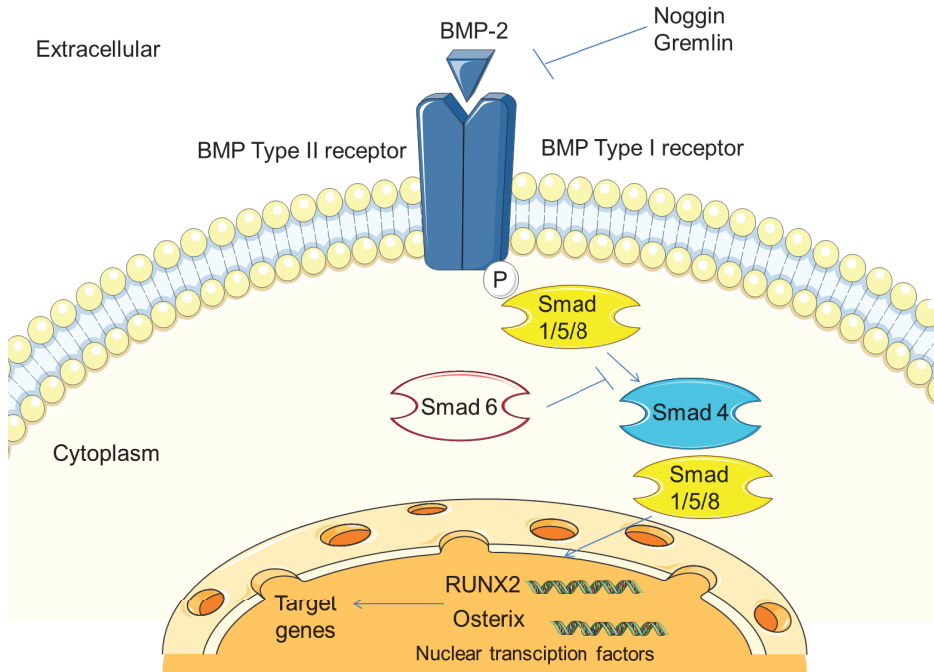


**Figure 1.3 Bone morphogenetic protein 2 canonical signalling cascade.** BMP-2 can bind to either preformed complexes of type I or type II receptors or to solitary receptors. The type II receptor kinase phosphorylates the type I receptor in the membrane proximal part initiating the cascade by recruiting (R)-Smad proteins 1, 5 and 8 (80). These Smad proteins bind to (C)-Smad 4 to translocate to the cell's nucleus inducing the expression of osteogenic transcription factors. Figure modified from (68) and made using Servier Medical Art.

#### 1.4 CLINICAL IMPLICATIONS OF BMP-2 DELIVERY - *Status Quo*

Several clinical orthopaedic trials have been carried out using the FDA approved rhBMP-2 product, Infuse<sup>®</sup> (Medtronic, Minneapolis, MN)/InductOs<sup>®</sup> (UK) (81). This BMP-2 is carried in an absorbable collagen sponge at a concentration of 1.5 mg/ml. Its approval was grounded on the results of a prospective clinical trial. The trial compared patients with degenerative disc disease randomised to receive either BMP-2/collagen sponge construct or autogenous bone from the iliac crest to treat anterior lumbar interbody fusion (to induce new bone formation in the disc space to fuse the vertebrae and alleviate pain). Radiographic evidence of osteogenic induction and maintained

fusion for 2 years were reported in BMP-2/collagen sponge group with improved neurological symptoms (81). More recent uses in posterolateral fusion to substitute for the gold standard procedures were also reported with positive results, however they were off-label uses, utilising much higher doses and different carrier and location than already approved (82). BMP-2 delivery and subsequent spinal fusion has also been facilitated by ceramics and synthetic polymers clinically in addition to the aforementioned collagen carriers (83).

A large randomised clinical trial including 450 patients to evaluate BMP-2 (Infuse<sup>®</sup>) reported accelerated bone regeneration from the test group of open tibial fracture repair surgeries with intramedullary nail fixation. The authors also described a dose dependant reduction of second surgical intervention and reduced infection for the group treated with BMP-2 in addition to standard care when compared to the group that received standard care alone (84). Despite the high costs of recombinant proteins, these results demonstrated that medical costs could be reduced due to reduced post-surgical interventions (85).

Oral and maxillofacial defects include causes such as congenital malformations, trauma, tumour removal and deficient bone in ridges for dental implants. The very first clinical study was a pilot evaluating the BMP-2/collagen sponge construct in maxillary sinus floor augmentation using a concentration varying from 1.77 to 3.40 mg per patient (86). Significant bone growth was seen in 91% of the patients but side effects of swelling in the face, redness and pain in the mouth were observed. A further randomised controlled trial reported 8 years later by the same group increased the dose to 0.75 mg/ml and 1.50 mg/ml and assessed bone induction after 4 and 6 months (87). It showed considerably increased alveolar ridge and bone density after 4 months in the treatment group, concluding that BMP-2/collagen sponge accelerated bone formation for the placement and functional loading of dental implants (87). Off-label use in mandibular continuity reconstructions in defects due to tumours or bone infections were evaluated in a few patients followed up to 18 months (88). This study demonstrated the ability of BMP-2 delivered in a collagen carrier without bone graft material to regenerate critical sized mandibular defects with a potential of enabling

prosthetic fitting (88). However, further studies will be required to assess the quality of the regenerated bone.

Due to the potential advantages of rhBMP-2 in a construct as a substitute for auto, allo- or xenografts deduced from pre-clinical studies, enthusiasm for rhBMP-2 led to its off-label usage for unapproved amounts indications, age groups or carrier. As a result, many complications were reported from its use in lumbar spine and cervical spine surgery, i.e. post-operative radiculitis and nerve injury, vertebral osteolysis and oedema, excessive bone formation heterotopically and hematomas obstructing respiration (89). A case of non-healing ulnar defect in a child's forearm was treated with BMP-2 and led to an unwanted inflammatory reaction with bone resorption (90), while a case in a child cleft palate treatment resulted in excessive gingival swelling (91).

The association of cancer with BMP-2 usage is controversial. A review trying to quantify cancer incidence and rate with spinal fusion using BMP-2 concluded that there might be an increased tumour risk but it was not statistically significant (92). Moreover, products with very high BMP-2 concentration (40 mg) used to treat spinal diseases have been connected with higher cancer risk when compared to controls (93). An *in vivo* pre-clinical analysis of oral squamous cell carcinoma (OSCC) cell line pre-treated with BMP-2 before xenografting reported that human oral cell carcinoma, when treated with BMP-2, became more locally aggressive and the host had decreased survival, suggesting the need for caution when using BMP-2 in reconstructing bone defects caused by oral cancers (94).

When loaded in collagen sponges, BMP-2 shows a pharmacokinetic profile of burst release (95). This required researchers to employ supra-physiological loading quantities to maintain BMP-2 biological activity in the vicinity in suitable amounts for longer times. Therefore efforts to design controlled release strategies for scaffold-based delivery of BMP-2 for dose reduction and localisation is an ongoing challenge.

## 1.5 STRATEGIES FOR A CONTROLLED BMP-2 DELIVERY- *Quo Vadis*

Localised, sustained release of BMP-2 can be potentially beneficial by lowering required doses and thus costs, and avoiding local or systemic side effects (58, 96). The concept of spatiotemporal dosage based on native ECM is challenging and significant research has focused on it.

In general, there are several approaches being developed to deliver BMP-2 from scaffolds: direct delivery of the protein itself, indirect delivery of genes encoding for BMP-2 or its peptides, or antibodies delivered to harness endogenous BMP-2. The use of scaffolds to deliver cells transduced *ex vivo* with virus encoding BMP-2 (97) or delivering the viral vector alone with no cells has the potential of rapidly achieving a high concentration of BMP-2 endogenously (98). Furthermore, gene therapy based on non-viral plasmid is being pursued to reduce immunogenicity (99). Synthetic peptides that mimic BMP-2 activity and activate receptors are smaller molecules that can easily be modified with chemical groups and have been shown to significantly stimulate heterotopic ossification *in vivo* (100). Entrapment of endogenous BMP-2 by using biomaterials to deliver murine monoclonal antibody demonstrated antibody-mediated *de novo* osseous regeneration (101). Safety concerns and production costs with gene therapy limit its clinical translation and due to advances in recombinant protein technology, delivery of the actual protein has become widely used. Researchers in the field have used a large variety of natural, synthetic and inorganic materials and their composites as carriers for BMP-2. The carrier or material is crucial for an optimal release profile (102), but a significant point also is the strategy of incorporating the protein in these materials, which exerts control on its release profile (58).

Discussion in the following sections considers the strategies envisioned for the incorporation of BMP-2 for a controlled release regardless of the specific material used.

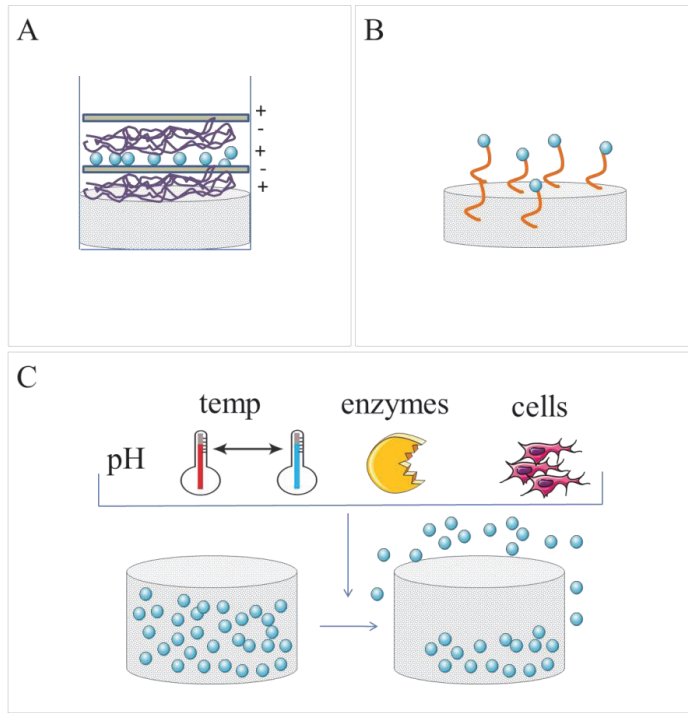


**Figure 1.4 Strategies for a controlled scaffold-based release of BMP-2.** Schematic illustrations of examples from the different strategies. **(A)** Physical entrapment using layer by layer polyelectrolyte multilayer. **(B)** Chemical immobilisation by heparin conjugation. **(C)** On demand release. Figure made using Servier Medical Art.

### 1.5.1 Physical mixtures/entrapment

The prevailing strategy of incorporating BMP-2 protein into polymer scaffolds is by directly mixing them into the matrix, either during the solidification of the polymer or after the fabrication of the scaffold (102). Adsorbing in prefabricated scaffolds is most easily achieved by dipping the scaffolds in a protein solution. However, during this process only minute amounts of protein are adsorbed to the scaffold, and in an uncontrolled fashion, resulting in similarly uncontrolled/unpredictable release profiles (103). Adsorbing BMP-2 onto a prefabricated scaffold leads to a variety of non-specific, non-covalent or electrostatic interactions (104). This has been associated with

a burst release and incomplete association of the BMP-2 to the carrier because most of it remains in the solution. Before scaffold fabrication, the entrapment of BMP-2 in porous scaffolds is most commonly carried out by the conventional method of solvent casting/particulate leaching, but the harmful solvents used may denature the BMP-2. In supercritical fluid, carbon dioxide under high pressure is used as an alternative solvent to produce porosity and entrapment of BMP-2. This method has shown suitability for sensitive growth factors (17).

A technology developed for the controlled release of growth factors adsorbed in scaffolds is layer by layer polyelectrolyte multilayer film (**Fig. 1.4 A**). Three-dimensional printed  $\beta$ -TCP/PCL scaffolds were repeatedly dipped in positively and negatively charged polymer baths, producing a film and trapping the charged BMP-2 while preserving its activity. This modality showed BMP-2 release in micrograms; 80% of the incorporated amount was released over a 2 day period with less than 1% in the first 3 hours and the remaining 20% over 2 weeks. Released BMP-2 induced differentiation of pre-osteoblasts and formed ectopic bone by 4 weeks (105). In another approach designed to produce a more sustained release that could last over several weeks, BMP-2 emulsified in acetic acid was incorporated in the polymer solution prior to electrospinning or by using co-axial electrospinning to produce a core containing BMP-2 surrounded by fibres. It was reported to accelerate bone regeneration and ossification foci in a 5 mm critical size rat calvarial defect (18). The pattern of release with these methods is usually a burst release followed by a continued slower release by diffusion through the polymer (104). Physical 3D printing technology has also been employed recently in order to achieve spatial control over BMP-2 by printing a pattern of BMP-2-containing bio-ink on the surface of circular acellular dermal matrix implants (106).

The major challenge associated with physical adsorption is the loss of bioactivity of the incorporated growth factors due to their undergoing conformational changes in the organic solvents at temperatures used or other harsh fabrication methods. Addition of a separate release system to the scaffold was introduced as a solution. Encapsulation within a biomaterial vehicle can provide protection from enzymes and increased

protein retention at the target site. Microspheres or nanospheres are particles with diameters from 10-1000  $\mu\text{m}$  and 10-1000 nm respectively (36). They were loaded with BMP-2 and incorporated into different types of scaffold matrices, either solid, hydrogel made of polymers or ceramics or fused together by sintering to make a scaffold (107). Microspheres typically exhibit burst release in the first few days followed by a more linear sustained release (108). When incorporating BMP-2 encapsulated in poly(lactic-co-glycolic acid) (PLGA) microspheres into polyurethane scaffolds, they reduced the burst release compared to scaffolds without microspheres (109).

A study comparing the release of BMP-2 from microspheres with or without being incorporated in a 3D scaffold showed that after 3 days, BMP-2 was released from PLGA microspheres and increased sharply with time for only 14 days. However, the 3D scaffolds with BMP-2-loaded microspheres released BMP-2 after 7 days but sustained linear release up to 4 weeks. This was attributed to the entrapped microspheres in the scaffold that have less surface exposed to the medium, reducing diffusion and hence sustaining BMP-2 for longer, forming more bone in a rat cranial defect (110). The particles can be made of different materials or different compositions or molecular weights compared to the matrix scaffold, which gives them the benefit of faster degradation while the scaffold still provides structural support. To bypass the drawback of exposure to organic solvents, techniques such as electro-spraying, with more control over the size of the sphere, have developed (111).

Besides adding separate release systems to enhance physical entrapment of BMP-2, attempts to increase electrostatic and non-covalent interactions by increasing the charged components in the surface, changing the pH of the media to increase the BMP-2 charge, or increasing the immersion time have been reported (104). Researchers have also expanded by developed nano-scale structures that provide increased surface area and non-covalent interactions that intensify binding between the protein and the scaffold or carrier (112). The surfaces of nanodiamond particles (nDP) show distinctive features depending on the production method (113). Detonation synthesis is a production method that has gained wide interest owing to the unique

mechanical, chemical and biological properties nDP acquire; making them useful in a variety of applications (114). In the case of detonation diamond, particle size of about 4-5 nm is yielded and a variety of functional oxygen-containing groups are usually present on the particle surface (**Fig. 1.5**).

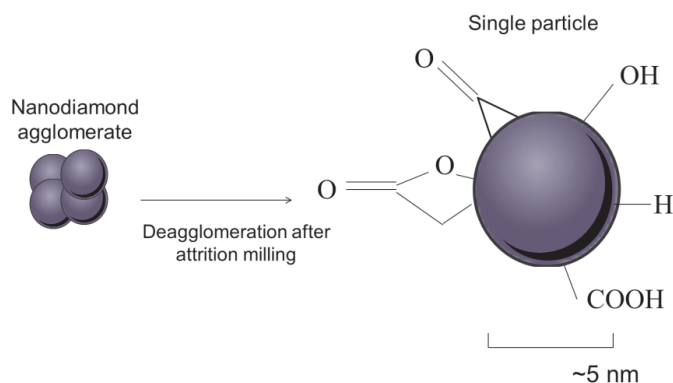


**Figure 1.5 Nanodiamond particles.** The structure and functional groups present in pristine nanodiamonds after purification with acidic treatment and deagglomeration with attrition milling. Adapted from (115).

These groups include carboxyl, lactone, ketone, hydroxyl as determined by infrared spectroscopy and mass spectrometry rendering it hydrophilic (116). These groups originate from the reaction in the detonation reactor and/or from the acid etching purification process (115). Also, more hydroxyl groups were found to be added from the milling process developed to deagglomerate/disperse them (117).

These nDP have many potential uses in a variety of biological applications (118). In BTE, BMP-2 was found to bind to nanocrystalline diamond (NCD) films produced by substrate-free chemical vapour deposition of acetylene in a microwave-enhanced plasma oven and then oxidised at high temperature (119). The oxygen-terminated nanocrystalline diamond (O-NCD) coating titanium implants showed highly stable, non-covalent physisorption of BMP-2 occurring in a reduced energy that would not alter the protein's conformation (119, 120). To confirm bioactivity of this bound BMP-2, MSC expressed high levels of osteogenic markers after being cultured on O-NCD implants and this same group also yielded enhanced osseointegration in sheep calvaria

defects (120). The nDP with hydrophilic oxygen-containing surface groups is very prone to adsorb molecules by hydrogen bonding and other polar interaction. In this study (120), theoretical calculations displayed BMP-2 binding with a combination of individual hydrogen bonds and van-der-Waals interactions up to 500 kJ/mol to the O-NCD. Therefore, comparable strengths to covalent binding were attained without chemical cross-linking providing sustained short distance BMP-2 delivery, which was confirmed histologically (120). In another study BMP-2 was delivered from NCD coated titanium screws in pig's mandible after 4 weeks of exposure to radiation; results showed osteoinductivity in irradiated bone (121). Drug delivery via nDP is an innovative matter in nanotechnology, and a few research groups have begun to investigate their uses for outstanding adsorption of biomolecules and bone regeneration.

In another recent study BMP-2 delivery from nDPs in suspension induced C2C12 myoblasts into alkaline-phosphatase (ALP) producing osteoblasts (122). There was a delayed cellular response observed in this study that was explained to be due to the strong binding and sustained delivery of BMP-2. This study showed how delivering BMP-2 in an nDP suspension can be a great advantage to bone defect surgeries where space is limited (122). nDP can also be incorporated into scaffolds for BTE to mediate the release of controlled therapeutics and at the same time provide structural support when the defect is large.

### **1.5.2 Chemical immobilisation**

The chemical immobilisation of BMP-2 inhibits nonspecific adsorption and may also reduce the amount of BMP-2 needed, preventing uncontrolled release (123). BMP-2 will be available to cells in contact with the scaffold, providing a highly localised signal and enhanced phosphorylation of receptor cascade (124). Techniques to chemically bind BMP-2 to scaffolds have been employed to control its release, either covalently or biochemically. This can be done after scaffold functionalisation by either using temporary or permanent and direct or indirect linkers (96). Non-covalent indirect interaction via proteins or other biological molecules such as oligopeptides can by

controlled by chemical conjugation onto scaffolds to provide binding sites and demonstrate a strong affinity to BMP-2 (96). A widely used example of this is heparin-conjugated systems that mimic the physiological role of heparin in regulating growth factors by binding proteins in the extracellular matrix (**Fig. 1.4 B**) (73). Studies verified that heparin-conjugated fibrin systems, after activating its carboxylic acid groups, enabled a slower and more controlled release of BMP-2 compared to BMP-2 absorbed in collagen sponge, leading to reduction in unwanted adipose tissue formation in ectopic sites and enhanced mineralisation (103, 125). The chemical functionalising of scaffolds with biomimetic peptides like arginine glycine-aspartic acid (RGD) has enhanced cell attachment and differentiation, while showing promise to reduce the doses of BMP-2 needed when combined with collagen sponges (126).

Covalent bonding on the other hand provides more prolonged attachment compared to physical and non-covalent chemical immobilisation, preventing its actual release in the vicinity until the scaffold degrades or the covalent bond is broken (123). One of its advantages is that the BMP-2 remains competent to activate receptors. A recently developed method to covalently tether BMP-2 by self-assembly using a bi-functional linker showed C2C12 myoblasts to express BMP-2 signalling pathway without BMP-2 being released in the medium (127). However, selection of the binding site of the protein without damaging the functional group activity is a challenge of covalently linking BMP-2, and the chemistries used to functionalise carriers and covalently immobilise BMP-2 can lead to protein denaturation or inactivation (123).

### 1.5.3 On-demand delivery and hybrids

‘Smart’ biomaterials release BMP-2 in response to surrounding environmental stimuluses. These factors commonly include changes in pH or temperature, presence of enzymes that cleave linkers used for immobilising or external factors such as drugs, light, electrical, magnetic or ultrasound applications (**Fig. 1.4 C**). In one study polyethylene glycol (PEG)-based scaffolds containing disulphide bonds were fabricated and implanted in a rabbit radius critical defect. This modification was made reactive to the cell-secreted redox microenvironment, thus the degradation rate and

subsequent BMP-2 release was dependent on the proteases secreted by the cells during remodelling (128). A pH/thermo-sensitive copolymer hydrogel showed high adsorbing efficacy of BMP-2 up to 85 % jellified in physiological pH and temperature. Release kinetics of the BMP-2 was not quantified but the scaffold formed mineralised tissue in an ectopic mouse model after 7 weeks (129).

Composite or hybrid materials are also used to improve the release profile of BMP-2. For example, this was seen in a study aimed to develop a system to release low amounts of BMP-2 from a collagen-HA scaffold. Preserved bioactivity of BMP-2 was seen up to 21 days, with enhanced mineralisation from cultured pre-osteoblasts and enhanced bone regeneration in rat calvaria after 8 weeks (130). In another study, a composite hybrid system using RGD- functionalised alginate hydrogel containing low amounts of BMP-2 was injected inside a PCL nanofiber mesh tube and compared it to the standard clinical method of absorbable collagen sponge delivery or alginate hydrogel alone to evaluate the regenerative process with respect to space and time (131). In a rat femoral segmental critical defect, the hybrid scaffolds slowed the release of BMP-2 and promoted significant increase in bone volume compared to the other groups while also preventing heterotopic mineralisation (131). Thermo-sensitive polymeric nanoparticles with hydrophobic and ionic complex interactions with BMP-2 in a hydrogel showed sustained release of BMP-2 for 3 weeks. These dual interactions led to increased bone regeneration in an ectopic and orthotopic model after a single injection (132).

## 1.6 CONSIDERATIONS FOR A SCAFFOLD DELIVERING BMP-2

The field of BTE is continuously developing; thus the definitions of an ideal scaffold construct delivering bioactive molecules continue to evolve. However, the optimal scaffold to deliver BMP-2 for bone regeneration should fulfil fundamental considerations in the clinic, in addition to the general scaffold requirements mentioned earlier (summarised in **Table 1.1**). These include the inter-related characteristics of; efficacy in *osteinduction* in addition to osteoconduction, *degradability* and, most importantly, to be *biologically harmless* for its host (133).

**Table 1.1. Scaffolds designed to deliver growth factors.** Necessary and desirable characteristics. Adapted and modified from (133, 134).

<b>Characteristic</b>	<b>Description</b>
Osteoinductivity	Release of a therapeutic dosage of bioactive growth factor over a period of time relevant to rate of bone formation
Biocompatibility	Low immunogenic response and no carcinogenicity
Degradability	Controllable degradation simultaneously with bone formation maintaining desirable mechanical properties
Readily sterilisable	Without loss of mechanical function or denaturation of growth factor
Ease of manufacture	Cost-effectiveness
Long shelf-life	Ease of access to the user

### 1.6.1 Osteoinductivity

Osteoinduction is the process by which osteoprogenitor cells are actively recruited and differentiate into osteoblasts under the influence of an osteogenic signal (65, 66). For effective osteoinduction, a scaffold must present bioactive signalling molecules to the tissues at a concentration that is optimal. It should be neither too low to be ineffective, nor so high as to cause toxic side effects. This optimum concentration range is called the therapeutic window (58). The mode of BMP-2 delivery to its potential site of action is an essential determinant of its osteoinductive *efficacy*. Preserved bioactivity at the site of interest is the primary goal, but effective concentration within the

therapeutic window is equally important. For BMP-2 as most growth factors, this index is rather small due to low solubility and short biological half-life (68).

### **1.6.2 Host response and degradability of implanted scaffolds**

Once a scaffold is implanted *in vivo*, the host responds by activating its defence mechanisms and an inflammatory/immune reaction, known as the foreign body response (FBR), is elicited (135). The interactions taking place between the implanted scaffold and its surrounding tissues significantly influence the ability of the scaffold to perform. This is described as biocompatibility (136). An appropriate host response must not only be local but also systemic, with an absence of cytotoxicity and carcinogenesis in addition to the ability of the scaffold to efficiently produce an osteoinductive response (136, 137). The innate defence system is a non-specific response that plays a crucial role in the early recognition and subsequent triggering of an inflammatory response to implanted scaffolds. The adaptive defence develops rapidly and efficiently to identify and respond to foreign materials that come in contact with the tissues, and is therefore referred to as specific or acquired (138). Scaffolds are associated with the innate immune response, and the adaptive response is only involved when they contain antigens (foreign proteins) that are recognised by the immune cells (139). The resultant tissue responses by the FBR are therefore quite complex, difficult to predict and involve both innate and adaptive immune cells with both short-term and long-term consequences (135, 137, 140).

The acute inflammatory host response towards the implanted scaffold is the beginning of the FBR, mediated by the injury of tissue vasculature during implantation and the adsorbed layer of blood plasma proteins on its surface (141). Fibrinogen with leukocyte integrin activation recruits macrophages and polymorphonuclear leukocytes that control severity of the response (141). These activated phagocytic cells then release cytokines and chemokines, including IL-1, TNF- $\alpha$ , and monocyte chemoattractant protein-1, which causes leukocytes extravasation and attract fibroblasts (142). Macrophages play important roles in the host response by secreting an array of products, including proteolytic enzymes, free radicals, and reactive oxygen

species (ROS) that degrade the scaffold and thus affect the release of BMP-2 (142, 143). They can also be differentiated towards pro- or anti-inflammatory phenotypes: M1 or M2 respectively (144). Macrophages have been shown to be capable of physiological osteoinduction by producing BMP-2, which promotes osteogenic differentiation of MSC *in vitro* (145). As the FBR progresses, the proinflammatory cells and cytokines decrease and macrophages express higher levels of anti-inflammatory IL-10, IL-4 and IL-13, which have been shown to have a role in macrophage fusion to form foreign body giant cells (FBGC) and in the inflammatory suppression (146). Recruited fibroblasts contribute to the formation of a fibrous capsule surrounding the implanted scaffold, isolating it from the surrounding vascularisation which may impair osteogenesis (135). Improved fibrous capsule vascularity has been stimulated through the local sustained release of BMP-2 from scaffolds (147).

#### ***1.6.2.1 The importance of the rate of degradation***

The long term host response to an implanted scaffold is affected by many factors, one of which is scaffold degradation (140) (**Fig. 1.6**). The optimal scaffold-based BMP-2 delivery should degrade at a rate corresponding to the rate of tissue restoration while maintaining release of the appropriate concentration of the protein. Resolution of the FBR is essentially dictated by the degradation profile and the products of scaffold degradation. The degradation process of degradable aliphatic polyesters generally occurs in two phases *in vivo*. First, hydrolysis causes cleavage of ester bonds and decrease in molecular weight of the material. When the oligomers are removed, there is a loss of mass and mechanical strength (37). The second phase is characterised by FBGC releasing degradation enzymes and ROS that begin to engulf the breakdown (148).

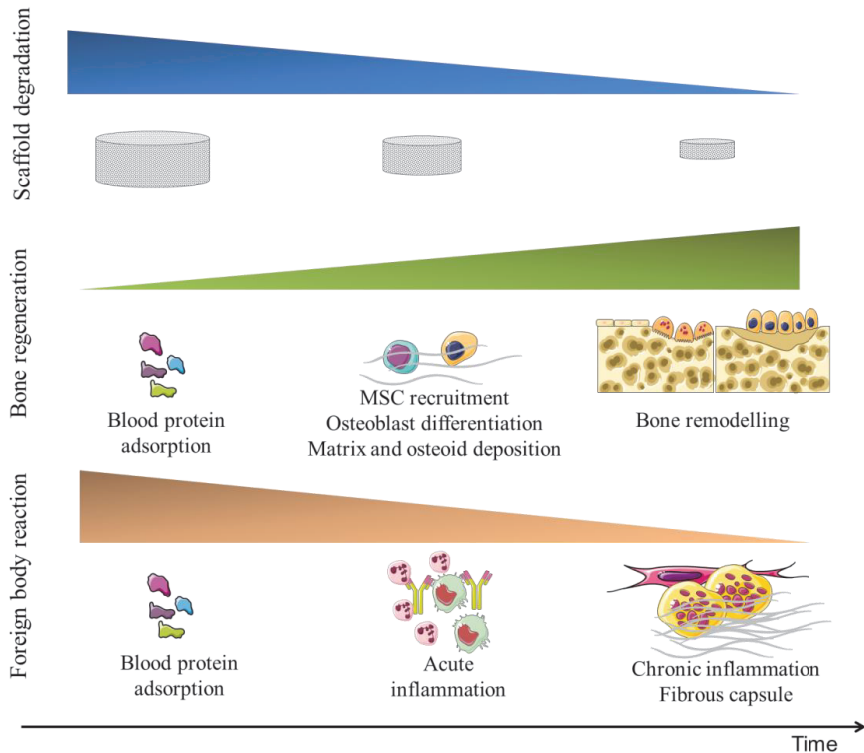


**Figure 1.6 Foreign body reaction to a degradable scaffold.** Schematic illustration of the inter-related stages of early and late host response and bone regeneration after implanting a degradable BTE scaffold. Inspired and modified from (140) and made using Servier Medical Art.

As the scaffold degrades, the acidic by-products, if not washed away, create an acidic environment shown to affect the inflammatory cytokines and neovascularisation and also to cause demineralisation of the bone formed (149). However, this acidity may be buffered by incorporating or coating polymer scaffolds with biomimetic agents (150). BMP-2 incorporated into a surface in polymer scaffolds coated with CaP compared to adsorbed directly onto the surface provided a slower, cell-mediated release as the scaffold degrades which was associated with a significant reduction of the inflammatory response, suppressing FBR and enhancing osteogenic potential (147, 151). In a rat mandible defect model, acidity from degrading polymer scaffolds affected bone formation and accordingly a continuous supply of BMP-2 was required

to overcome the drawbacks (152). The delivery of immunosuppressive agents with BMP-2 has been shown to modulate host response and enhance osteogenesis (153).

### ***1.6.2.2 Host response and its long-term consequences***

There may be many long-term consequences of a FBR or when an inflammation gets out of control, but the most alarming is tumour formation. Based on increasing evidence, it appears that the cause of foreign-body sarcomas is not the chemical content of the biodegradable polymer alone, but also promoting events that lead to tumours due to prolonged presence of the irritant in tissues (154). The implantation of several materials in rodents can produce tumours. These effects have been described as solid-state carcinogenicity and it has been assumed that the mechanism is related to the development of the FBR (154). There has been an increasing emphasis on the role of inflammation on cancer (155). Irreversible genetic damage leads to a neoplastic state which, when exposed to chronic inflammatory chemokines, progresses through cell proliferation and reduced genetic repair (156). Chronic inflammation such as that seen with the prolonged presence of an implanted scaffold plays a promoting role. A study using p53 tumour suppressor gene deficient mice, where plastic discs were implanted subcutaneously, found that sarcomas developed in 79% of the mice with implants compared to those without. This was found to be associated with increased oxidative stress from chronic inflammation (157). Rats also developed a peri-implantation chronic inflammatory FBR reaction and a high incidence of malignant mesenchymal tumours in response to different implanted biomaterials (158).

A thick fibrous capsule associated with a chronic inflammatory foreign body presence was frequently related to carcinogenicity, due to the acellularity and avascularity which render the environment susceptible for mutations with no repair (154). Foreign body carcinogenesis has a rare incidence in humans (159). In rodents, it contains stages that involve at least half its life-span, making it species-dependant (159-161). Although rarely encountered, it cannot be ignored and all new biomaterials require rigorous testing. Scaffolds are associated with many factors that influence host response, including the chemistry, ability to degrade, surface and bulk architecture (160, 161). In the case of the presence of a bioactive ligand such as in BMP-2 carriers,

the side effects can be attributed to uncontrolled release of high amounts of BMP-2. The observed increase in the cancer incidence remains a real concern for the carcinogenic potentials of BMP-2 (89, 92). Concern also arises for the safe delivery of BMP-2 from scaffolds when reconstructing bone defects caused by carcinomas, since both chronic inflammation as well as the effects of BMP-2 can have effects on areas prone to recurrence (94, 162, 163). Therefore, this necessitates long-term safety biocompatibility evaluations of a scaffold delivering BMP-2.

### ***1.6.2.3 Evaluating host response and its unwanted consequences***

Extensive assessments relevant to Standardisation and Regulatory Body Guidelines are commonly followed for biomaterial safety and registration purposes (164, 165). Assessments are primarily based on the evaluation of cytotoxicity, immune response, genotoxicity, mutagenesis and/or carcinogenesis, in addition to the primary function, which is, in the current case, bone formation (166). *In vitro* cytotoxicity testing using direct contact with cell lines or elution of biomaterials into cell lines cultures has been used to make testing of BTE scaffolds reproducible (45). Although many complex *in vitro* cell culture models have been employed, animal testing is still considered to be the most reliable system. *In vivo* evaluation of immune response typically uses rodents, where the scaffolds or biomaterials are implanted subcutaneously, intramuscularly or in the bone itself, and evaluated after various time points. Depending on the degradation rate of the scaffold tested, sample harvesting between 6-12 months may be used to allow time for degradation, regeneration and remodelling to take place (167). Organ and body weights and blood biochemistry all serve as evaluation tools (168). Histopathology has been the gold standard, however, traditional histological evaluation is unable to identify the dynamics between different cell types.

Therefore, real-time non-invasive models to monitor inflammatory host response have been developed recently. A model to measure the release of ROS which were found to be involved in early and late FBR to evaluate biocompatibility using bioluminescence has been reported (148). Another model using a fluorescence imaging probe system that allows the assessment of the recruitment and interactions between polarised M1 and M2 macrophages has recently been developed (169).

Biomaterials used in fabricating tissue engineering scaffolds and drug delivery were used to develop the model and find approaches that optimised macrophage response (169, 170).

*In vitro* genotoxicity and mutagenicity utilising proto-oncogenes and tumour suppressor genes from mammalian or bacterial cells exposed to biomaterials of interest have been used as methods for evaluating chromosomal damage (166, 171). Carcinogenicity or tumorigenic potential of biomaterials in general is typically tested in rodent 2-year cancer bioassays (160, 161, 172). However, these assays are no longer the only efficient or feasible way to detect possible human carcinogenicity; alternative mouse models are now available for increased sensitivity (172-174).

Few reports of scaffold constructs tested *in vivo* for carcinogenicity currently exist, as this is more commonly done for physical materials or chemicals. Bioglass-poly(lactic acid) composite scaffolds populated with progenitor cells were evaluated in a rat calvarial critical size defect and tumorigenicity potential was evaluated based on the activity in serum of the free radicals involved in tumorigenicity (168). Carbon nanotubes, another type of scaffold, have been tested in rasH2 mouse models expressing human-derived c-H-ras proto-oncogene (175). Non-invasive real time methods have not been developed to monitor carcinogenesis in response to biomaterials such as those recently developed for inflammatory responses.

## 1.7 RATIONALE

Previous efforts from our research group examined degradable aliphatic polyester porous scaffolds, poly(LLA-co-CL) as candidates for BTE. These scaffolds showed cytocompatibility (45) and encouraging potential for osteoconductivity (16, 44). Also, attempts to enhance their mechanical properties (52) and wettability by modifying the surface with nDP improved cellular responses and bone formation (54). Functionalising these copolymer scaffolds and immobilising BMP-2 could augment their osteoinductive properties. The development of more effective, sustained and controlled scaffold-based BMP-2 delivery systems in the near future is crucial. Enormous efforts have been made in recent years in this field in order to overcome side effects, however, optimal controlled release and a sustained therapeutic concentration has yet to be attained.

Several aspects will need to be considered concerning the efficacy of the bioactive scaffold. The scaffold and mode of growth factor delivery determines the efficacy of the bioactive scaffold; i.e. bioactivity, release kinetics, biocompatibility and degradability. Evaluation of these requires an understanding of inflammatory and regenerative tissue responses as the scaffold degrades. The host response to a bioactive scaffold may lead to the development of responses that adversely affect the host tissues, thus early and late host responses to degradation of these functionalised scaffolds will direct their success or failure. Validated animal models need to be developed together with *in vitro* models, to facilitate investigations of long-term responses.

## 2. AIMS

The aim of the work described in the following chapters was generally to determine efficient modes of delivering bioactive signalling molecules from copolymer scaffolds for bone regeneration with minimal adverse host reactions.

### Specific Aims:

- 1 To determine the release profile and efficacy of recently developed and established functionalising techniques for delivering BMP-2 from poly(LLA-co-CL) scaffolds (**Paper I**).
- 2 To evaluate the *in vivo* host response and degradation of functionalised bioactive poly(LLA-co-CL) scaffolds (**Paper II**).
- 3 To develop a non-invasive *in vivo* model to evaluate the tumorigenic potential of scaffolds used in tissue engineering (**Paper III**).
- 4 To assess the tumorigenic potential of functionalised bioactive poly(LLA-co-CL) scaffolds (**Paper IV**).

### 3. METHODOLOGICAL CONSIDERATIONS

#### 3.1 THE CHOICE OF METHODS

To evaluate a bone regenerating scaffold while observing active bone formation and preventing adverse effects, clinically-relevant *in vivo* environments are strongly required. Despite the criticism of *in vivo* research due to ethical and economic reasons, this helps to evaluate complex interactions between different cells, growth factors and scaffold biomaterials. The methods used in the four papers are summarised in **Fig. 3.1**.

In **Paper I**, *in vitro* and *in vivo* methods were used to evaluate the bioactivity of BMP-2 incorporated on copolymer scaffolds using four different modalities. The relative release of the incorporated BMP-2 was quantified using SRM. Assays were performed in order to confirm that the scaffolds supported MSC attachment, cytoskeletal re-organisation and proliferation. Furthermore, differentiation of MSC cultured on the different scaffolds *in vitro* was evaluated at the mRNA level. The effects of the different modes of delivery on the scaffolds' osteoinductivity were compared in a rat mandible critical-size defect. Based on data obtained from **Paper I**, the most distinctive BMP-2 functionalising modality was chosen to conduct the following investigations where effects of nDP modification and BMP-2 physisorption on copolymer scaffolds on their degradation and host response were determined using Balb/c mice (**Paper II**). Molecular weights of the degrading scaffolds were analysed after 1, 8 and 27 weeks. Correspondingly, host response was evaluated using a customised RT<sup>2</sup> Profiler PCR Array and infiltration of inflammatory cells was quantified in H&E sections. To investigate potential harmful properties of the functionalised bioactive scaffolds, the tumorigenic potential was evaluated. For this purpose, a non-invasive BLI microenvironmentally-induced oral carcinogenesis model was first established using NSG mice in **Paper III**. Early neoplastic oral keratinocytes (DOK) were first transduced with luciferase (DOK<sup>Luc</sup>) and cultured with or without CAF to develop the model. To confirm that the DOK phenotype was preserved after transduction, the development of tumours from orthotopic and ectopic xenografts of DOK<sup>Luc</sup> or DOK<sup>Luc</sup>+CAF inoculations was monitored manually and by BLI.

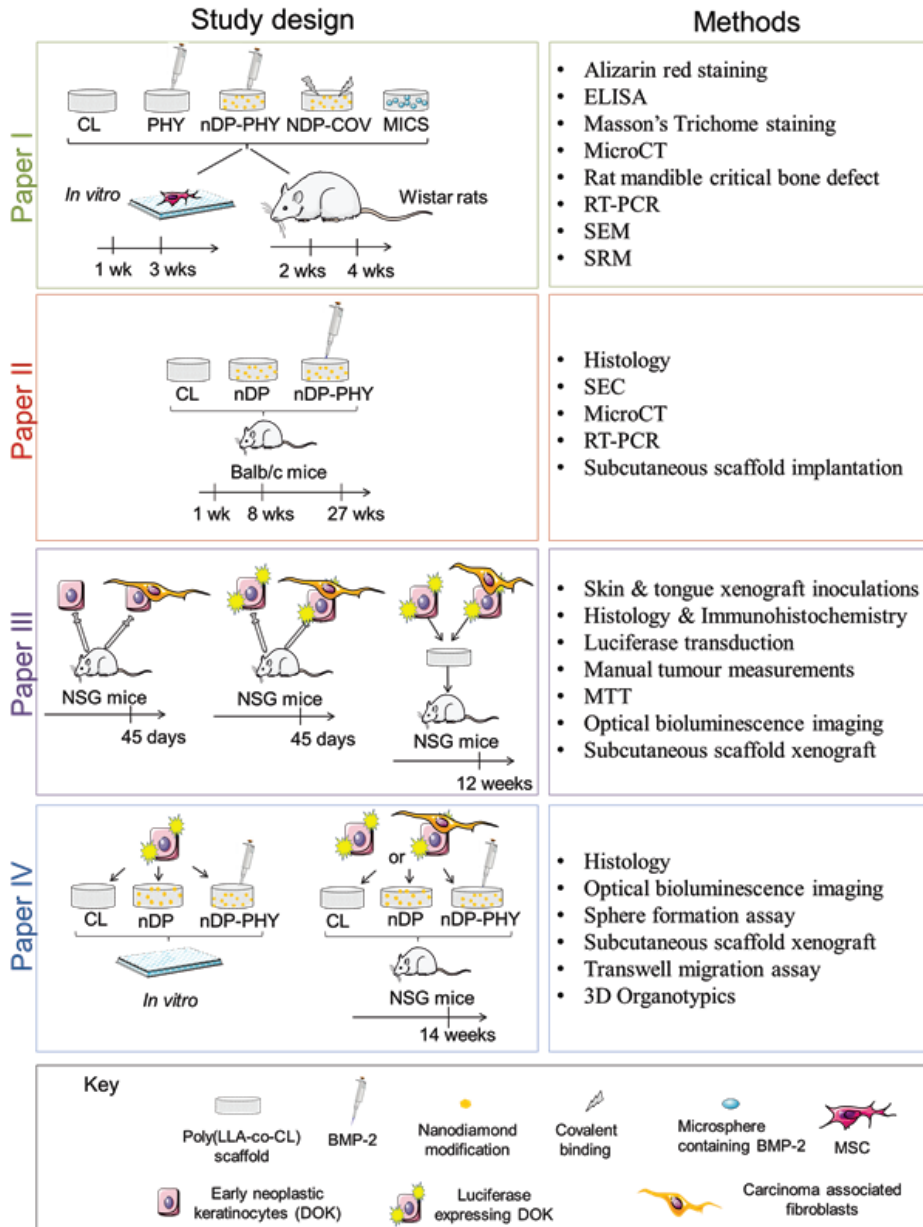


Figure 3.1. Schematic summary of the study designs used in the four studies. Figure made using Servier Medical Art.

Development of tumours from DOK<sup>Luc</sup> grown on poly(LLA-co-CL) scaffolds under different microenvironmental cues was monitored non-invasively by BLI. In **Paper IV**, the *in vivo* model established as part of this thesis was applied to study the tumorigenic potential of copolymer scaffolds modified with nDP and nDP plus physisorbed BMP-2, and tumour formation was followed with BLI for 14 weeks. Harvested tumours were evaluated immunohistologically. Also, after being cultured on modified and non-modified scaffolds, DOK<sup>Luc</sup> were evaluated by functional *in vitro* tumorigenicity assays including a 3D organotypic model.

### 3.2 SCAFFOLD FABRICATION

The poly(LLA-co-CL) was synthesised from 75 mol % LLA (Boehringer Ingelheim, Germany) and 25 mol %  $\epsilon$ -CL (Sigma-Aldrich, , St Louis, MO, USA), by ring opening polymerisation at 110°C for 72h using stannous 2-ethylhexanoate as catalyst and ethylene glycol as the initiator. The composition was determined by proton nuclear magnetic resonance spectrometry (Bruker AC 400, Bruker, Switzerland). Poly(LLA-co-CL) with about 25 mol%  $\epsilon$ -CL provides amorphous, elastic physical properties which makes it suitable for cell applications (42). The polymer number average molecular weight ( $M_n$ ) was measured on a Verotech PL-GPC 50 size-exclusion chromatography system (SEC) (Polymer Laboratories, Varian Inc., USA) described in **Section 3.6**. 3D porous scaffolds were prepared by the solvent-casting particulate-leaching method described earlier (16). Briefly, the copolymer was dissolved in chloroform (1g/ml) and mixed with sodium chloride particles by a weight ratio of 10:1 before being poured into moulds. Scaffolds were punched out in different dimensions. Salt particles were removed by soaking in deionised water and then scaffolds were vacuum dried and electron beam sterilised. Scaffold porosities were characterised using a micro-CT (SkyScan 1172, Kontich, Belgium) using 40 kV and 2.4 micron voxel.

### 3.2.1 Scaffold functionalisation and BMP-2 immobilisation

rhBMP-2 expressed in *Escherichia coli* (*E. coli*) was produced and obtained from our collaborator at The University of Wuerzburg, Germany as described previously (176). In (**Paper I, II and IV**), poly(LLA-co-CL) scaffolds were modified to deliver BMP-2 using different modalities as follows:

#### 3.2.1.1 Physisorbed BMP-2 on unmodified scaffolds (*PHY scaffold*)

A total of 1 µg of BMP-2 in 50 µl phosphate buffered saline (PBS) (Gibco, Thermo Scientific, MA, USA) was added in two increments onto the unmodified poly(LLA-co-CL) scaffolds.

#### 3.2.1.2 Physisorbed BMP-2 on scaffolds modified with nDP (*nDP-PHY scaffold*)

Detonation nDP were purchased from Gansu Lingyun Corp. (Lanzhou, China), acid-purified and dispersed according to previously described protocols (117). The particles were attrition milled with micro-sized zirconia beads producing particles of ~5 nm diameters. Mechano-chemical reactions during the milling produced particles with hydrophilic surface, containing oxygen-containing terminal groups detected by infrared spectroscopy. Scaffolds were then modified with the nDP solution (2% (w/v) by a vacuum technique described in **Paper I**. Later, physisorption of BMP-2 on the nDP modified scaffolds was carried as **Section 3.2.1.1**.

#### 3.2.1.3 Scaffolds modified with nDP covalently functionalised with BMP-2 (*nDP-COV scaffold*)

First nDP were functionalised with benzoquinone by adding 189 mg of deagglomerated nDP in 20 ml of PBS (pH 8) and 150 mg of benzoquinone (1.38 mmol) (VWR International, Radnor, PA, US) for 24h at room temperature. This was followed by the immobilisation of BMP-2 to the functionalised nDP in PBS (pH 6) for 24h. The scaffolds were then finally modified with the functionalised nDP by the vacuum technique.

After the reaction of functionalising the nDP with BMP-2, which corresponds to a loading of 0.5 mg BMP-2 per 1 g of nDP (approx. 19 nanomoles/g), the supernatant solution was found not to contain any organic material (checked by thin layer chromatography and infrared). It can thus be assumed that all of the BMP-2 was bound to the diamond surface, likely due to the large excess of reactive diamond surface moieties. This amount is too small to be analysed by quantitative methods, as the expected changes are within the error range of the instruments.

#### ***3.2.1.4 Microsphere preparation and scaffold modification (MICS scaffold)***

It has been shown that the properties of the microspheres have a major effect on their efficacy (36). PLGA was chosen owing to its biocompatibility and FDA approval. The molecular weight of PLGA5050 purchased was very close to that used in a previous report (108). BMP-2-loaded PLGA5050 (Purac Biochem, Gorinchem, Netherlands) microspheres were fabricated using a previously described water-in-oil-in-water double emulsion solvent extraction technique, detailed in **Paper I**. The microspheres were incorporated into the porous scaffold using a seeding technique (177). The loading efficiency of the microspheres was determined using a solvent-extraction technique (178) and the concentration of BMP-2 was analysed by a commercially available human BMP-2 enzyme-linked immunosorbent assay (ELISA) (RnD Systems, Minneapolis, Minnesota, USA). With an evaluated loading efficiency of 0.04%, the amount of microspheres needed to contain exactly 1 µg of BMP-2 was calculated. The morphology and distribution of microspheres in the scaffolds were examined using scanning electron microscope.

### **3.3 CELL SOURCE AND MAINTAINENCE**

#### **3.3.1 Cell culture**

##### ***3.3.1.1 Primary human MSC***

Primary human MSC (StemCell™ Technologies, Vancouver, BC, Canada) were expanded in MSCGM™ complete medium (Lonza, Basel, Switzerland). Passages 3 to 6 were seeded ( $2 \times 10^5$  cells per scaffold). Once they reached confluence, the medium

was replaced with osteogenic medium (**Paper I**). MSC cultures were performed in a minimum of triplicates and the experiments were repeated three times.

### **3.3.1.2 Human osteoblast-like cells (HOB)**

HOBs were used as a positive control for the *in vitro* mineralisation staining in **Paper I**. They were isolated using a protocol that has been previously described (179). They were maintained in the alpha modification of Minimum Essential Medium supplemented with 1% antibiotic and 10% Foetal Calf Serum (FCS) (all from Gibco).

### **3.3.1.3 Early neoplastic, dysplastic oral keratinocytes (DOK)**

Transformed, non-tumorigenic DOK were purchased from The European Collection of Cell Cultures (Salisbury, Wiltshire, UK) (180) and were routinely maintained in Dulbecco's Modified Eagle's Medium (DMEM), 10% FCS, 20µg/ml L-glutamine and 5µg/ml hydrocortisone (all from Sigma-Aldrich).

#### *3.3.1.3.1 DOK cells as a screening tool for developing the tumorigenicity model*

Over 90% of head and neck cancers are, as are the majority of human malignancies, of epithelial origin and their consequences for patients are dramatic. In addition, most of the bone defects are due to resection of OSCC (181). Since scaffolds used for bone regeneration in the oral and maxillofacial area might come in contact with the oral epithelium and be influenced by their components, there is a need to study the potential carcinogenic effect of degradable bioengineered scaffolds on oral epithelial cells. In **Paper III**, we chose to develop an animal model with DOK cell line derived from premalignant oral mucosa (180). The use of normal cells in tumour models is time consuming and it is difficult to reproduce the several mutagenic events required for carcinogenesis in an experimental setting (155). DOK was established from a tongue dysplasia that progressed after 11 years into a well-differentiated OSCC. They were found to be partly transformed but non-tumorigenic in NUDE mice and our previous research on non-obese diabetic/severe combined immunodeficient (NOD/SCID) mice (182) showed that DOK at a low density were tumorigenic only when co-inoculated with carcinoma associated fibroblasts (CAF). Spontaneously

immortalised cells possess a more stable phenotype than virally immortalised cells. Thus they are preferred in models of tumorigenesis (183).

#### 3.3.1.3.2 Luciferase transduction of DOK

The process of transducing DOK wild type (DOK<sup>WT</sup>) cells is explicitly described in the methodological paper (**Paper III**). Briefly, infectious retroviral vector particles were produced in Phoenix A cells (LGC Standards AB, Borås, Sweden) and DOK<sup>WT</sup> cells transduced with a luciferase expressing construct, L192, coding for the luciferase enzyme and co-transduced with the tetracycline-regulated transactivator (tTA) (184) and gene transfer enhanced with protamine sulfate (5µg/mL) as previously described (**Paper III**). L192 has a puromycin resistance gene, so cells were selected with 1µg/ml puromycin (Sigma).

Proliferation of transduced DOK<sup>WT</sup> and DOK<sup>Luc</sup> was compared using Methyliazol Tetrazolium Assay (Sigma). Both cell types, DOK<sup>WT</sup> and DOK<sup>Luc</sup> were seeded (1000 cells/well) in 96-well plates (n=6). Cells were fixed every 24h for 7 days and the absorbance expressed as optical density using a microplate reader.

#### 3.3.1.4 Carcinoma associated fibroblasts (CAF)

CAF were obtained from patients with oral cancer after informed consent and histologically confirmed OSCC lesions. They were isolated using the previously described explant technique (185). They were maintained in FAD medium (DMEM/Ham's F12 1:3 mixture, 1% L-glutamine, 0,4µg/ml hydrocortisone, 50µg/ml ascorbic acid, 10 ng/ml EGF, 5µg/ml insulin and 20µg/ml transferrin and linoleic acid (all from Sigma), with 10% FCS.

CAF were characterised by fluorescence-activate cell sorting for expression of lineage-specific markers such as: epithelial specific antigen 0.00%, leukocyte marker CD45 0.02%, endothelial cell marker CD31 0.09%, pericyte marker/MSC marker CD146 1.48% and mesenchymal markers: CD140b 95.67%. Immunohistochemistry carried on culture dishes showed expression of vimentin 99.5% and  $\alpha$  smooth muscle actin 50.2% of cells.

To collect the conditioned medium, medium from CAF at 70-80% confluence was replaced for 18-24h by serum-free DMEM (Sigma). That was then replaced with half the volume of their routine medium for another 24h before the conditioned medium was collected, centrifuged and filtered through 0.40  $\mu\text{m}$  filters.

### 3.3.1.5 Primary gingival fibroblasts (GF)

GF were isolated from samples of normal human oral mucosa of individuals with no clinical signs of inflammation at time of undergoing third molar extraction after informed consent. They were isolated using the explant technique protocols previously described (185). They were maintained in DMEM high glucose + 10% FCS (Sigma).

## 3.4 QUANTIFYING THE RELEASE OF BMP-2 FROM SCAFFOLDS

Selected reaction monitoring (SRM) was used to relatively quantify the release kinetics of BMP-2 in **Paper I**. The scaffolds were immersed in PBS at dynamic conditions and the supernatant was collected and replaced at determined time points up to 70 days. Briefly, the SRM strategy involved quantitative comparison of endogenous peptides and a spiked-in peptide standard, referred to as light and heavy peptides respectively, to determine the relative abundance of the protein. The method consists of a triple quadrupole (QQQ) mass spectrometer, as illustrated in **Fig. 3.2**. The mixture was subjected to digestion and the proteolytic peptides exposed to liquid chromatography (LC) and electrospray ionisation (ESI). The heavy and the light peptides were eluted with the same retention time from the LC column. In the QQQ, a predefined precursor peptide (the light and heavy forms of the signature peptide respectively characterised by different masses) is selected and isolated in Q1. In Q2, the collision energy produces charged fragments of a target peptide and in Q3 predefined fragment ions selected by mass are transmitted for detection. A chromatogram shows retention time and signal intensity for each transition.

rhBMP-2 (residues 283-396) expressed in *E. coli* was purchased (RELIATech GmbH, Wolfenbüttel, Germany). A preliminary step in SRM strategy consists of choosing a peptide that is ideal for SRM method based on specific criteria. An ideal

SRM peptide has to be present in a unique form for the targeted protein and post-translational and chemical modifications must be considered (186). To choose the peptide, the protein was digested and run in a mass spectrometer (MS), after which each peptide with a specific mass was fragmented in MS-MS (Orbitrap, ThermoScientific). The four representative peptides of BMP-2 that showed high intensities in the MS spectrum were tested in SRM mode.

rhBMP-2 expressed in *E.coli* is a small protein of no more than 13 kilo Dalton molecular mass as monomer, so due to a short protein sequence (total 114 amino acid residues) the number of tryptic peptides was limited, with only 4 peptides providing strong specific signals. After testing all 4 peptides with direct infusion on 5500QTRAP for transitions status, it was found that only 1 peptide, NYQDMVVEGCGCR, revealed good transitions and was therefore selected for relative quantification of BMP-2. This peptide, is however, not optimal for absolute quantification as it contains 2 cysteines (C) able to form inter- and intra-chain disulfide bridges. De-folding of protein by urea followed by carbamidomethylation of cysteine was performed in the *in vitro* SRM assay. The peptide contains glutamine (Q) and asparagine (N) residues but their conversion to aspartate and glutamate, depending on the surrounding sequence, would probably not occur (187). Therefore, it was selected as stable isotope-labelled internal standard (SIS) candidate as there was no better alternative. A SIS (heavy peptide) corresponding to that signature peptide was purchased in AQUA QuantPro quality (ThermoScientific). The C-terminal arginine for the SIS was labelled with  $^{13}\text{C}$  and  $^{15}\text{N}$  resulting in a peptide with 10 Dalton additional mass compared to the non-labelled peptide. In addition cysteines were carbamidomethylated. In order to obtain the chosen peptide in a unique form, methionine residue had to be oxidised.

The assay for detection of peptide was optimised by direct infusion on a Q-Trap 5500 (AB SCIEX, MA, USA). SIS peptide NYQDMoxVVEGCcmGCcmR $^{13}\text{C}^{15}\text{N}$  [25 femtomoles (fmole)] were spiked into samples containing unknown amounts of BMP-2. The mixture was lyophilised (Centrivap<sup>®</sup> Centrifugal, USA) prior to in-solution protein digestion according to a previously established protocol (<http://www.uib.no/file-archive/in-solution-proteindigestion.pdf>). Prior to liquid

chromatography SRM-MS (LC SRM-MS) analysis, the mixtures of reduced and alkylated tryptic peptides were desalted as described previously (188). LC SRM-MS analysis was performed on a Q-Trap 5500 coupled to a Dionex Ultimate system (Thermo Scientific) as previously described (188). For quantification of the signature peptide from BMP-2, all y transitions with significant intensity were used to obtain ratio Light/Heavy (L/H).

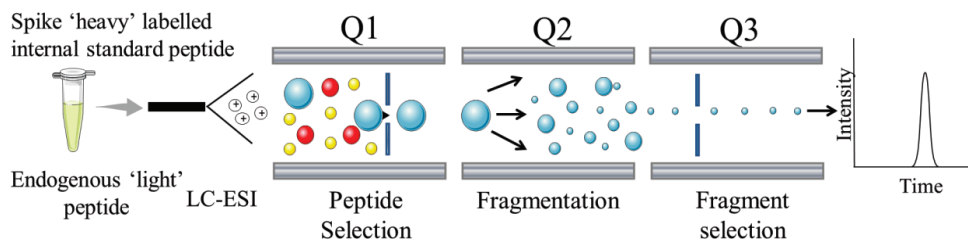


**Figure 3.2 Schematic workflow of SRM-based proteomic experiment.** A triple quadrupole (QQQ) mass spectrometer (Q-Trap). Figure modified from (186).

### 3.4.1 Optimising the use of MS as a method for assessing release of BMP-2

ELISA is the most commonly used method for detecting protein release from scaffolds (189), provided the amount is within the detection range. The BMP-2 Quantikine ELISA kit (RnD) was used initially when designing the study, but no BMP-2 could be detected. Kits commonly used, detect mammalian BMP-2 which is glycosylated, and the rhBMP-2 used in this study is bacterial BMP-2 and thus non-glycosylated. Protein labelling techniques to quantify fluorescence have been employed previously but unreliable release profiles have been encountered because they depend on the fluorophore tagging which in return depends on its dissociation factor (95). Using radiolabelled proteins commonly radioactive  $^{125}\text{I}$ iodine requires adjusting for radioactive decay and accompanying risks and drawbacks of radioactivity are not sustainable for longer periods (190). Hence, to quantify low abundant amounts released for a long period a highly sensitive, selective and reproducible method was required. SRM was thus chosen as a new strategy for quantification of BMP-2. We tested 3 assays (series) with slightly different SRM methods and progressively improved the ability to measure the release of BMP-2.

In all triplicate samples (series), the heavy signature peptide with the following sequence NYQMVVEGCGCR was spiked in samples with endogenous BMP-2. However, in the first run, the heavy signature peptide was NYQMVVEGCGCR with labelled R and spiked-in in the amount of 5 fmoles. In the second run, due to the fact that the signature peptide contains a methionine (M), making the side chain of the amino acid prone to oxidation, the heavy signature peptide used was not only labelled on R, but in addition synthesised with M oxidised (Mox) NYQMVVEGCGCR and spiked-in in the amount of 5 fmoles. In this assay, M residues from the endogenous samples were oxidised *in vitro*. In third run, an assay similar to that described in the 2<sup>nd</sup> was performed, with the exception that 25 fmoles (instead of 5 fmoles) of heavy peptide were spiked-in, in order to obtain more robust results and because the SIS peptide should be added to the sample in amounts corresponding to the endogenous peptide levels. All 3 series analysed with slightly different SRM conditions revealed comparable profile of BMP-2 release from the different scaffolds (data not shown).

Finally, in an attempt to obtain not only a relative quantification of BMP-2 expressed as ratio (L/H), but an absolute quantification of BMP-2, standard curves were generated alongside our analyses of series samples. Values of peak area for various samples (heavy peptide with Mox spiked in various amount of synthetic light peptide with Mox) prepared for the standard curve were highly reproducible under our assay conditions.

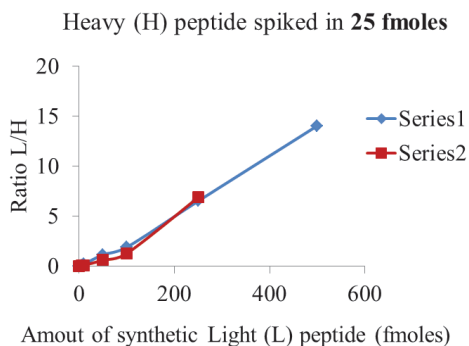


**Figure 3.3 SRM standard curves generated.** Standard curve performed with spiked-in 25 fmoles heavy peptide in various amount of synthetic L peptide NYQDMVVEGCGCR. Data (blue, red) from 2 experiments performed on different occasions.

Data from various analyses (different colours in **Fig. 3.3** correspond to experiments performed on different days) show good correlation and a relatively good linearity, arguing for reproducibility using our developed method and parameters for SRM assay and encourage efforts for future absolute quantification. The slight discrepancy may be attributed to the fact that the SIS could not be synthesised by the manufacturer in the quality required for absolute quantification.

The SRM work was carried out in collaboration with the Proteomics Unit (PROBE) with the help of Dr. Anne P. Døskeland.

### 3.5 INVESTIGATING OSTEOINDUCTIVITY AND HOST REPSONSE

#### 3.5.1 *In vitro* experiments

##### 3.5.1.1 *Cell attachment and mineralisation*

Attachment and spreading of MSC on the scaffolds at days 1 and 3 post-seeding in **Paper I** were analysed by scanning electron microscopy (Jeol JSM 7400F, Tokyo, Japan). To evaluate the mineralisation in the scaffolds as evidence of MSC developing an osteogenic phenotype and depositing calcium, the MSC /scaffold constructs were harvested after 1 week culture and stained with Alizarin red (2%).

### **3.5.1.2 Real-time reverse transcribed polymerase chain reaction (PCR) and PCR Array**

Total RNA was isolated from *in vitro* cultures (**Paper I**) and *in vivo* samples (**Paper II**) using a Tissue RNA isolation kit (Maxwell®, Promega, Madison, WI, USA). Quantity and purity were checked using a Nanodrop spectrophotometer (ThermoScientific, Wilmington, Delaware, USA). Total RNA was reverse transcribed according to the manufacturer's instructions using the High-capacity complementary DNA Reverse Transcription Kit (Applied Biosystems, Carlsbad, CA, USA) in **Paper I** and reverse transcribed according to the manufacturer's instructions using the Rt<sup>2</sup> PCR Array First Strand Kit (SABiosciences, Hilden Germany) in **Paper II**. Quantitative real time PCR was conducted on a StepOne Plus system, using TaqMan gene expression assays (Applied Biosystems) (**Paper I**) and a customised Rt<sup>2</sup> Profiler PCR Array (Superarray Bioscience) was used and PCR was performed on a StepOne Plus system with Rt<sup>2</sup> Real-time SyBR Green/Rox PCR mix (SABiosciences) in **Paper II**. Reference genes were glyceraldehyde 3-phosphate dehydrogenase (GAPDH) in **Paper I** and GAPDH, beta-actin, and beta-2 microglobulin in **Paper II**.

### **3.5.1.3 ELISA**

MSC and scaffold culture constructs were incubated with RIPA buffer, 1×Halt™ protease and phosphatase inhibitor cocktail (all from ThermoScientific) to extract total intracellular protein and quantitate intracellular BMP-2. To measure the endogenous BMP-2 released extracellularly, culture medium was collected at week 1 and 3. Human BMP-2 ELISA Development Kit (Peprotech, Rocky Hill, NJ, USA) was used to measure extracellular and intracellular endogenous BMP-2 from MSC in **Paper I**.

## **3.5.2 In vivo experiments**

### **3.5.2.1 Rat mandible defect model and subcutaneous ectopic mouse model**

Several critical-sized defect models have been described in the literature including calvarial defects (46) and long bone segmental defects (48), but none of them simulate the specific microenvironment and masticatory stresses seen in the oral and

maxillofacial area. An incision was made along the lower border of the mandible of male Sprague–Dawley rats (300–350 g) and after muscle retracting a round-shaped bone defect was created using a trephine burr (Komet Medical, Lemgo, Germany) (5 mm diameter) in the mandibular angle region (**Fig. 3.4 A, B**). The defect was filled with a scaffold (n = 8 per scaffold type). Rats were sacrificed after 2 weeks.

In **Paper II**, two (1 cm length) incisions were made on the back of 8-10 weeks old Balb/c mice (**Fig. 3.4 C, D**) (n = 4 scaffolds implanted per animal). Mice were sacrificed after 1, 8 and 27 weeks (n = 8 per scaffold type).

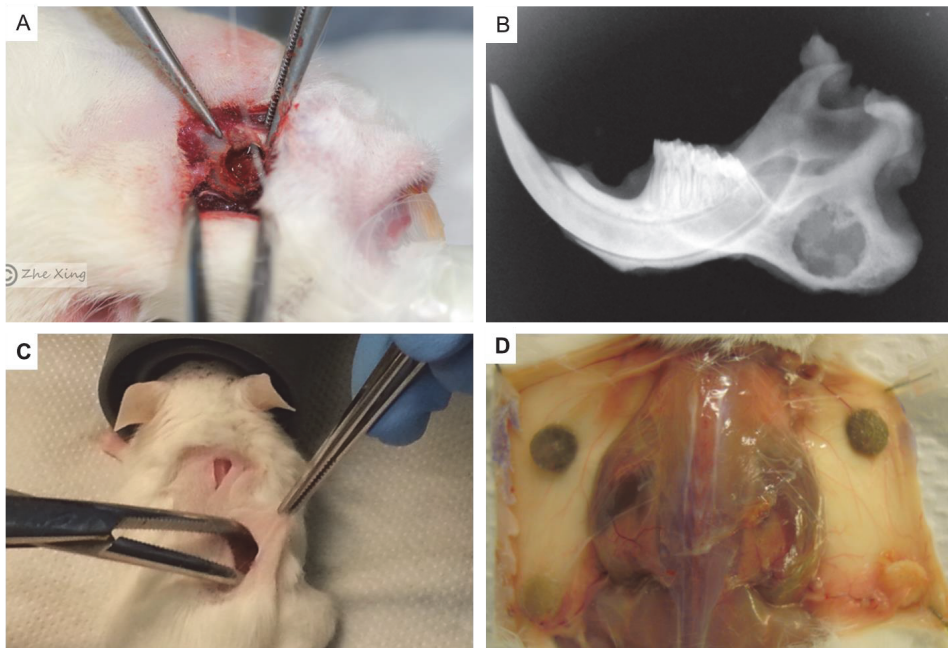


**Figure 3.4** Animal procedures to evaluate osteoinductivity and host response. **(A)** Anaesthetised rat through a custom-made mask and an incision along the lower border of the mandible showing a defect made in the mandibular angle region. **(B)** X-ray of a rat mandible showing the defect's location. **(C)** Two incisions made in the back of a mouse and scaffolds being carefully placed. **(D)** Dissection of a mouse after 1 week showing distribution of 4 scaffolds distributed in the subcutaneous scaffold implantation model.

### 3.5.2.2 *Histologic and histomorphometric analysis*

All harvested samples were fixed in 4% paraformaldehyde (PFA) before they were decalcified. Paraffin embedded sections (3-4  $\mu\text{m}$ ) were stained with Masson's Trichome to confirm the osteoid-like tissue (**Paper I**) and stained with hematoxylin-eosin (H&E) in **Paper II**. The amount of bone formation within the mandible defects (**Paper I**) was examined using micro-CT after 4 weeks (micro-CT 40, Scanco Medical AG, Bruettisellen, Switzerland). In **Paper II**, mineralised ectopic areas were evaluated within the scaffolds using micro-CT (Skyscan 1172) after 8 weeks.

Qualitative and semi-quantitative histological evaluation was carried out to assess the host response to implanted scaffolds based on the morphology of infiltrating inflammatory cells and connective tissue surrounding the scaffold area in **Paper II**. H&E sections were evaluated in six fields of vision (magnification 40 $\times$ ) using a modified scoring system (150) by two blinded examiners. The H&E sections were also visualised with an ultra-resolution imaging system (Cytoviva<sup>TM</sup> 130, Auburn USA) to identify nanodiamond particles still present in the implantation site.

## 3.6 CHEMICAL ANALYSIS OF DEGRADING SCAFFOLDS

In **Paper II** the  $M_n$  of the scaffolds degrading *in vivo*, after 1, 8 and 27 weeks, was analysed after dissolving the harvested scaffolds in chloroform.  $M_n$  were recorded by SEC on a Verotech PL-GPC 50 (Polymer Laboratories, Varian Inc., MA, USA), with a refractive index detector and two Polar-Gel-M organic SEC columns (300 $\times$ 7.5 mm) from Varian Inc. Samples were injected using chloroform and the system was calibrated against a narrow polystyrene standards. The decrease in  $M_n$  was calculated.

## 3.7 NON-INVASIVE MICROENVIRONMENTALLY-INDUCED ORAL CARCINOGENESIS: AN *IN VIVO* BLI MODEL

### 3.7.1 *In vivo* experiments

#### 3.7.1.1 *Orthotopic and ectopic cell inoculation and tumour measurements*

The tumorigenic potential of human cells in an animal can be tested only in an environment which favours tumour development, hence the need for immunodeficient animals. In this context, non-obese diabetic severe combined immunodeficient IL2rgnull (NSG) mice with multiple immunological dysfunctions provide a high engraftment level for xenografts and more rapid tumour formation and progression than less immunodeficient mice (191). The cell inoculation method in orthotopic and heterotopic sites was used in **Paper III** to assess the tumorigenic potential of DOK before and after cell transduction with luciferase and the effect of co-inoculation with CAF. This method was also used to assess the sensitivity of bioluminescence imaging (BLI) to differentiate between tumours formed by different strains of CAF.

Both DOK<sup>WT</sup> and DOK<sup>Luc</sup> were cultured and allowed to reach their log phase before they were suspended in 50 µl of growth factor reduced matrigel (BD Biosciences, San Jose, CA, USA). The cells were inoculated at two different densities, low ( $1 \times 10^3$ ) and high ( $1 \times 10^5$ ), in the tongue (**Fig. 3.5 A**) and subcutaneously in the back of 8-10 weeks old male NSG mice (University of Bergen, Norway) (n = 6 per group).

To create a positive tumour formation control as a reference,  $1 \times 10^3$  DOK<sup>WT</sup> were suspended with  $1 \times 10^5$  CAF in 50 µl matrigel and co-inoculated in the tongue (n=6 per group). To assess the sensitivity of BLI to differentiate between tumours formed by different strains of CAF, DOK<sup>Luc</sup> ( $1 \times 10^3$ ) were co-inoculated with  $1 \times 10^5$  of one of two different strains of CAF (CAF15\_13 and CAF15\_23) in the tongue (n=6 per CAF strain). The development of the tumours formed was followed manually by digital calliper (**Fig. 3.5 B**) and by BLI weekly for approx. 45 days. The tumour volumes from inoculations were calculated using the formula: Volume = [length × (width<sup>2</sup>)/2]

(192). In addition, the tumour areas were calculated from areas of interest in H&E sections using Olympus DP Soft 5.0 software (Munster, Germany).

### 3.7.1.2 Scaffold xenotransplantation subcutaneously and optical *in vivo* imaging

The scaffolds were first pre-wet with DOK medium before being seeded with DOK<sup>Luc</sup> alone or DOK<sup>Luc</sup>+CAF and then allowed to attach overnight. Three different densities of DOK were used ( $1 \times 10^3$ ), ( $1 \times 10^5$ ) and ( $1 \times 10^6$ ) in **Paper III** and in **Paper IV** the density was only ( $1 \times 10^4$ ). The density of CAF was fixed to  $1 \times 10^5$  in all experiments. The different densities were distributed among all mice ( $n = 6$ ) in **Paper III** and in **Paper IV**  $n = 6$  per each scaffold type. The same subcutaneous operating procedure as in **Section 3.5.2.1** was followed but only 2 scaffolds were implanted into each NSG mouse, one scaffold with DOK<sup>Luc</sup> alone and the other with DOK<sup>Luc</sup>+CAF. At 12 weeks (**Paper III**) or 14 weeks (**Paper IV**) animals were euthanized and scaffolds harvested.

To monitor tumour formation *in vivo* non-invasively, mice were depilated and scanned 10 min after intraperitoneal injection with 150 mg/kg of D-luciferin (Biosynth AG, Staad Switzerland) (**Fig. 3.5 C**). Images were captured using *In Vivo* MS FX PRO (Carestream Health Inc. Rochester, NY) and analysed using Carestream MI SE version 5.0.6.20. For the bioluminescent reaction to happen: the catalyst enzyme (luciferase) and the luciferase substrate (D-Luciferin) are needed. The general mechanism is the decarboxylation of the luciferin in the presence of oxygen to produce light.

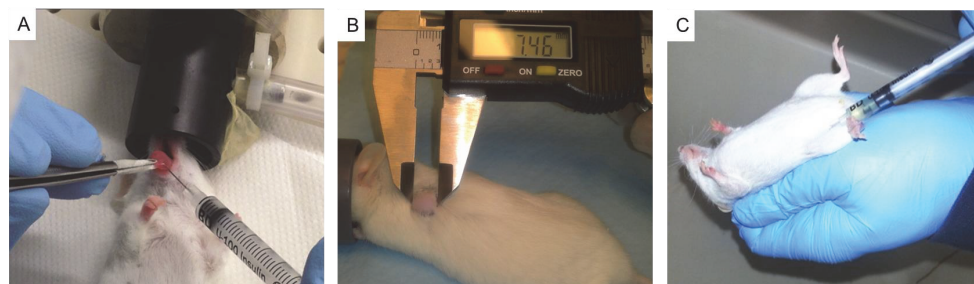


**Figure 3.5** *In vivo* cell inoculation and optical imaging. **(A)** Inoculation of DOK into the tongue of an NSG mouse under gas anaesthesia. **(B)** Manually measuring a subcutaneous tumour 8 weeks post-inoculation using a calliper. **(C)** Intraperitoneal injection of a depilated mouse with D-luciferin.

### 3.7.1.3 Immunohistochemistry of tumour xenotransplants

In **Paper III** and **IV**, 3-4  $\mu\text{m}$  paraffin sections of tumour xenotransplants were stained with H&E (Sigma). Immunostaining of xenotransplants was also performed on paraffin sections as follows (**Table 3.1**). All bound reactions were visualised using 3, 3'-diaminobenzidine tetra hydrochloride.

**Table 3.1 Immunostaining of tumour xenotransplants.**

Primary antibody	Dilution	Manufacturer	Paper
Monoclonal Mouse Anti-human p53	1:50	Dako	III
Monoclonal Mouse Anti-human Vimentin	1:1000	Dako	III
Monoclonal Mouse Anti-human Involucrin	1:500	Novocastra	IV

## 3.8 FUNCTIONAL *IN VITRO* TUMORIGENICITY ASSAYS

### 3.8.1 *In vitro* assays

In **paper IV**, DOK<sup>Luc</sup> ( $2.5 \times 10^4$  per scaffold) were cultured on 3 different scaffolds: unmodified poly(LLA-co-CL) scaffolds (*CL scaffold*), poly(LLA-co-CL) scaffolds modified with nanodiamond particles (*nDP scaffold*) and nDP scaffold plus physisorbed BMP-2 (*nDP-PHY scaffold*) for 1 week. After seeding adherent cells like DOK in copolymer scaffolds, extracting viable cells required a careful optimising procedure. Several concentrations of Trypsin/EDTA (Sigma) were used along with several initial seeding densities and culture days as well as methods of manipulating and cutting the scaffolds. The final protocol involved adding warm (0.25%) Trypsin/EDTA followed by plate vortexing for 30s followed by incubation for 5min. The plate was removed for mechanical trypsinisation before further incubation for 3min. Supernatant was removed and the trypsin was then deactivated with FCS in a separate tube to prevent clumping of cells in the scaffold. The DOK<sup>Luc</sup> trypsinised from the different scaffolds were allowed to propagate before they were subjected to the following *in vitro* functional tumorigenicity assays:

### **3.8.1.1 Transwell migration assay**

A cell's migratory and invasive behaviour is a surrogate measure, used to evaluate its tumorigenic and metastatic potential (155). Inserts (8  $\mu\text{m}$ , Corning Incorporated, NY, USA) were used in 24-well plates (Nunc, Roskilde, Denmark). The DOK<sup>Luc</sup> were allowed to migrate against one of 2 gradients; (1) high serum or (2) conditioned medium from CAF (in a 1:1 mix with fresh routine culture medium). The DOK<sup>Luc</sup> extracted from the scaffolds were re-suspended in DOK medium and seeded on top of the insert. The lower chamber contained either DOK medium with 20% FCS or conditioned medium from CAF (**Fig. 3.6 C**). After 18-20h, the cells were fixed and stained with DAPI (1:1000). Inserts were imaged to count migrated cells using a fluorescence microscope (Nikon TE 2000, Nikon, Japan).

### **3.8.1.2 Sphere formation assay**

This assay tests the ability of a cell to grow independent of anchorage, giving an understanding to its renewal potential and resistance to anoikis and hence its tumorigenic potential. Plates (48-well) were coated overnight to obtain the non-adherent surface with 1% solution of poly 2-hydroxyethyl methacrylate (Sigma) in 95% methanol. DOK<sup>Luc</sup> were seeded (500 cells per well) in 500  $\mu\text{l}$  of FAD medium + 10% matrigel (BD Biosciences). The cells were allowed to grow for 21 days and the spheres with diameter > 40  $\mu\text{m}$  were counted.

### **3.8.1.3 3D Organotypic cultures (3D-OT)**

Organotypic culture help overcome the limitations of 2D culture which lack complex microenvironment, intercellular and dynamic interactions. These models have been considered as high throughput preclinical models in tumorigenesis (193), although they are limited by a short culture span (they can only last for approx. 12 days) and the lack of vascular and immune compartments. These limitations have been compensated for here by the parallel use of *in vivo* experiments.

We attempted the reconstruction of an oral mucosa that mimics the primary tissue by co-culturing epithelial and mesenchymal (stromal) cells in a 3-D model. To assess the invasive potential of the DOK<sup>Luc</sup> extracted from the scaffolds, they were seeded on

a matrix incorporating different types of fibroblasts (GF or CAF). CAF were used as a positive control for invasion, since a previous report from our group (182) showed that an oral cancer cell line underwent deeper invasion in organotypic cultures populated with CAF compared to normal oral fibroblasts. Using a well-established protocol in our laboratory (194), the fibroblasts were seeded on prepared collagen bio-matrices (constituents described in **Paper IV**) at a final concentration of  $2.5 \times 10^5$  cells per matrix. They were incubated until the matrix solidified before adding the routine culture medium for the respective fibroblasts.

One day later, DOK<sup>Luc</sup> extracted from the scaffolds were re-suspended in DOK medium and seeded on top of the collagen bio-matrices populated with fibroblasts at a concentration of  $5 \times 10^5$  per matrix to re-construct the epithelial compartment of the 3D-OT. After 2 days of co-culture, the OT were detached and lifted on a stainless steel metal grid to keep them at an air-liquid interface and cultured in serum-free OT medium (constituents described in **Paper IV**) (**Fig. 3.6 A**). Two thirds of the medium was changed every 2<sup>nd</sup> day and the 3D-OT were harvested after 10 days of co-culture and fixed.

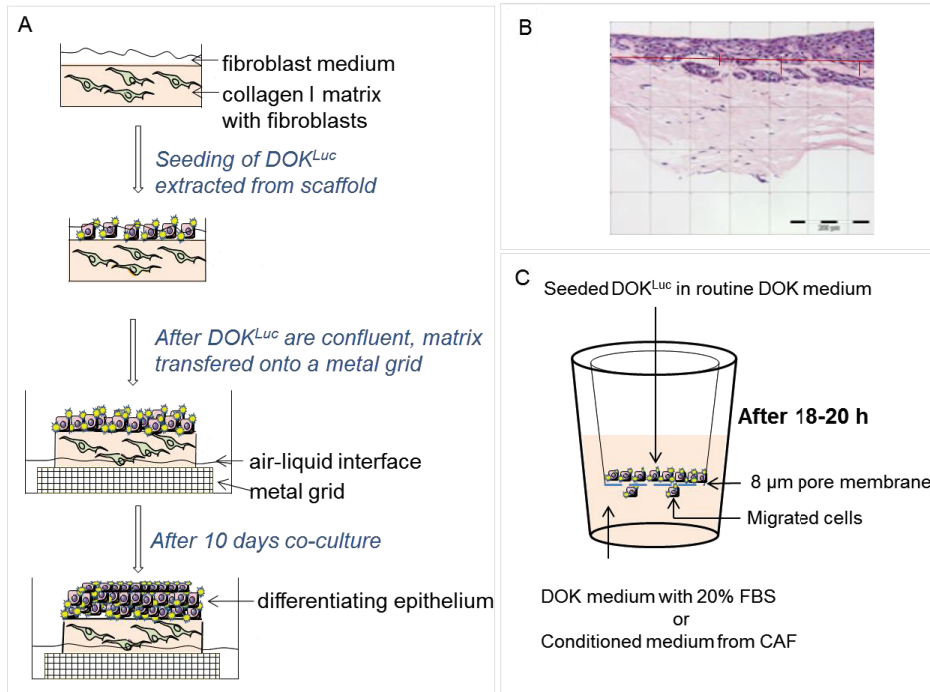


**Figure 3.6** *In vitro* functional tumorigenicity assays. (A) Schematic diagram of reconstructing oral mucosa in a 3-D organotypic culture. (B) Measuring invasion of  $DOK^{Luc}$  in the sectioned 3D-OT (red line). (C) Illustration of the transwell migration assay. Figure made using Servier Medical Art.

Preliminary tests using different seeding densities were performed to optimise the 3D-OT. In higher fibroblast densities the matrices were found to contract earlier than expected preventing the fibroblasts from multiplying and at higher DOK seeding densities, it caused rolling of the 3D-OT from the sides. The best architecture was found from 3D-OT made of GF in densities mentioned above.

#### 3.8.1.4 Histomorphometry and immunohistochemical quantification of 3D-OT

Paraffin sections of 3D-OT (3-4  $\mu m$ ) were stained with H&E (Sigma) for measuring invasion using the software Olympus DP.Soft 5.0. The sections were imaged and analysed for invasive capacity. Briefly, in the section, the central and the two outer parts of the 3D-OT were excluded because these areas were usually found to show

variable invasion since they are the focal points of the matrix handling and seeding of DOK<sup>Luc</sup>. The depth of invasion was determined every 100 µm from a line drawn through the upper remnants of the collagen bio-matrix towards the epithelium (**Fig. 3.6 B**). This line was considered to represent the original, upper level of the collagen bio-matrix and thus the basement membrane. The depth of invasion was measured from this line to the deepest point of invading DOK<sup>Luc</sup>. Two areas per section were evaluated, with 3 readings per area.

Immunostaining of 3D-OT was also performed on paraffin sections (**Table 3.2**). All bound reactions were visualised using 3, 3'-diaminobenzidine tetra hydrochloride. The open resource digital image analysis software ImageJ (v.1.46r) (National Institute of Health, USA) was used to count positively stained Ki67 cells. To quantify cells positively stained for involucrin, epithelial growth factor receptor (EGFR) and E-cadherin cells, a plug-in IHC Profiler compatible with ImageJ was used for scoring (195).

**Table 3.2 Immunostaining of 3D-OT.**

Primary antibody	Dilution	Manufacturer
Monoclonal Mouse Anti-human Ki67	1:25	Dako
Monoclonal Mouse Anti-human Involucrin	1:500	Novocastra
Monoclonal Mouse Anti-human E-cadherin	1:3000	Dako
Monoclonal Mouse Anti-human EGFR	1:1000	Dako

EGFR, epidermal growth factor receptor

### 3.9 STATISTICAL ANALYSIS

All data are presented as the mean values together with either the standard deviation or the standard error of the mean or 95% confidence interval. For Real time RT-PCR analysis (**Paper I**), the comparative Ct method ( $2^{-\Delta\Delta Ct}$ ) was used to analyse data and One-way ANOVA was used followed by a multiple comparison Tukey test. The *in vivo* data (**Paper I**) were analysed with the Kruskal–Wallis test. PCR Array data in **Paper II** were analysed using the web-based analysis software RT<sup>2</sup> Profiler PCR Array Data Analysis (v 3.5, Superarray Bioscience).

In **Papers III** and **IV**, paired t-test or the independent Mann Whitney U tests were used to compare differences between the tumours. Spearman's correlation was used to correlate the manual tumour measurements and histological measurements with corresponding BLI signals (**Paper III**). In **Paper IV**, significant difference in the sphere formation, depth of invasion between groups in 3D-OT, and significant difference in immunostaining quantification was tested using One-way ANOVA followed by a multiple comparison Tukey test. SPSS ver. 21/22 (IBM, NY, USA) was used for the evaluation and the level of significance was set to  $p < 0.05$ .

### **3.10 ETHICAL STATEMENT**

All animal experiments were approved by the Norwegian Animal Research Authority and conducted in strict accordance with the European Convention for the Protection of Vertebrates used for Scientific Purposes (FOTS nos. 2012/4178, 2013/5042, 2013/4643, 2012/3961 and 2013/5297). All animals were anaesthetised with isoflurane (IsobaVet®; Schering-Plough, Kenilworth, NJ, USA) combined with O<sub>2</sub> and were euthanized with an overdose of CO<sub>2</sub>. The ethical approvals for OSCC patient samples and individuals undergoing third molar extraction samples were obtained from the Regional Committee for Medical and Health Research Ethics (REK # 2010/48 and REK Vest# 177.04). The samples were collected following an informed consent of the patients.

## 4. MAIN RESULTS AND GENERAL DISCUSSION

### 4.1 OSTEOINDUCTIVITY

#### 4.1.1 Osteogenic potential of a controlled, sustained release of BMP-2

In **Paper I**, we investigated how the release and bioactivity of BMP-2 from copolymer scaffolds are affected by binding techniques. Four different functionalising techniques were used to immobilise a low dose of 1  $\mu\text{g}$  rhBMP-2 on recently developed poly (LLA-co-CL) scaffolds. BMP-2 was either (i) physisorbed onto unmodified scaffolds (PHY), (ii) physisorbed onto scaffolds modified with nDP (nDP-PHY), (iii) covalently linked onto nDPs that were used to modify the scaffolds (nDP-COV) or (iv) entrapped in microspheres distributed on the scaffolds (MICS).

BMP-2 administered in excess amounts in order to efficiently repair bone creates undesirable side effects which limits its therapeutic use (92, 94). In a clinical trial of alveolar cleft palates in children the high concentrations of BMP-2 delivered resulted in a significant amount of severe unwanted postoperative swelling (91). Furthermore, studies emphasised the necessity of using a controlled, sustained release of BMP-2 within physiological and therapeutic limits for clinical success (196, 197). Hence it was fundamental to understand the release kinetics of the loaded BMP-2, before further bioactivity evaluations were initiated. The SRM method used was able to detect released quantities from the different scaffolds producing a release curve (**Fig. 4.1**).

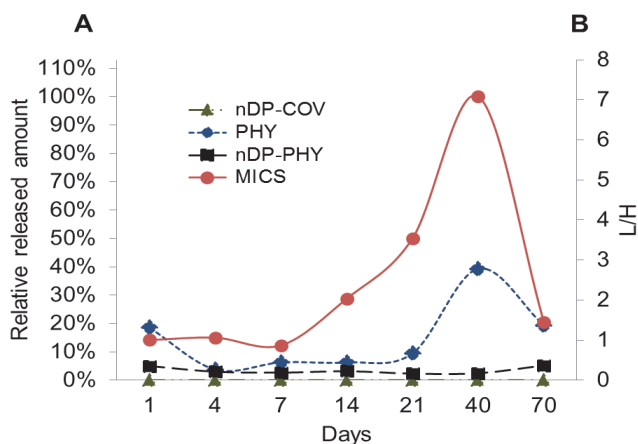


**Figure 4.1 Release profile of BMP-2 from different scaffolds.** Axis-(A) Relative amount released where 100% value corresponds to the highest value observed for the total amount of BMP-2 measured at a specific time point. Axis-(B) Release over time of BMP-2 from the different scaffolds expressed by the ratio (L/H) between endogenous light (L) and heavy synthetic (H) peptide spiked-in our sample. Figure reprinted with permission from Elsevier Ltd. (**Paper I**).

The early time points gave a vivid depiction of the variation between the different modes of binding; the PHY scaffolds showed an initial burst of release followed by a drop and MICS showed a higher level of release starting at 24 h (compared to nDP-COV and nDP-PHY scaffolds) and remained steady up to 7 days only. Passively adsorbed BMP-2, such as on the PHY scaffold, is the easiest way to load growth factors onto a carrier since it simply requires immersion in protein solution but has the disadvantages of uncontrolled release and short release duration caused by the burst release. This mode of delivery can be used when delivering multiple growth factors and wanting to tailor release onsets; i.e. wanting to initiate vascularisation first by a spurt of VEGF before commencing prolonged osteogenesis (198). This can be needed in cases where vascularisation is impaired, for example due to radiation therapy. However, for our purpose (**Paper I**) a prolonged controlled delivery of growth factors might be the best option since it promotes healing coordinated with the normal physiological expressions of these factors. It has also been proposed that the ideal pharmacokinetics for BMP-2 should include an initial burst first to recruit

osteoprogenitor cells followed by sustained release to induce osteogenesis (199). Studies have shown burst followed by a sustained release of BMP-2 regenerated 50% more new bone than a collagen sponge loaded with BMP-2, whereas a sustained release without the burst did not enhance bone more than a scaffold without BMP-2 (199). It seems reasonable that the delivery of BMP-2 ought to be based on the normal physiological microenvironment of bone, where it is an extended dynamic process. This would necessitate maintaining protein bioactivity in the carrier for a sustained release. The ideal time point of BMP-2 delivery has not been elucidated yet, but the increased expressions at 1 and 21 days after injury is remarkably useful (58, 96, 200). Several studies explored the spatiotemporal effect of BMP-2 delivery; some suggested that BMP-2 plays an important role in osteoinduction, especially at the early stages (201). However, there is evidence suggesting that sustained delivery of BMP-2 enhances bone formation, attributed to its effect on a larger population of osteoprogenitor cells at the fracture site at later stages following injury (197).

In comparison to the MICS scaffolds, the PHY scaffolds showed a smaller increase in release between days 21 and 40 than that seen from MICS, probably attributed to degradation of the scaffold and/or microspheres and liberating the low amounts entrapped (37). The difference seen between MIC and PHY scaffolds in amounts released suggests that perhaps not all the BMP-2 added to PHY scaffolds was able to be adsorbed. The nDP-PHY was seen to have a controlled release sustained in comparable low amounts compared to the other groups until the termination of the *in vitro* release experiment. In a rat tibia osteotomy model, sustained BMP-2 delivery resulted in enhanced mineralised bone healing and biomechanical properties at 84 days compared to BMP-2 delivered at much higher amounts released in a burst fashion (202). Also in line, a larger animal model showed efficient bone healing when using a slow sustained release of BMP-2 (203). In nDP-PHY, BMP-2 was strongly bound to the nDP, since protein interactions with nDP are known to be relatively strong (204) (discussed further in **Section 4.1.2**).

ALP expression is an early differentiation marker of the osteoblast phenotype and studies often test bioactivity of BTE scaffolds using ALP expression from cells in the osteoblastic lineage, considering it a robust cytochemical marker for mineralisation (205). Our findings of increased ALP mRNA *in vitro* at 3 weeks from cells on nDP-PHY scaffolds in **Paper I** are in line with the significant increase in ALP mRNA expression ( $p = 0.014$ ) from the first week for nDP-PHY implanted subcutaneously compared to nDP and CL scaffolds in **Paper II**. Osteosarcoma cells cultured on BMP-2 treated O-NCD implant surfaces were reported to significantly increase ALP activity in less than 2 weeks of culture (119). Another study showed polyester carriers with hydroxyl terminals similar to those terminating nanodiamond particles used here promoted increased ALP activity in differentiating osteogenic cells (206). However, in **Paper I**, *in vivo* significance for ALP mRNA at 2 weeks was only demonstrated from MICS scaffolds compared to other osteogenic markers, but micro-CT and histology supported the interpretations and conclusions related to the comparable osteogenic potential of MIC, nDP-PHY and PHY scaffolds. The bioactive BMP-2 might have caused the recruitment of osteogenic progenitor cells from the local circulation, leading to the pronounced ectopic mineralisation in nDP-PHY scaffolds (**Paper II**) and de novo bone formation in the critical-sized mandible defect (**Paper I**). Previous reports have shown that a controlled local concentration of BMP-2 modifies the recruitment of osteogenic progenitor cells and regulates the formation of bone (207).

mRNA of the potent osteogenic markers osteocalcin and BMP-2, was highly expressed from MSC grown on nDP-PHY and MICS scaffolds at week 1 and week 3 *in vitro* and at week 2 *in vivo*, implying increased osteogenic potential in comparison to that seen from PHY scaffolds (**Paper I**). Confirmed by the *in vitro* mineralisation assay, nDP-PHY and MICS scaffolds demonstrated vast extracellular dark spots evident of calcium deposits in the matrix produced by seeded MSC while on PHY scaffolds which showed less extracellular matrix staining indicating lack of sustained mineralisation. Corroborating to this pattern in PHY scaffolds are the high levels of mRNA collagen type I, an early marker of bone formation, produced by cells in the PHY group *in vitro* as well as *in vivo* in **Paper I**. Release as a burst from PHY was

perhaps above therapeutic threshold, and then rapidly declined to levels that were too low for effective mineralisation.

The data from **Paper I** confirmed that nDP-PHY and MICS scaffolds showed both *in vitro* and *in vivo* evidence that a more controlled release is needed to induce a commitment to bone phenotype. Furthermore, the amounts released from nDP-PHY scaffolds were far less than from MIC, and release continued until 70 days with bioactivity also displayed in an ectopic model (**Paper II**).

#### 4.1.2 Effects of nanodiamond particles on the scaffold's osteogenic potential

Nanodiamonds are known to amplify surface areas due to their size, providing chances of surface functionality in addition to their biocompatibility, rigidity and chemical stability (115). The nanodiamond particles used to modify the poly(LLA-co-CL) scaffolds in this work increased hydrophilicity of the scaffold material via the previously described increased oxygen-containing groups which also facilitate strong binding of organic groups (114). Unpublished data from optimising experiments demonstrated a reduction from 119° contact angle on pure Teflon to almost <10° when modified with nDP. Poly(LLA-co-CL) scaffolds modified with nDP terminated with oxygen-containing groups produced composites that are not only mechanically reinforced (52) but also enhanced hydrophilicity and thus cellular responses and *de novo* bone formation in a sheep defect (54). Another study using titanium implant surfaces coated with O-NCD and physisorbed BMP-2 demonstrated enhanced bone to implant contact ratio which was not entirely due to the activity of BMP-2 since O-NCD implants on their own, still improved healing when comparing the results (120). The nDP scaffolds without BMP-2 (**Paper II**) also showed enhanced osteogenic potential and this was in line with recent reports that showed cultivated osteoblast-like cells in O-NCD films exhibited a higher growth rate compared to hydrogen-terminated NCD, and supported more deposition of ECM proteins and ECM mineralisation (208). A study exploiting functionalised monolayers containing various surface chemistries demonstrated that the hydrophilic monolayers selectively permit osteoblastic differentiation, inhibiting adipocytic differentiation, while the positively charged

monolayers supported both adipocytic and osteoblastic differentiation (209). The osteoconductivity demonstrated by our data can also be attributed to the difference in surface charge in the modified scaffolds that caused wettability, that in return modulates the absorption of cell adhesion molecules and proteins from the surrounding fluids *in vivo* (210, 211). O-NCD coating titanium implants bound BMP-2 physically by electrostatic interactions, van der Waals forces and hydrogen bonds (119), supporting the contention that nanodiamonds in nDP-PHY scaffolds express similar properties and bind BMP-2 by increasing the magnitude of the electrostatic interactions between BMP-2 and the scaffold, which in turn decrease the initial burst release.

Several drug delivery systems have been reported that take advantage of the unique nDP electrostatic surfaces, daunorubicin (anti-cancer drug), for instance, has been reversibly bound to nDP, providing a sustained and steady release profile *in vitro* and *in vivo* (212). The nDP conjugate (212) improved drug maintenance in target cells along with treatment safety. Acidic pH was found to be a trigger for the anti-cancer drug's release from nDP and also shown to affect the release in another study where BMP-2 was delivered from nDP in suspension (122). In our release profile we demonstrated a slight increase in release kinetics from nDP-PHY scaffolds at day 40 and this correlates with increase in the scaffold degradation (37) and the subsequent acidic environment may be caused by polymer hydrolysis.

In addition to the results of **Paper I** discussed above, osteoconductivity from nDP modified scaffolds was further shown in a mouse ectopic model (**Paper II**) by virtue of mRNA levels of selected osteogenic markers. At week 1 nDP and nDP-PHY scaffolds expressed upregulated trends of osteogenic markers (such as RUNX2, Collagen type I $\alpha$ 2, Collagen type I $\alpha$ 1, BMP-2) compared to the unmodified scaffolds, CL. The effect of nDP modification was also underlined after physisorbing BMP-2 in this study. These osteogenic markers were more upregulated in nDP-PHY compared to the other two groups. In **Paper II**, BMP-2 receptors and transcripts' activation in the host showed that the mRNA levels of BMPRIA and RUNX2 were upregulated in the nDP-PHY scaffold group at week 1, demonstrating conserved bioactivity of the

physisorbed BMP-2 and indicating activation of the BMP signalling pathway and a consequent increase of osteogenicity (213).

With regards to the nDP functionalising in nDP-COV (**Paper I**), this modification was not as successful as the nDP-PHY scaffolds. No BMP-2 release was detected during the course of the *in vitro* release experiment. Furthermore, reduced osteogenic potential both *in vitro* and *in vivo* was observed. This can be attributed to increased strength of the covalent immobilisation of the protein on the diamond surface, as was previously reported with enzymes (214). The loss of the BMP-2 functionality might also indicate that the protein was deformed during binding onto the nanodiamond surface by the covalent linker or the BMP-2 denatured during scaffold sterilisation, which had to take place after functionalising. BMP-2 engineered to irreversibly bind to titanium did not induce osteogenic gene expression in C2C12 cells compared to BMP-2 that were reversibly bound to titanium surfaces (215). Nonetheless, nDP-COV can be improved to be a good modality for immobilising molecules that do not require release, for example adhesion molecules (216). In such circumstances, controlled release of adhesion molecules can be considered as the controlled provision of a bioactive molecule in its most appropriate state, not necessarily in a diffusible state.

#### **4.1.3 Importance of a controlled release of BMP-2 in low amounts**

Our release profiles from MICS and PHY scaffolds in **Paper I** showed a starting higher release followed by a sustained release but this soon increased again to very high levels compared to other scaffolds. The FDA approved BMP-2 carrier Infuse<sup>®</sup> delivers BMP-2 from an absorbable collagen sponge and shows a burst release profile, and complications have been reported due to uncontrolled release of high amounts (89). Reports underscored the importance of decreasing the dose of BMP-2 to the lowest level that is compatible with the desired degree of bone formation (217). Cells with osteogenic potential can be recruited and differentiated at low doses. In addition, the rapid release of BMP-2 may result in transient osteoclast-mediated resorption of newly formed bone whereas osteoclasts are transiently activated at high doses of BMP-2 (218). This was seen with the significantly increased *in vivo* expression of

tartrate-resistant acid phosphatase (TRAP) and Cathepsin K (CTSK) in the MICS scaffolds followed by a high trend in PHY scaffolds for TRAP, which could cause resorption of bone before its maturation (**Paper I**). Another *in vivo* study using the rat femoral segmental defect model indicated that an increased concentration of BMP-2 above a certain threshold did not improve bone healing and could actually promote lower bone quality with an abnormal structure and potentially inferior mechanical properties (219). It has been reported that high concentrations significantly inhibited Wnt signalling pathway activity by a dramatic increase in released inhibitory proteins that lead to potential toxicity and side effects such as decreased human periosteal cell proliferation and induced apoptosis (220).

There is a large disparity in BMP-2 concentration between clinical and experimental use, with clinical trials using high doses of at least 1 mg BMP-2 per ml, and higher doses of BMP-2 mask differences in bone regeneration, as we have observed for different release profiles. The dose used in the present thesis, 1  $\mu$ g, falls in the lower range used for osteogenic threshold in rodents with similar defects (221). However, it is important to be careful when extrapolating results across different animal models and sites. The protein on nDP-PHY was bioactive with comparable efficacy to MICS *in vitro* and *in vivo* despite being strongly bound to the carrier, holding greater promise compared to growth factors adsorbed onto a polymer in the PHY scaffolds. The osteogenicity observed *in vivo* with PHY scaffolds compared to other groups in **Paper I** is intriguing despite its burst release, but the current inability to control burst release within the therapeutic window makes us favour a more controlled sustained release of low amounts.

Taken together from the data in **Papers I** and **II** of osteogenic importance, nDP modification of the poly(LLA-co-CL) scaffolds was found to enhance osteoconductivity. nDP modification also provided a platform for binding BMP-2 strongly, allowing its sustained release in low amounts and rendering the scaffold osteoinductive. These attributes suggest they may provide ideal growth factor carrier characteristics and lead to further investigations into the characteristics of this scaffold

and mode of BMP-2 delivery, including evaluating the host response during degradation as described below.

## 4.2 DEGRADABILITY

### 4.2.1 Degradation of functionalised poly(LLA-co-CL) scaffolds

The degradation profile of unmodified poly(LLA-co-CL) porous scaffolds with similar compositions to those used in this work has been evaluated previously (37). In **Paper II** the effect on degradation of modifying these scaffolds with nDP or nDP and BMP-2 was evaluated up to 6 months. Greater molecular weight loss was observed from the nDP and nDP-PHY scaffolds than from the CL scaffolds at time points 1, 8 and 27 weeks. The data showed that after 27 weeks, all three scaffolds lost almost 90% of molecular weight. Hydrolysis is the main mechanism for the degradation of these synthetic polymers, where the speed and amount of water capable of diffusing throughout the polymer determines the degradation rate. The nDP used to modify our scaffolds has been shown previously to increase hydrophilicity due to the hydroxylated surfaces, thus absorbing water (115). A more hydrophobic scaffold, such as CL scaffold, will make it difficult for water to be absorbed. This promotion of hydrolysis may have increased polymer degradation seen in nDP and nDP-PHY scaffolds relative to unmodified counterparts at weeks 1 and 8. It has been reported that incorporating hydrophilic bioactive fillers such as TCP into hydrophobic polymers caused the composite PCL/TCP scaffolds to degrade faster than PCL homopolymer scaffolds in a 6 months rabbit model. This acceleration in degradation is owed to the increase in water diffusion into the composite bulk (222).

Increased water diffusion into the nDP modified scaffolds may have promoted a bulk pattern of erosion. In bulk erosion, the polymer chain scission occurs throughout the scaffold in the amorphous part of the polymer, thus although it does not change much in external dimensions, the molecular weight decreases early. This was seen in the macroscopic pictures (**Paper II**) of the harvested scaffolds after 8 and 27 weeks where the nDP and nDP-PHY scaffolds were physically present but showed considerably thinner and translucent areas in the centre. The decrease in  $M_n$  from the

first week in these scaffold groups compared to CL also reflects their bulk degradation. Our data demonstrated that after 2 months almost 60% of  $M_n$  of unmodified scaffolds decreased and previously reported data (37) demonstrated that these same scaffolds implanted into rat calvaria decreased around 70% of the molecular weight after 91 days. Hence a comparable rate of degradation is appreciated although the implantation site and size of the animal were different. Mechanical properties were outside the scope of this paper but they would have added complementary information to the degradation characteristics of the modified scaffolds.

Tissue response also plays a role in *in vivo* degradation. The nDP modified scaffolds exerted an upregulated inflammatory response at the mRNA level (**Section 4.3.1**) relative to the CL scaffolds, suggesting the presence of the early stage ROS, which has been reported to degrade polymers. The ROS induce migration of inflammatory cells that can oxidise polymer chains (199). Previous studies reported that relatively delayed degradation of a biomaterial enhances biocompatibility, reducing the inflammatory cells infiltration (150). However, this was not the case in **Paper II**, where it is more likely the result of nDP and BMP-2 additions.

## 4.3 HOST RESPONSE

### 4.3.1 Inflammatory response

Bone regeneration after scaffold implantation starts with an inflammatory reaction that initiates the healing process, but chronic persisting inflammation or lack of initial/acute inflammation affects the process of regeneration (223). Thus, when evaluating host response it is important to discriminate between the short-lived inflammation that is a normal component of the healing response and a long-term, persistent chronic inflammation that may indicate an adverse response such as tumorigenesis. A shortcoming of **Paper II** design was the absence of a sham surgical control. Another study comparing the immune response towards different scaffold carriers concluded that the implantation of scaffolds itself caused tissue injury that intensified immune response (224). Thus it might be either important to deliver the

tissue-engineered construct as non-invasively as possible or to include a sham control in order to avoid overlooking any immunological responses to implantation itself. However, in **Paper II** the initial inflammatory response between the scaffolds groups differed, which is more likely to be related to the modifications than to the surgical injury.

In **Paper II**, proinflammatory markers at the mRNA level displayed a gradual decrease with time from week 1 to week 8 in all groups, with the highest week 1 expressions being from the nDP scaffolds followed by nDP-PHY scaffolds. The mRNA level of tissue healing markers showed almost the reverse pattern, with the up-regulation at week 8. Here too, the greatest expression was from nDP and nDP-PHY scaffolds. The early upregulated proinflammatory expressions from nDP scaffolds can be attributed to nano-scale particles that have been shown to induce a low to intermediate amount of oxidative stress from the generation of ROS (225). This might induce proinflammatory responses, which here were initiation of a regeneration or healing phase. Previous reports showed similar patterns *in vitro* where adherent monocytes on hydrophilic polymers expressed higher amounts of proinflammatory cytokines such as IL-1 $\beta$  and IL-6 than cells from corresponding hydrophobic polymers detected at protein level up to 10 days (226, 227). It has been shown that there were fewer cells and minimal FBGC formation on the hydrophilic/neutral surface but these adherent cells demonstrated greater levels of activation and produced significantly greater amounts of cytokines/chemokines tested than the other surfaces (226). This is in agreement with the upregulated proinflammatory mRNA expressions, such as TNF $\alpha$ , IL-1 $\beta$ , Chemokine C-C motif ligand 5 (CCL5), CCL12 and IL6 seen here at week 1 from the implanted nDP scaffolds followed by nDP-PHY scaffolds, which have been previously shown to be hydrophilic, again supporting the idea that material surface chemistry is a factor in modulating the phenotypic expression of FBR cells.

Histologically, the presence of inflammatory cells and FBGC was more prominent in the CL scaffold group than in the nDP and nDP-PHY scaffolds, except that at 8 weeks more lymphocytes were present in nDP-PHY scaffolds (**Paper II**). Hydrophilic surfaces have also been reported to show reduced adhesion of monocytes and

macrophages and a reduced amount of macrophage fusion into FBGC (226, 228), which may explain the reduced number of inflammatory cells or FBGC on nDP modified scaffolds. It was reported that hydrophilic surfaces promote the apoptosis of biomaterial adherent FBGC and the authors proposed that inducing apoptosis in the adherent FBGC would reduce the negative effects and improve tissue remodelling (229).

The reason for the persistent presence of FBGC around a scaffold or a degradable implant in general has been an area of controversy. It has been considered as an indication of foreign bodies with lack of biocompatibility and inflammation or a sign of degradation leading to regeneration. Another postulation is the faster degradation of the modified scaffolds and hence less number of FBGC required or observed at the certain time point (140, 147). Also, hydrophilic titanium surfaces decreased macrophage immune response and reduced FBGC formation by promoting the polarisation of macrophages towards a pro-healing phenotype via (Nuclear factor) NF-kappaB signalling (230). A recent study showed that it is not only chemistry by itself, but selective adsorption of proteins by different surfaces and ligand orientation could account for observed differences in FBR and have a potential to modulate immune response and macrophage polarisation from pro to anti-inflammatory (227, 231).

Moreover, fibrous capsule formation as a result of extended inflammation may impair the capacity of the scaffolds to degrade in the intended manner or to promote tissue regeneration. The reduction in the fibrous capsule thickness and the chronic inflammatory cells' infiltrate after 8 weeks in nDP and nDP-PHY scaffolds suggests the good compatibility of these scaffolds. Previous reports demonstrated the attenuation of inflammation by the slow release of BMP-2 from polymeric scaffolds (151). The efficacy of the BMP-2-functionalised scaffolds in reducing the fibrous capsule and the FBR has also been attributed to the initiation of the formation of ectopic bone in this group (147); therefore, homing of endogenous MSC (64) may also be involved, since MSC have been shown to demonstrate immunomodulatory and immunosuppressive effects (232). The nDP and nDP-PHY scaffolds showed superior osteogenic potential as described earlier and higher proinflammatory markers (TNF- $\alpha$

and IL-6) at week 1, although the inflammatory cellular infiltrate was less in these groups than in CL. The cytokines TNF- $\alpha$ , IL-6 and stromal cell-derived factor 1 have been associated with migration of MSC *in vivo* (233) and mice deficient in IL6 have shown compromised bone regeneration (234). While TNF $\alpha$  is generally considered to be a proinflammatory cytokine, it also has confirmed important roles in bone by promoting vascularisation and recruitment of osteogenic cells; however, persistent upregulation of TNF $\alpha$  negatively affects the bone (235, 236). Exaggerated inflammatory environments decreased induced bone mass *in vivo* after implanting a scaffold carrying BMP-2, by suppressing BMP-2-induced osteoblastic differentiation and by increasing the number or activity of osteoclasts (237). This highlights the concept that immune cells and inflammatory cytokines play an important role in the bone healing process and are required from its initiation, but over a prolonged period can have adverse effects.

The relatively avascular fibrous capsule that encapsulates foreign bodies limits its interaction with the host tissue and the subcutaneous area is relatively lacking in circulation (238), which is a challenge for tissue regeneration after scaffold implantation. Angiogenesis is perceived as being able to reduce fibrous capsule formation (239). Levels of angiogenic markers' mRNA (ANGPT1 and FGF2) were significantly upregulated in nDP and nDP -PHY scaffolds at week 1 compared to CL. Previous reports have shown the hydrophilic surface in O-NCD titanium implants to enhance vascularisation when implanted subcutaneously in rats, in addition to decreasing the inflammatory response (211). This may explain the reduction in the fibrous capsule thickness in these groups at 27 weeks.

As time progressed, the level of proinflammatory cytokines reduced, and higher levels of healing/regenerating marker (IL-4) showed higher trends in nDP scaffolds at 1 week and were significantly higher in nDP-PHY scaffolds at 8 weeks. These levels may play a role in macrophage fusion, suppression of inflammatory responses during the FBR and leading to a healing phase (240). In a study of ectopic bone induction by demineralised xenogenic bone matrix, the expression of angiogenic markers were affected by deficiency of IL-4 and IL-13 (241). The observed increase in expression of

IL-4 in nDP and nDP-PHY scaffolds is in agreement with the enhanced angiogenic markers and resolved FBR. It has also been reported that IL-4 and IL-13 positively influence the migration of osteoblastic cells (242). The role of BMP-2 as a chemoattractant and angiogenic factor, recruiting endothelial cells has also been displayed in studies *in vitro* (243). This highlights the interdependence of inflammation, angiogenesis, and tissue regeneration, and the necessity of immunomodulation to prevent impaired regeneration.

To conclude, this demonstrates the osteoconductivity and osteoinductivity of nDP and nDP -PHY scaffolds respectively in **Paper II**. nDP and nDP-PHY modification of scaffolds offer the prospect of modulating cellular activation and cytokine profiles that may provide a means to control or manipulate inflammation, the foreign body reaction, and ultimately biocompatibility and regeneration.

#### **4.3.2 Persistence of nanodiamond particles at the implantation site**

The presence of nanodiamond particles in the implantation site of the scaffolds at week 27 indicated that the particles stayed in the tissue even after almost 90% of the scaffold has degraded without eliciting side effects (**Paper II**). It can be postulated that the acidic environment created from the by-products of the polymer scaffold degradation led to the agglomeration of the particles, which immobilised them and thus were not able to distribute in cells or elicit nano-scale side effects (244). One must therefore be careful when considering this copolymer/nDP scaffold construct degradable. Thus, this motivated our following evaluations of long-term tumorigenicity (**Paper IV**). nDP is a factor determining the host tissue response towards the functionalised scaffold. The host response to nDP as a construct with a polymer scaffold/carrier *in vivo* has limited reports in the literature. Investigations on the cytotoxicity and genotoxicity of nDP in suspension have been commonly carried out by exposing cells to the particles in suspensions or by growing the cells on nanodiamond coated substrates/scaffolds (53). Results were controversial, most studies concluded that they do not alter cellular proliferation and that they have no obvious

cytotoxic effects (245), but others revealed size and concentration dependence on macrophages (246).

*In vivo* assessments, more relevant to our current study, injected nDP into the peritoneum, and into the tail vein to study their biocompatibility, distribution and fate. Most of them reported absence to minimal inflammatory responses with slightly elevated blood indices in rabbits after intravenous administration (247). Previous reports reported them to accumulate mostly in the liver, followed to a lesser extent by the lungs and some traces detected around other organs such as the brain, bone, muscle, stomach and intestines after intravenous administration in mice (248). The observation of nDP remaining in the implantation site after 27 weeks was accompanied with no macroscopic adverse effects in **Paper II**. However, harvesting organs to monitor distribution, if any, may have added information. Preliminary unpublished data from our laboratory have shown the highest tolerated dose of nDP (3 times higher than what is added in a scaffold) suspended in glucose and injected intravenously in rats did not affect the haematological profile.

### 4.3.3 Tumorigenicity

The scaffold construct and its degradation products should not have any potential adverse systemic effects including carcinogenicity. Since the nDP and nDP-PHY scaffolds elicited inflammatory responses that initiated bone formation or foreign body reactions and the nanodiamond particles do not degrade, it was necessary to carry out long-term biocompatibility evaluations, such as the tumorigenic potential.

#### 4.3.3.1 Developing an non-invasive carcinogenicity testing model *in vivo*

The selection and relevance of DOK as a ‘screening sensor’ in this developed model has been discussed in **Section 3.3.1.3.1**. To achieve real-time BLI and facilitate non-invasive visualisation after xenotransplantation, DOK cells were transduced with the luciferase gene, successfully generating a new cell line, DOK<sup>Luc</sup> (**Paper III**). DOK<sup>Luc</sup> retained comparable morphology, growth *in vitro*, and *in vivo* behaviour after inoculation in mice compared to DOK<sup>WT</sup>. Introducing viral vectors into primary cells or cell lines carries many risks, including the risk of causing phenotypic variations

(249). After transduction, DOK demonstrated bioluminescent stability together with preservation of the phenotype, proving thus to be a valuable tool for screening tumorigenesis and ruled out the possibility that transduction can be the cause of tumour formation in **Papers III** and **IV**.

Manual measurement of the size of tumours formed by both DOK<sup>Luc</sup> and DOK<sup>WT</sup> showed that when injected in the tongue of NSG mice at high density, bigger tumours resulted than when low density was used at all time points (6 weeks). The tumour area measured from the histological sections after 6 weeks was also bigger when high density inoculation was used. The growth of DOK *in vitro* depends on seeding density; in an orthotopic site (tongue) this phenomenon would be expected due to the favourable surrounding environment (250). Similar *in vivo* growth curves were observed in the tongue between DOK<sup>Luc</sup> and DOK<sup>WT</sup> with low density inoculations. However, in the skin, an ectopic site for the DOK, tumours were only formed by the high density inoculation, possibly due to the injection technique or the site.

In addition to the manual measurement by digital calliper for 6 weeks, tumour volumes formed by skin and tongue inoculations were also measured weekly by BLI for the DOK<sup>Luc</sup> group only. The BLI signals were always significantly higher ( $p < 0.01$ ) for the inoculations of DOK<sup>Luc</sup> at higher density at both tongue and skin, in line with the tumour growth curve as assessed by manual measurements. BLI proved sensitivity and validity during detection of tumours formed by DOK<sup>Luc</sup> inoculations, where 50% of the total number of tumours formed in the tongue by DOK<sup>Luc</sup> was detected by BLI much earlier than manual detection, even by the first week. Therefore, the detection of tumours was consistent between manual and BLI measurements, but BLI detection of tumours was more sensitive than manual measurement. In the skin more than 85% of the tumours were visible by BLI from the first week.

BLI is performed in darkness with no interference from background light or autofluorescence, which makes it possible to detect small tumours. A study comparing the sensitivity of BLI with another non-invasive optical imaging modality, fluorescence, suggested that BLI was more sensitive due to the lower background

(251). One of the tumours detected by BLI in **Paper III**, which was from a low density inoculation, was not detected by manual detection but was confirmed histologically. A stronger significant correlation ( $r = 0.846$ ,  $p < 0.001$ ) was found between the tumour area from histological sections and BLI signals at the last time point than between the tumour area from histological sections and the manual measurement ( $r = 0.739$ ,  $p < 0.001$ ). Previous reports developing a model for a brain tumour also showed correlation and validation of BLI with MRI, a more established method for that tumour, and their results also corresponded with histology (252).

Important for this screening model using DOK, was the inclusion of a positive control as a reference or guideline. The duration of the screening and the end point were set based on this positive control. Previous work has shown the significant role of microenvironmental cues, specifically CAF, in tumour progression (182, 253). In line with these findings, our data showed that co-inoculating DOK<sup>WT</sup> with  $1 \times 10^5$  CAF in the tongues of NSG mice significantly increased tumour incidence by 40.48% and the tumours showed typical OSCC histology with invasive epithelial islands growing in the host stroma and keratin pearl formation. The only considered tumour formed here by the DOK<sup>WT</sup>, detected only manually, was found histologically to be surviving DOK<sup>WT</sup> cells within remnants of undissolved matrigel underscoring the drawbacks of manual measurements that include subjective evaluations. The sensitivity of the BLI was again confirmed when DOK<sup>Luc</sup> was co-inoculated with two different types of CAF and their effect on tumour formation compared. BLI seemed to be more sensitive than manual measurement in detecting differences in the tumour growth of xenografts, although not statistically significant.

#### ***4.3.3.2 Using the newly established model to test tumorigenicity of scaffolds***

DOK<sup>Luc</sup> were cultured on unmodified poly(LLA-co-CL) scaffolds at three different densities with or without CAF and implanted subcutaneously in NSG mice. BLI showed significantly higher intensity from scaffolds xenotransplanted with DOK<sup>Luc</sup> + CAF compared to DOK<sup>Luc</sup> alone at all densities throughout the 12 weeks of *in vivo* imaging ( $1 \times 10^6$ :  $p < 0.001$ ,  $1 \times 10^5$ :  $p < 0.001$ ,  $1 \times 10^3$ :  $p = 0.017$ ). A challenge for using BLI method would be monitoring of bigger tumours. We monitored a drop in intensity

for a tumour developed from the highest seeding density of DOK<sup>Luc</sup> + CAF xenografts. This tumour was found to be cystic, thus we considered this drop to be an underestimation of the real BLI signal from the DOK<sup>Luc</sup> cells. The formation of bioluminescence requires the coenzyme adenosine triphosphate and therefore only metabolically active cells can produce it. Cystic content can occur in large tumours, reducing the overall signal due to decreased proliferation or hypoxia (252). Oxyhemoglobin and deoxyhemoglobin in the bloody content of the tumour might also absorb light output in the visible spectrum, reducing the signal output.

In a study of orthotopic bladder xenografts correlating BLI with MRI results of tumour volume to determine the role of hypoxia and necrosis, they found the correlation to be variable and reduced in xenografts that got too large for their vascularisation (254). Another study found that changes in hypoxic conditions affected the reported BLI by affecting tumour cell growth (255). Thus it may be challenging to use the BLI method for monitoring bigger tumours. To circumvent these limitations and monitor tumour formation for longer period of times, a relatively smaller number of DOK<sup>Luc</sup> ( $1 \times 10^4$ ) cells were used to test functionalised scaffolds (**Paper IV**). Several studies investigated the sensitivity of BLI in different tumour models using different inoculation sites, i.e. subcutaneously, intravenously, intraperitoneally, intramuscularly, intracranially, or via bone marrow (256, 257) and concluded that sensitivity is highest when the tumours are solid masses closer to the surface of the animal. These studies support our choice of implanting the scaffolds subcutaneously for testing.

The histology of the xenografts of DOK<sup>Luc</sup>+CAF scaffolds (**Paper III**) showed squamous epithelial tumour nests (confirmed by p53 positive staining) with many of the islands retaining differentiation and containing keratin pearls, growing within and outside the scaffold area, invading the surrounding connective tissue and musculature as small groups or cords of infiltrating cells of greater than 15 cells in number. Staining for human specific vimentin showed few human CAF were still found in the tumours formed by the xenotransplants after 12 weeks of growth in mice. When this *in vivo* model was applied to study the tumorigenic potential of nDP scaffolds and nDP-PHY scaffolds (**Paper IV**), the positive control of DOK<sup>Luc</sup>+CAF showed the same histological features, displaying the characteristic hallmarks of OSCC. However, the

number of invading tumours in positive control xenografts formed by nDP-PHY scaffolds was higher (100%) when compared to the CL (50%) and nDP scaffolds (only 30%). The increased invasion in nDP-PHY scaffolds is in line with the increasing evidence for the role played by BMPs in the promotion of tumours derived from epithelium. A study evaluating the expression of BMP-2/4 and their receptor and their implications for the prognosis of OSCC from patient specimens found strong expression of these proteins in both metastatic and non-metastatic cases, suggesting disturbances in the BMP-mediated signalling pathway during malignant developments (258).

The pro-tumour activity of BMPs occurs in more advanced stages of neoplastic development and exhibits metastasis by inducing VEGF, thus inducing neovascularisation. Elevated expression of this cytokine in tumours may be associated with a poor prognosis (259). This is in agreement with results from **Paper II**, where mRNA expression of VEGFA from the nDP-PHY scaffolds was upregulated at both 1 and 8 weeks compared to CL and nDP scaffolds. Although it is a different animal model, these results support the enhanced invasive potential observed in **Paper IV**.

When considering the nDP scaffolds in **Paper IV**, BLI from the positive xenografts carrying DOK<sup>Luc</sup>+CAF in this scaffold group showed a decreasing trend from 8 weeks until it reached values comparable to the negative control, indicating a reduction in the size of the tumour in this scaffold group. This conclusion was supported by the histological examination of these tumours that showed least number of invasive tumours formed with nDP scaffolds compared to the higher number of invasive tumours from nDP-PHY and CL scaffolds. Hence tumours formed by xenografts carrying DOK<sup>Luc</sup>+CAF in nDP scaffolds had the least aggressive potential.

A similar pattern of invasion was displayed when *in vitro* functional assays were used to assess the tumorigenic potential of the functionalised scaffolds were carried. Significant decrease in DOK<sup>Luc</sup> invasion was also observed *in vitro* in the 3D-OTs that were seeded with DOK<sup>Luc</sup> from nDP scaffolds compared to DOK<sup>Luc</sup> previously seeded on nDP-PHY scaffolds and to the positive control in 3D-OT (**Paper IV**). The role of

BMP-2 was further demonstrated in a migration assay where preliminary results showed that when DOK<sup>Luc</sup> were grown on nDP-PHY scaffolds they displayed an enhanced potential to migrate towards a high serum gradient and with an even higher migration capacity towards conditioned medium from CAF (**Fig. 4.2**). Invasive and migratory phenotypes are caused by a complex process where the cell loses epithelial morphology and gains a motile fibroblast-like mesenchymal phenotype. Of the epithelial markers that are lost during this process, the E-cadherin molecules are some of the most thoroughly investigated (260). Recent studies have reported that stimulation of human pancreatic cancer cells with BMP-2 induces epithelial-mesenchymal transition (EMT) by reducing E-cadherin expression and MMP-2 secretion, which contributes to increased invasiveness (261). These results are in line with E-cadherin staining results from 3D-OT, where DOK<sup>Luc</sup> previously grown in nDP-PHY scaffolds showed weaker expression accompanied with negative areas superficially in the epithelium. DOK<sup>Luc</sup> previously grown in nDP scaffolds had the strongest expression of E-cadherin in the epithelial compartment of the 3D-OT. There are reports that suggest stem-like properties generated by EMT are accompanied by an increase in expression of stemness markers, which would then increase in sphere-forming ability *in vitro* (262). This was in agreement with our results where the extracted DOK<sup>Luc</sup>, after being cultured on nDP-PHY scaffolds, formed more spheres than cells from CL and nDP scaffolds. A recent study also showed that BMP-2-treated colon cancer cells formed spheres that displayed significantly elevated expression of stemness markers via STAT3 activation (263). Cells from nDP scaffolds formed significantly reduced number of spheres compared to cells cultured on the other type of scaffold.

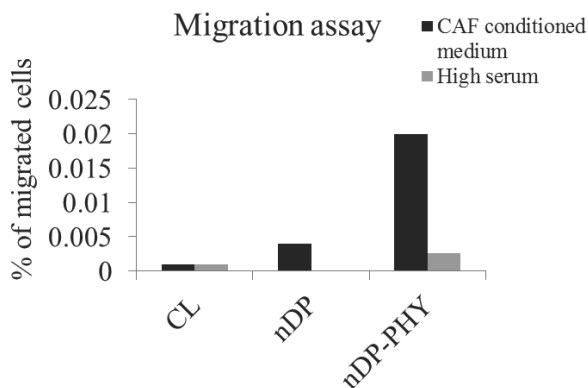


**Figure 4.2 Results of migration assays.**  $DOK^{Luc}$  cells after culture on different scaffolds for 1 week migrating against CAF conditioned medium and against a high serum gradient.

#### 4.3.3.3 *nDP promoted $DOK^{Luc}$ differentiation and decreased their tumorigenic potential*

Although controversial, there are studies that show a clinical correlation between the degree of differentiation of a tumour and its clinical behaviour; generally, a poorly differentiated tumour is more aggressive than the more (well-) differentiated tumours (264). In **Paper IV**, the epithelial differentiation marker involucrin was assessed *in vitro* in the 3D-OTs formed by  $DOK^{Luc}$  previously grown on the different scaffolds. Cells from nDP-PHY scaffolds showed a significantly reduced expression of involucrin with low expression in the supra-basal layers and abnormal expression in the para-basal layers of the epithelium in the 3D-OT. This suggests an abnormal pattern of differentiation, similar to the positive controls for tumorigenesis of  $DOK^{Luc}$  populated on CAF biomatrices. In the 3D-OT formed by  $DOK^{Luc}$  extracted from nDP scaffolds, involucrin was significantly more strongly expressed in the supra-basal epithelial layers, as evidenced by higher staining score compared to the 3D-OT made by  $DOK^{Luc}$  from nDP-PHY scaffolds and the positive control. This pattern of expression was the closest to that in normal human oral mucosa. Recent research efforts have attempted to exploit the reprogramming of cancer cells in order to drive them towards terminal differentiation with consequent loss of tumorigenicity (265).

The nDP scaffolds exhibited a favourable topography and charge for the cells as described previously, and may have played a role in enhancing the differentiation of DOK<sup>Luc</sup>, suppressing their tumorigenic ability as a result.

Dedifferentiation is a process by which cells develop from a more differentiated to a less differentiated state. BMP-2 has been recently shown to engage in signalling to Smad2/3, causing progression from benign to metastatic disease, and showing that BMP-2 is a critical component of dedifferentiation and cancer progression (266). This may explain why some parts of the epithelium in 3D-OT made by DOK<sup>Luc</sup> from nDP-PHY scaffolds were completely negative for involucrin. *In vivo*, all the different scaffolds carrying the negative control (DOK<sup>Luc</sup> alone) showed constant low photon intensities in BLI and histologically presented with proliferating DOK<sup>Luc</sup> accompanied with fibrous tissue and few differentiated keratin pearls confined to only the scaffold's area (**Papers III and IV**). Although not statistically significant, the nDP modification also enhanced the differentiation pattern *in vivo*, with stronger involucrin staining in nDP and nDP-PHY scaffolds carrying DOK<sup>Luc</sup> alone than in CL scaffolds.

Proliferation is a fundamental biological process because of the role it plays in tissue homeostasis, and it is highly perturbed in cancer, with cancer cells being able to survive beyond the life span of a normal cell and to proliferate abnormally (155). Dysregulations of homeostasis and the inverse association of differentiation with cell proliferation capacity appear to be associated with many different human tumours (155). Ki-67 expression in our re-constructed 3D-OTs showed the DOK<sup>Luc</sup> cells from the nDP and CL scaffolds had proliferation more confined to the basal layer, like the normal pattern of proliferating cells in oral epithelium. DOK<sup>Luc</sup> previously grown on nDP scaffolds had significantly reduced proliferation in the supra-basal layers, compared with cells from nDP-PHY scaffolds ( $p = 0.11$ ) and the positive control ( $p = 0.007$ ). It is generally accepted that presence of cell proliferation in the supra-basal layers marks the switch from normal oral epithelium to dysplasia and malignancy. Previous authors have showed Ki-67 to be over expressed in the supra-basal epithelium in dysplastic lesions and correlated with the severity of dysplasia (267). Studies have revealed that the invasive tumour front of an OSCC is composed of

highly proliferative cells expressing Ki-67 and positively correlated with histological grading in malignancy (268). The increased expression of Ki-67 in the basal and supra-basal epithelial layers of 3D-OTs formed by DOK<sup>Luc</sup> from nDP-PHY scaffolds parallels the increased invasion seen *in vitro* and *in vivo* (**Paper IV**). These findings argue for the role played by BMP-2 in enhancing proliferative capacity and thus motility of DOK<sup>Luc</sup>, in line with studies which showed the effect of BMP-2 in enhancing aggressiveness of OSCC (94) and evidence from lung cancer after suppressing BMP-2 activity significantly inhibited proliferation and migration of lung cancer cell lines (269).

These results again highlight the role nanodiamonds might play in suppressing an abnormal epithelial phenotype, thus pinpointing their potential for reducing the tumorigenic risk of scaffold materials.

#### ***4.3.3.4 BMP-2 plays dual roles in modulating tumorigenesis and inflammation***

The action of BMPs during carcinogenesis is complex and involves both pro-(oncogenes) and anti-tumour (tumour suppressor) characteristics. This has been reported to be dependent on the stage of the disease and cell type. The physiological concentration of the BMP-2 has been also considered a factor affecting tumorigenesis (270). Several studies have investigated the biologic effects of BMPs on cancer cells (271). BMP-2 has been shown to stimulate cancer cells such as lung, breast and prostate (272, 273). Other reports suggest that BMP-2 may have inhibitory effects on tumours of gastrointestinal origin, for example, inhibits gastric and colorectal cancer cell growth (274, 275). However, the effects of BMPs on oral cancer cells *in vitro* or *in vivo* are poorly understood. It has been reported that OSCC frequently expresses BMP-2/4, BMP-5, and BMP-1A protein (276) and others reported lack of biological adverse effects on OSCC as far as proliferation and angiogenesis are concerned (277). The use of BMP-2 for bone regeneration in the oral cavity is contraindicated for oral cancer patients because the effects of stimulating the BMP signalling pathway on these cancer cells are contradictory.

Prolonged inflammatory response has been reported to be associated with several chronic inflammatory diseases, such as gingivitis and lichen planus as well as playing roles in modulating cancer (278). Studies of the role played by BMP-2 in inflammation have produced conflicting results, which appear to be related to the dose administered (218, 237). Our results showed an attenuated inflammatory reaction at cellular level from nDP-PHY scaffolds compared to CL and nDP scaffolds, and this was attributed to the controlled delivery of low amounts of BMP-2. Nevertheless, cells from nDP-PHY scaffolds showed the most aggressive tumorigenic activities *in vitro*, and the *in vivo* invasiveness was also most pronounced in nDP-PHY scaffolds. As the difference in invasiveness was seen in the positive control only, the contribution of CAF and its secretome and the synergy between their secreting molecules and BMP-2 also have to be taken into consideration when evaluating these results.

Nevertheless, this points out the suppressive effect of nDP scaffolds on malignant progression of early neoplastic cells. While this malignant progression may have been due to the presence of early neoplastic cells, the model used is representative of the postsurgical situation in oral cancer patients where the tumour has been removed but the oral mucosa may contain spots of transformed, premalignant oral cells due to the field cancerisation phenomenon, well described for OSCC (279). This again points out the necessity of delivering BMP-2 in a controlled manner to avoid adverse effects. It also suggests that detection of premalignant signs is important prior to BMP-2 treatment and that clinicians should recognise the possible patient-dependant dangers of BMP-2, as smokers and patients with previous OSCC have patches of cells molecularly altered (p53 mutations) that are not detectable clinically or even by routine histology (280).

#### 4.3.3.5 *The carcinogenicity BLI model: an alternative to the 2-year rodent model?*

Regulatory experts advise that a biomaterial that will be implanted for more than 30 days to be screened for carcinogenicity using the two-year 'life time' carcinogenicity assays in rodents (172, 174). This has been considered difficult for several reasons, and questions have been raised regarding the extrapolation of results to humans. This long period of testing has been justified with the likelihood of a latent period before tumour formation, which may be measured in years (159). Furthermore, the *rasH2* transgenic mouse has often been used to shorten the duration of screening to 6 months (175). The nDP used to modify our scaffolds renders them topographically and physically altered and warrant screening in a relevant model. It was reported that contact by pre-neoplastic cells with an implanted biomaterial surface may promote carcinogenesis in animals (281), rather than the biomaterial initiating tumorigenesis. Several studies support the concept that carcinogenesis, including head and neck cancer, is a multistep involving a premalignant phase of long-term accumulated chromosomal alterations (181). We therefore chose to use early neoplastic cells such as DOK as a tool to evaluate the tumour promoting potential of scaffolds, providing a faster alternative to the long 'life-time' models.

The functionalised bioactive scaffolds showed success in a critical defect in the mandible area (**Paper I**); hence they can be developed for use in the oral maxillofacial area. Experimental data and clinical experience suggest that BMP-2 can be used to regenerate bone in segmental defects of the mandible (88). However, the most common reason for bone regeneration in the maxillofacial region is resection due to OSCC, and the biological effects of BMP-2 on these carcinoma cells are unknown. The use of human cells also brings to our model a substantial benefit with respect to clinical safety in humans.

Non-invasive *in vivo* monitoring for only 12-14 weeks using BLI gives robust evaluation in a shorter period than the aforementioned established carcinogenicity testing systems. While ISO 10993-3 standards require the inclusion of a positive control of comparable form and shape when screening an implantable biomaterial (166), the use of these controls is not necessary since the inclusion of a positive

environment with the use of CAF has been developed. In addition, this model is also highly practical because it provides quantitative analysis and is the only approach that can image cancer burden from the moment the cancer cells are administered to the animals. The processing time is reduced due to the ability of screening several animals simultaneously. BLI is also starting to expand in regenerative medicine and might become a powerful tool to gain more insights into the development of cell-engineered constructs (282).

## 5. CONCLUDING REMARKS

The main conclusions based on the findings of the studies in this thesis are:

1. The amounts of BMP-2 released from nDP-PHY scaffolds were found to be far less than MIC and PHY scaffolds and its release continued up to 70 days *in vitro*. Therefore, compared to BMP-2 adsorbed onto a polymer, nanodiamond particles provided a platform for strongly physisorbing BMP-2 with sustained release in low amounts, holding great potential promise for bone tissue engineering.
2. A low dose of 1  $\mu\text{g}$  of BMP-2 was found to be bioactive for bone regeneration in a rodent model.
3. PHY, MICS and nDP-PHY scaffolds showed accelerated bone regeneration in a rat mandible critical-sized defect after 4 weeks; both nDP-PHY and MICS scaffolds showed osteogenic potential both *in vitro* in MSC culture and *in vivo*. nDP-COV showed reduced osteogenic potential *in vitro* and *in vivo*. The mode of binding BMP-2 to poly(LLA-co-CL) scaffolds was thus shown to have a significant effect on their osteogenic potential *in vitro* and *in vivo*.
4. nDP and nDP-PHY scaffolds showed enhanced osteoconductive and osteoinductive potential respectively, in a mouse ectopic model.
5. nDP functionalisation of poly(LLA-co-CL) not only promoted osteogenicity but also reduced foreign-body reactions, confirming that this new modality of nDP-PHY attenuates inflammation while lowering the pharmacological dose of BMP-2, promoting its clinical application.

6. nDP and nDP-PHY scaffolds exhibited faster degradation than unmodified CL scaffolds. Nanodiamond particles were found in the implantation site after 27 weeks when 90% of the scaffolds degraded.
7. A sensitive and reliable *in vivo* model was established using DOK<sup>Luc</sup> and CAF for monitoring microenvironmentally-induced carcinogenesis providing early, non-invasive surveillance of tumour development associated with implantation of scaffolds. The model was successfully applied to evaluating functionalised copolymer scaffolds.
8. In an *in vitro* 3D-OT, DOK<sup>Luc</sup> cells demonstrated a reduced tumorigenic potential after being cultured on nDP modified scaffolds, as shown by proliferation, invasiveness and differentiation compared to DOK<sup>Luc</sup> from nDP-PHY and CL scaffolds.
9. The nDP modified scaffolds reduced the bioluminescence intensity from positive control xenograft scaffolds of DOK<sup>Luc</sup>+CAF, suggesting tumour suppressing effects.
10. The nDP-PHY scaffolds showed enhanced tumorigenic potential *in vitro* in the 3D-OT and *in vivo* in the positive control xenografts, but not the negative control xenografts with DOK<sup>Luc</sup> alone. This raises concerns for the delivery of BMP-2 in reconstruction of bone defects in oral cancer patients.

## 6. FUTURE PERSPECTIVES

The future of growth factors' use in bone tissue engineering applications seems promising. Most studies and clinical trials to date have focused on single growth factor delivery (rhBMP-2 or rhBMP-7). However, an ideal growth factor-delivery system should mimic the natural healing process, which involves the complex participation of multiple growth factors that perform their functions in a specific sequence and at specific concentrations. The findings from nDP-PHY and MICS mode of delivery here may serve as a basis for future investigations. They can be combined together in one scaffold system and assessed for sequential release of the growth factors to imitate the natural healing process. Studies with longer time points will allow evaluation of the sustainability of bioactivity of the delivered growth factors *in vivo*, and to evaluate the quality of the bone formed. Further improvement of fabrication technologies and introduction of computer aided 3D scaffold fabrication techniques may allow production of patient-specific, custom-made treatment options. In this way, it may be possible to regenerate more complex bone defects and osteochondral tissues in larger animals.

With regard to the tumorigenicity results in **Paper IV**, study of the MAPK/ERK pathway and the EGFR pathways may help elucidate the underlying molecular mechanisms behind reduction of tumorigenic potential by the nanodiamond particles. In addition, it would be of interest to apply our established model to different cell lines of different origins to see if the nanodiamond modification has the same effect on other tumour types.

Application of the nDP-PHY scaffolds offers intriguing possibilities as a drug delivery system. This would be of relevance for example, in the case of oral cancer after resection of a cancerous lesion, where there is a need for a system that can support the generation of new bone as well as delivering localised chemotherapy. *In vivo* established rodent OSCC cancer models can be used to test this, with additional bone defects created.

Another interesting area of investigation would be evaluating the phenotypic dichotomy of macrophages. Macrophages are known to play switching roles in inflammation and cancer. Further investigations of the switching phenomenon between M1 and M2 in our harvested samples will be of great value to elucidate the role played by scaffolds modified with nanoparticles with or without BMP-2 in inflammation and carcinogenesis.

## ACKNOWLEDGEMENTS

I would like to express my gratitude to the Department of Clinical Dentistry, Department of Clinical Medicine (Gade Laboratory of Pathology) and the Center for International Health for providing me the opportunity and an inspiring working environment. I thank the Norwegian State Educational Loan Fund (Quota scholarship programme) for funding my PhD and the FP7 EU Project (VascuBone) for supporting this work.

Words cannot express my gratitude to those who stood by me throughout this journey.

I was blessed with a remarkable team of supervisors who created a wonderful learning experience for me. I want to sincerely thank my main supervisor **Kamal Mustafa** for his unwavering support and patience. *I appreciate your exquisite and natural goodness and insightful guidance on my PhD and professional career. Thank you for your trust and for being there during the difficult times.* **Daniela Elena Costea** – *I am indebted to your exceptional encouragement and unfailing dedication throughout. Your friendly supervisory style taught me unique lessons in team work that I will not forget.* **Anne Christine Johannessen** - *I am grateful for your guidance and for keeping your doors always open, the fruitful discussions and support during my hardships.* **Ying Xue** – *Thank you for your enduring support, patience when teaching me ABCs of laboratory work and answering my mindless questions.*

I would like to extend this gratitude to my co-workers/co-authors at UIB or the VascuBone project consortium, without them this work would not have been possible; **Torbjorn Pedersen, Anna Døskeland, Emmet McCormack, Tereza Osdal, Xujun Wu, Frank Kloss, Thilo Waag, Frode Berven, Henning Lygre, Himalaya Parajuli, Zhe Xing.** A special thanks to **Anke Krueger** and **Anna Finne-Wistrand** - *Thank you for kindly hosting me in your labs, and for the fruitful discussions. I enjoyed being a chemist amateur for a while during my stay.* **Yang Sun**, *thanks for being an efficient 'scaffold fabricator' and for keeping up with my short deadlines.* **Doris Steinmüller-Nethl**, *thanks for your continuous support.* **Joachim Nickel** *thanks for the stimulating*

*discussions and continuous supply of BMP-2. Heike Walles, Bettina Hafen, Endre Hellem, Tian Yuan, Magdalena Schmike, Christoph Rucker, Alexander Kahlig, Ram Kumar, Anup James, Regina Ebert, Mihaela Popa – I appreciate our fruitful collaboration and thanks for positively influencing my work. Sarah Schweetberg and Andreas, thanks for your prolific help during my visit to Wurzburg.*

I am grateful for the support I got from the academic, technical and administrative staff at the different departments. **Siren Hammer Østfold** - *thanks for making the 'fourth floor' a cheerful place, Rita Griener-Simonsen, Kaia Berstad, Randi Sundfjord, Gunnvor Øijordsbakken, Edith Fick, Bendik Nordanger, Knut Buanes – thank you all for your technical support. June-Vibecke Knudtsen, Linda Forshaw, Mona Isakson, Marit Stubdal, among others – Thanks for facilitating my study period.*

**Cecilie Gjerde, Solve Hellem, Stein Atle, Anne Nordrehaug Åstrøm, Mihaela Cimpan, Nils Roar Gjerdet, Asgeir Bårdsen, Anne Isine Bolstad, Rune Nilsen, Kathrine Skarstein, Inge Fristad, Gunhild Strand** – *you have all been generous to me at various phases of my PhD*

I had the pleasure of working and interacting with a number of great colleagues at CIH, Gade and IKO: **Xiao, Maryam, Khadija, Elisabeth Nginamau, Julia Irani, Janne Gjerde, Hilde Sellevol, Jörn Blume, Lara Aqrawi, Pugazendhi, Alemnesh, Ferda Gulcan, Niyaz, Bass, Julie Schölermann, Tarig, Kemal, Dipak, Victoria, Eivind, Sushma, Sunita, Dagmar, Nancy, Israa, Masahito, Kenji, Kathrin, Ahmad,** among others – *words cannot express how each one of you positively influenced my experience. Thank you all!*

**Hager, Hisham, Hiba Baldo, Sally Eltayeb, Manal Mustafa, Amani, Dalia, Hasaan, Mohammed Y, Mohammed I, Elwalid Fadul, Nada Suliman, Shaza Idris, Salah Ibrahim, Ahmed Elmokashfi, Houwaida, Rabab, Wigdan, Omnia, Salma, Samih** - *You were my family in Bergen, thanks for making me feel at home.*

**Alsheima, Nafisa, Sarah I, Hadeel, Azza N, Azza A, Azza E, Eman** - *This journey would not have been possible without your support, and thanx for making me feel I was not too far away.*

I would not have been addressing you today were it not for my family's fortification. To my parents, my pillars, I owe this accomplishment - *Thank you for believing in me and for being my powerhouse, my strength and backbone. Thanks for your prayers!* The loving support, prayers and patience of my sisters **Nasreen** and **Nazik**, my brother **Mohammed** and my brother-in-law **Montasir** helped me get through the hardest times. My nephew **Kareem**, (*our sunshine*)!

This list is by no means exhaustive for those who contributed to this work. Many people I met in this journey inspired me in different ways – *Thank you all!*

Above all, I thank Allah the Almighty for giving me the courage to complete this research.

Salwa Suliman

September 2015, Bergen

**BIBLIOGRAPHY**

1. Buck DW, 2nd, Dumanian GA. Bone biology and physiology: Part I. The fundamentals. *Plast Reconstr Surg*. 2012;129(6):1314-20.
2. Giannoudis PV, Dinopoulos H, Tsiridis E. Bone substitutes: an update. *Injury*. 2005;36 Suppl 3:S20-7.
3. Athanasiou VT, Papachristou DJ, Panagopoulos A, Saridis A, Scopa CD, Megas P. Histological comparison of autograft, allograft-DBM, xenograft, and synthetic grafts in a trabecular bone defect: an experimental study in rabbits. *Med Sci Monit*. 2010;16(1):BR24-31.
4. Langer R, Vacanti JP. Tissue engineering. *Science*. 1993;260(5110):920-6.
5. Vacanti JP, Langer R. Tissue engineering: the design and fabrication of living replacement devices for surgical reconstruction and transplantation. *Lancet*. 1999;354 Suppl 1:SI32-4.
6. Shrivats AR, McDermott MC, Hollinger JO. Bone tissue engineering: state of the union. *Drug Discov Today*. 2014;19(6):781-6.
7. Hutmacher DW. Scaffolds in tissue engineering bone and cartilage. *Biomaterials*. 2000;21(24):2529-43.
8. Tsang KY, Cheung MC, Chan D, Cheah KS. The developmental roles of the extracellular matrix: beyond structure to regulation. *Cell Tissue Res*. 2010;339(1):93-110.
9. Huebsch N, Arany PR, Mao AS, Shvartsman D, Ali OA, Bencherif SA, et al. Harnessing traction-mediated manipulation of the cell/matrix interface to control stem-cell fate. *Nat Mater*. 2010;9(6):518-26.
10. Hynes RO. The extracellular matrix: not just pretty fibrils. *Science*. 2009;326(5957):1216-9.
11. Lin F, Ren XD, Pan Z, Macri L, Zong WX, Tonnesen MG, et al. Fibronectin growth factor-binding domains are required for fibroblast survival. *J Invest Dermatol*. 2011;131(1):84-98.
12. Polo-Corrales L, Latorre-Esteves M, Ramirez-Vick JE. Scaffold design for bone regeneration. *J Nanosci Nanotechnol*. 2014;14(1):15-56.
13. Cipitria A, Lange C, Schell H, Wagermaier W, Reichert JC, Hutmacher DW, et al. Porous scaffold architecture guides tissue formation. *J Bone Miner Res*. 2012;27(6):1275-88.
14. Karageorgiou V, Kaplan D. Porosity of 3D biomaterial scaffolds and osteogenesis. *Biomaterials*. 2005;26(27):5474-91.
15. Bose S, Roy M, Bandyopadhyay A. Recent advances in bone tissue engineering scaffolds. *Trends Biotechnol*. 2012;30(10):546-54.
16. Danmark S, Finne-Wistrand A, Wendel M, Arvidson K, Albertsson AC, Mustafa K. Osteogenic Differentiation by Rat Bone Marrow Stromal Cells on Customized Biodegradable Polymer Scaffolds. *J Bioact Compat Polym*. 2010;25(2):207-23.
17. Gruber R, Weich H, Dullin C, Schliephake H. Ectopic bone formation after implantation of a slow release system of polylactid acid and rhBMP-2. *Clin Oral Implants Res*. 2009;20(1):24-30.
18. Schofer MD, Roessler PP, Schaefer J, Theisen C, Schlimme S, Heverhagen JT, et al. Electrospun PLLA nanofiber scaffolds and their use in combination with BMP-2 for reconstruction of bone defects. *PloS one*. 2011;6(9):e25462.
19. La Carrubba V, Pavia FC, Brucato V, Piccarolo S. PLLA/PLA scaffolds prepared via Thermally Induced Phase Separation (TIPS): tuning of properties and biodegradability. *Int J Mater Form*. 2008;1:619-22.

20. Peltola SM, Melchels FP, Grijpma DW, Kellomaki M. A review of rapid prototyping techniques for tissue engineering purposes. *Ann Med.* 2008;40(4):268-80.
21. Zein I, Hutmacher DW, Tan KC, Teoh SH. Fused deposition modeling of novel scaffold architectures for tissue engineering applications. *Biomaterials.* 2002;23(4):1169-85.
22. Hutmacher DW, Sittinger M, Risbud MV. Scaffold-based tissue engineering: rationale for computer-aided design and solid free-form fabrication systems. *Trends Biotechnol.* 2004;22(7):354-62.
23. Bandyopadhyay A, Espana F, Balla VK, Bose S, Ohgami Y, Davies NM. Influence of porosity on mechanical properties and in vivo response of Ti6Al4V implants. *Acta Biomater.* 2010;6(4):1640-8.
24. Balla VK, Bodhak S, Bose S, Bandyopadhyay A. Porous tantalum structures for bone implants: Fabrication, mechanical and in vitro biological properties. *Acta Biomater.* 2010;6(8):3349-59.
25. Gao C, Deng Y, Feng P, Mao Z, Li P, Yang B, et al. Current progress in bioactive ceramic scaffolds for bone repair and regeneration. *Int J Mol Sci.* 2014;15(3):4714-32.
26. Zhou J, Lin H, Fang T, Li X, Dai W, Uemura T, et al. The repair of large segmental bone defects in the rabbit with vascularized tissue engineered bone. *Biomaterials.* 2010;31(6):1171-9.
27. Reppenhausen S, Reichert JC, Rackwitz L, Rudert M, Raab P, Daculsi G, et al. Biphasic bone substitute and fibrin sealant for treatment of benign bone tumours and tumour-like lesions. *Int Orthop.* 2012;36(1):139-48.
28. Yuan H, Fernandes H, Habibovic P, de Boer J, Barradas AM, de Ruiter A, et al. Osteoinductive ceramics as a synthetic alternative to autologous bone grafting. *Proc Natl Acad Sci U S A.* 2010;107(31):13614-9.
29. Oliveira SM, Ringshia RA, Legeros RZ, Clark E, Yost MJ, Terracio L, et al. An improved collagen scaffold for skeletal regeneration. *J Biomed Mater Res A.* 2010;94(2):371-9.
30. Liu H, Ge Z, Wang Y, Toh SL, Sutthikhum V, Goh JC. Modification of sericin-free silk fibers for ligament tissue engineering application. *J Biomed Mater Res B Appl Biomater.* 2007;82(1):129-38.
31. Place ES, George JH, Williams CK, Stevens MM. Synthetic polymer scaffolds for tissue engineering. *Chem Soc Rev.* 2009;38(4):1139-51.
32. Welle A, Kroger M, Doring M, Niederer K, Pindel E, Chronakis IS. Electrospun aliphatic polycarbonates as tailored tissue scaffold materials. *Biomaterials.* 2007;28(13):2211-9.
33. Lee JW, Lan PX, Kim B, Lim G, Cho DW. Fabrication and characteristic analysis of a poly(propylene fumarate) scaffold using micro-stereolithography technology. *J Biomed Mater Res B Appl Biomater.* 2008;87B(1):1-9.
34. Mitchell A, Kim B, Cottrell J, Snyder S, Witek L, Ricci J, et al. Development of a guided bone regeneration device using salicylic acid-poly(anhydride-ester) polymers and osteoconductive scaffolds. *J Biomed Mater Res A.* 2014;102(3):655-64.
35. Woodruff MA, Hutmacher DW. The return of a forgotten polymer-Polycaprolactone in the 21st century. *Prog Polym Sci.* 2010;35(10):1217-56.
36. Nugraha C, Bora M, Venkatraman SS. Release retardation of model protein on polyelectrolyte-coated PLGA nano- and microparticles. *PLoS one.* 2014;9(3):e92393.
37. Danmark S, Finne-Wistrand A, Schander K, Hakkarainen M, Arvidson K, Mustafa K, et al. In vitro and in vivo degradation profile of aliphatic polyesters subjected to electron beam sterilization. *Acta Biomater.* 2011;7(5):2035-46.
38. Low SW, Ng YJ, Yeo TT, Chou N. Use of Osteoplug polycaprolactone implants as novel burr-hole covers. *Singapore Med J.* 2009;50(8):777-80.

39. Suzuki T, Kawamura H, Kasahara T, Nagasaka H. Resorbable poly-L-lactide plates and screws for the treatment of mandibular condylar process fractures: a clinical and radiologic follow-up study. *J Oral Maxillofac Surg.* 2004;62(8):919-24.
40. Liu XH, Holzwarth JM, Ma PX. Functionalized Synthetic Biodegradable Polymer Scaffolds for Tissue Engineering. *Macromol Biosci.* 2012;12(7):911-9.
41. Andersson SR, Hakkarainen M, Albertsson AC. Tuning the Polylactide Hydrolysis Rate by Plasticizer Architecture and Hydrophilicity without Introducing New Migrants. *Biomacromolecules.* 2010;11(12):3617-23.
42. Odelius K, Pliikk P, Albertsson AC. Elastomeric hydrolyzable porous scaffolds: copolymers of aliphatic polyesters and a polyether-ester. *Biomacromolecules.* 2005;6(5):2718-25.
43. Mistura DV, Messias AD, Duek EA, Duarte MA. Development, characterization, and cellular adhesion of poly(L-lactic acid)/poly(caprolactone triol) membranes for potential application in bone tissue regeneration. *Artif Organs.* 2013;37(11):978-84.
44. Xue Y, Danmark S, Xing Z, Arvidson K, Albertsson AC, Hellem S, et al. Growth and differentiation of bone marrow stromal cells on biodegradable polymer scaffolds: an in vitro study. *J Biomed Mater Res A.* 2010;95(4):1244-51.
45. Idris SB, Danmark S, Finne-Wistrand A, Arvidson K, Albertsson AC, Bolstad AI, et al. Biocompatibility of Polyester Scaffolds with Fibroblasts and Osteoblast-like Cells for Bone Tissue Engineering. *J Bioact Compat Polym.* 2010;25(6):567-83.
46. Xing Z, Xue Y, Danmark S, Schander K, Ostvold S, Arvidson K, et al. Effect of endothelial cells on bone regeneration using poly(L-lactide-co-1,5-dioxepan-2-one) scaffolds. *J Biomed Mater Res A.* 2011;96(2):349-57.
47. Akkouch A, Zhang Z, Rouabhia M. A novel collagen/hydroxyapatite/poly(lactide-co-epsilon-caprolactone) biodegradable and bioactive 3D porous scaffold for bone regeneration. *J Biomed Mater Res A.* 2011;96A(4):693-704.
48. Reichert JC, Wullschleger ME, Cipitria A, Lienau J, Cheng TK, Schuetz MA, et al. Custom-made composite scaffolds for segmental defect repair in long bones. *Int Orthop.* 2011;35(8):1229-36.
49. Chuenjitkuntaworn B, Inrung W, Damrongsri D, Mekaapiruk K, Supaphol P, Pavasant P. Polycaprolactone/Hydroxyapatite composite scaffolds: Preparation, characterization, and in vitro and in vivo biological responses of human primary bone cells. *J Biomed Mater Res A.* 2010;94A(1):241-51.
50. Jiao YP, Cui FZ. Surface modification of polyester biomaterials for tissue engineering. *Biomed Mater.* 2007;2(4):R24-37.
51. Tang Y, Zhao Y, Wang X, Lin T. Layer-by-layer assembly of silica nanoparticles on 3D fibrous scaffolds: enhancement of osteoblast cell adhesion, proliferation, and differentiation. *J Biomed Mater Res A.* 2014;102(11):3803-12.
52. Sun Y, Finne-Wistrand A, Waag T, Xing Z, Yassin M, Yamamoto A, et al. Reinforced Degradable Biocomposite by Homogenously Distributed Functionalized Nanodiamond Particles. *Macromol Mater Eng.* 2015;300(4):436-47.
53. Zhang Q, Mochalin VN, Neitzel I, Knoke IY, Han J, Klug CA, et al. Fluorescent PLLA-nanodiamond composites for bone tissue engineering. *Biomaterials.* 2011;32(1):87-94.
54. Xing Z, Pedersen TO, Wu X, Xue Y, Sun Y, Finne-Wistrand A, et al. Biological effects of functionalizing copolymer scaffolds with nanodiamond particles. *Tissue Eng Part A.* 2013;19(15-16):1783-91.
55. Danmark S, Finne-Wistrand A, Albertsson AC, Patarroyo M, Mustafa K. Integrin-mediated adhesion of human mesenchymal stem cells to extracellular matrix proteins adsorbed to polymer surfaces. *Biomed Mater.* 2012;7(3):035011.

56. Schindeler A, McDonald MM, Bokko P, Little DG. Bone remodeling during fracture repair: The cellular picture. *Semin Cell Dev Biol.* 2008;19(5):459-66.
57. Tsiridis E, Upadhyay N, Giannoudis P. Molecular aspects of fracture healing: which are the important molecules? *Injury.* 2007;38 Suppl 1:S11-25.
58. Santo VE, Gomes ME, Mano JF, Reis RL. Controlled release strategies for bone, cartilage, and osteochondral engineering--Part I: recapitulation of native tissue healing and variables for the design of delivery systems. *Tissue Eng Part B Rev.* 2013;19(4):308-26.
59. Schmidt-Bleek K, Schell H, Schulz N, Hoff P, Perka C, Buttgerit F, et al. Inflammatory phase of bone healing initiates the regenerative healing cascade. *Cell Tissue Res.* 2012;347(3):567-73.
60. Gurkan UA, Gargac J, Akkus O. The Sequential Production Profiles of Growth Factors and their Relations to Bone Volume in Ossifying Bone Marrow Explants. *Tissue Eng Part A.* 2010;16(7):2295-306.
61. Caplan AI, Correa D. PDGF in bone formation and regeneration: new insights into a novel mechanism involving MSCs. *J Orthop Res.* 2011;29(12):1795-803.
62. Kigami R, Sato S, Tsuchiya N, Sato N, Suzuki D, Arai Y, et al. Effect of basic fibroblast growth factor on angiogenesis and bone regeneration in non-critical-size bone defects in rat calvaria. *J Oral Sci.* 2014;56(1):17-22.
63. Pedersen TO, Blois AL, Xing Z, Xue Y, Sun Y, Finne-Wistrand A, et al. Endothelial microvascular networks affect gene-expression profiles and osteogenic potential of tissue-engineered constructs. *Stem Cell Res Ther.* 2013;4(3):52.
64. Zhang W, Zhu C, Wu Y, Ye D, Wang S, Zou D, et al. VEGF and BMP-2 promote bone regeneration by facilitating bone marrow stem cell homing and differentiation. *Eur Cell Mater.* 2014;27:1-11; discussion -2.
65. Urist MR. Bone: formation by autoinduction. *Science.* 1965;150(3698):893-9.
66. Urist MR, Strates BS. Bone morphogenetic protein. *J Dent Res.* 1971;50(6):1392-406.
67. Reddi AH. BMPs: from bone morphogenetic proteins to body morphogenetic proteins. *Cytokine Growth Factor Rev.* 2005;16(3):249-50.
68. Carreira AC, Lojudice FH, Halcsik E, Navarro RD, Sogayar MC, Granjeiro JM. Bone morphogenetic proteins: facts, challenges, and future perspectives. *J Dent Res.* 2014;93(4):335-45.
69. Sipe JB, Zhang J, Waits C, Skikne B, Garimella R, Anderson HC. Localization of bone morphogenetic proteins (BMPs)-2, -4, and -6 within megakaryocytes and platelets. *Bone.* 2004;35(6):1316-22.
70. Matthews SJ. Biological activity of bone morphogenetic proteins (BMP's). *Injury.* 2005;36 Suppl 3:S34-7.
71. Cheng H, Jiang W, Phillips FM, Haydon RC, Peng Y, Zhou L, et al. Osteogenic activity of the fourteen types of human bone morphogenetic proteins (BMPs). *J Bone Joint Surg Am.* 2003;85-A(8):1544-52.
72. Chen G, Deng C, Li YP. TGF-beta and BMP signaling in osteoblast differentiation and bone formation. *Int J Biol Sci.* 2012;8(2):272-88.
73. Scheufler C, Sebald W, Hulsmeier M. Crystal structure of human bone morphogenetic protein-2 at 2.7 Å resolution. *J Mol Biol.* 1999;287(1):103-15.
74. Bais MV, Wigner N, Young M, Toholka R, Graves DT, Morgan EF, et al. BMP2 is essential for post natal osteogenesis but not for recruitment of osteogenic stem cells. *Bone.* 2009;45(2):254-66.
75. Panetta NJ, Gupta DM, Lee JK, Wan DC, Commons GW, Longaker MT. Human adipose-derived stromal cells respond to and elaborate bone morphogenetic protein-2 during in vitro osteogenic differentiation. *Plast Reconstr Surg.* 2010;125(2):483-93.

76. Mostafa NZ, Fitzsimmons R, Major PW, Adesida A, Jomha N, Jiang H, et al. Osteogenic differentiation of human mesenchymal stem cells cultured with dexamethasone, vitamin D3, basic fibroblast growth factor, and bone morphogenetic protein-2. *Connect Tissue Res.* 2012;53(2):117-31.
77. Tsuji K, Bandyopadhyay A, Harfe BD, Cox K, Kakar S, Gerstenfeld L, et al. BMP2 activity, although dispensable for bone formation, is required for the initiation of fracture healing. *Nat Genet.* 2006;38(12):1424-9.
78. Wang Q, Huang C, Xue M, Zhang X. Expression of endogenous BMP-2 in periosteal progenitor cells is essential for bone healing. *Bone.* 2011;48(3):524-32.
79. Yang W, Harris MA, Cui Y, Mishina Y, Harris SE, Gluhak-Heinrich J. Bmp2 is required for odontoblast differentiation and pulp vasculogenesis. *J Dent Res.* 2012;91(1):58-64.
80. Retting KN, Song B, Yoon BS, Lyons KM. BMP canonical Smad signaling through Smad1 and Smad5 is required for endochondral bone formation. *Development.* 2009;136(7):1093-104.
81. Burkus JK, Transfeldt EE, Kitchel SH, Watkins RG, Balderston RA. Clinical and radiographic outcomes of anterior lumbar interbody fusion using recombinant human bone morphogenetic protein-2. *Spine.* 2002;27(21):2396-408.
82. Glassman SD, Carreon L, Djurasovic M, Campbell MJ, Puno RM, Johnson JR, et al. Posterolateral lumbar spine fusion with INFUSE bone graft. *Spine J.* 2007;7(1):44-9.
83. Dawson E, Bae HW, Burkus JK, Stambough JL, Glassman SD. Recombinant Human Bone Morphogenetic Protein-2 on an Absorbable Collagen Sponge with an Osteoconductive Bulking Agent in Posterolateral Arthrodesis with Instrumentation A Prospective Randomized Trial. *J Bone Joint Surg Am.* 2009;91A(7):1604-13.
84. Govender S, Csimma C, Genant HK, Valentin-Opran A, Amit Y, Arbel R, et al. Recombinant human bone morphogenetic protein-2 for treatment of open tibial fractures: a prospective, controlled, randomized study of four hundred and fifty patients. *J Bone Joint Surg Am.* 2002;84-A(12):2123-34.
85. Alt V, Donell ST, Chhabra A, Bentley A, Eicher A, Schnettler R. A health economic analysis of the use of rhBMP-2 in Gustilo-Anderson grade III open tibial fractures for the UK, Germany, and France. *Injury.* 2009;40(12):1269-75.
86. Boyne PJ, Marx RE, Nevins M, Triplett G, Lazaro E, Lilly LC, et al. A feasibility study evaluating rhBMP-2/absorbable collagen sponge for maxillary sinus floor augmentation. *Int J Periodontics Restorative Dent.* 1997;17(1):11-25.
87. Boyne PJ, Lilly LC, Marx RE, Moy PK, Nevins M, Spagnoli DB, et al. De novo bone induction by recombinant human bone morphogenetic protein-2 (rhBMP-2) in maxillary sinus floor augmentation. *J Oral Maxillofac Surg.* 2005;63(12):1693-707.
88. Herford AS, Boyne PJ. Reconstruction of mandibular continuity defects with bone morphogenetic protein-2 (rhBMP-2). *J Oral Maxillofac Surg.* 2008;66(4):616-24.
89. Tannoury CA, An HS. Complications with the use of bone morphogenetic protein 2 (BMP-2) in spine surgery. *Spine J.* 2014;14(3):552-9.
90. Ritting AW, Weber EW, Lee MC. Exaggerated Inflammatory Response and Bony Resorption From BMP-2 Use in a Pediatric Forearm Nonunion. *J Hand Surg Am.* 2012;37A(2):316-21.
91. Neovius E, Lemberger M, Docherty Skogh AC, Hilborn J, Engstrand T. Alveolar bone healing accompanied by severe swelling in cleft children treated with bone morphogenetic protein-2 delivered by hydrogel. *J Plast Reconstr Aesthet Surg.* 2013;66(1):37-42.
92. Vavken J, Mameghani A, Vavken P, Schaeren S. Complications and cancer rates in spine fusion with recombinant human bone morphogenetic protein-2 (rhBMP-2). *Eur Spine J.* 2015.(pub ahead of print)

93. Carragee EJ, Chu G, Rohatgi R, Hurwitz EL, Weiner BK, Yoon ST, et al. Cancer Risk After Use of Recombinant Bone Morphogenetic Protein-2 for Spinal Arthrodesis. *J Bone Joint Surg Am.* 2013;95A(17):1537-45.
94. Kokorina NA, Lewis JS, Jr., Zakharkin SO, Krebsbach PH, Nussenbaum B. rhBMP-2 has adverse effects on human oral carcinoma cell lines in vivo. *Laryngoscope.* 2012;122(1):95-102.
95. Boerckel JD, Kolambkar YM, Dupont KM, Uhrig BA, Phelps EA, Stevens HY, et al. Effects of protein dose and delivery system on BMP-mediated bone regeneration. *Biomaterials.* 2011;32(22):5241-51.
96. Mehta M, Schmidt-Bleek K, Duda GN, Mooney DJ. Biomaterial delivery of morphogens to mimic the natural healing cascade in bone. *Adv Drug Deliv Rev.* 2012;64(12):1257-76.
97. Jiang J, Fan CY, Zeng BF. Experimental construction of BMP2 and VEGF gene modified tissue engineering bone in vitro. *Int J Mol Sci.* 2011;12(3):1744-55.
98. Dupont KM, Boerckel JD, Stevens HY, Diab T, Kolambkar YM, Takahata M, et al. Synthetic scaffold coating with adeno-associated virus encoding BMP2 to promote endogenous bone repair. *Cell Tissue Res.* 2012;347(3):575-88.
99. Rose LC, Kucharski C, Uludag H. Protein expression following non-viral delivery of plasmid DNA coding for basic FGF and BMP-2 in a rat ectopic model. *Biomaterials.* 2012;33(11):3363-74.
100. Lin ZY, Duan ZX, Guo XD, Li JF, Lu HW, Zheng QX, et al. Bone induction by biomimetic PLGA-(PEG-ASP)<sub>n</sub> copolymer loaded with a novel synthetic BMP-2-related peptide in vitro and in vivo. *J Controlled Release.* 2010;144(2):190-5.
101. Ansari S, Freire MO, Pang EK, Abdelhamid AI, Almohaimeed M, Zadeh HH. Immobilization of murine anti-BMP-2 monoclonal antibody on various biomaterials for bone tissue engineering. *Biomed Res Int.* 2014;2014:940860.
102. Jung S-Y, Ko Y-J, Jang H-S, Kang S-W, Park J-H. The effect of carrier for BMP-2 delivery on histological aspects of tissue-engineered bone. *Tissue Engineering and Regenerative Medicine.* 2013;10(6):341-6.
103. Yang HS, La WG, Cho YM, Shin W, Yeo GD, Kim BS. Comparison between heparin-conjugated fibrin and collagen sponge as bone morphogenetic protein-2 carriers for bone regeneration. *Exp Mol Med.* 2012;44(5):350-5.
104. King WJ, Krebsbach PH. Growth factor delivery: how surface interactions modulate release in vitro and in vivo. *Adv Drug Deliv Rev.* 2012;64(12):1239-56.
105. Macdonald ML, Samuel RE, Shah NJ, Padera RF, Beben YM, Hammond PT. Tissue integration of growth factor-eluting layer-by-layer polyelectrolyte multilayer coated implants. *Biomaterials.* 2011;32(5):1446-53.
106. Smith DM, Cray JJ, Jr., Weiss LE, Dai Fei EK, Shakir S, Rottgers SA, et al. Precise control of osteogenesis for craniofacial defect repair: the role of direct osteoprogenitor contact in BMP-2-based bioprinting. *Ann Plast Surg.* 2012;69(4):485-8.
107. Wang H, Leeuwenburgh SC, Li Y, Jansen JA. The use of micro- and nanospheres as functional components for bone tissue regeneration. *Tissue Eng Part B Rev.* 2012;18(1):24-39.
108. Kempen DH, Lu L, Hefferan TE, Creemers LB, Maran A, Classic KL, et al. Retention of in vitro and in vivo BMP-2 bioactivities in sustained delivery vehicles for bone tissue engineering. *Biomaterials.* 2008;29(22):3245-52.
109. Li B, Yoshii T, Hafeman AE, Nyman JS, Wenke JC, Guelcher SA. The effects of rhBMP-2 released from biodegradable polyurethane/microsphere composite scaffolds on new bone formation in rat femora. *Biomaterials.* 2009;30(35):6768-79.

110. Lee JW, Kang KS, Lee SH, Kim JY, Lee BK, Cho DW. Bone regeneration using a microstereolithography-produced customized poly(propylene fumarate)/diethyl fumarate photopolymer 3D scaffold incorporating BMP-2 loaded PLGA microspheres. *Biomaterials*. 2011;32(3):744-52.
111. Bock N, Woodruff MA, Hutmacher DW, Dargaville TR. Electrospraying, a Reproducible Method for Production of Polymeric Microspheres for Biomedical Applications. *Polymers*. 2011;3(4):131-49.
112. Li XM, Wang L, Fan YB, Feng QL, Cui FZ, Watari F. Nanostructured scaffolds for bone tissue engineering. *J Biomed Mater Res A*. 2013;101(8):2424-35.
113. Krueger A. The structure and reactivity of nanoscale diamond. *J Mater Chem*. 2008;18(13):1485-92.
114. Krueger A, Lang D. Functionality is Key: Recent Progress in the Surface Modification of Nanodiamond. *Adv Funct Mater*. 2012;22(5):890-906.
115. Krueger A. New carbon materials: biological applications of functionalized nanodiamond materials. *Chemistry*. 2008;14(5):1382-90.
116. Krueger A, Ozawa M, Jarre G, Liang Y, Stegk J, Lu L. Deagglomeration and functionalisation of detonation diamond. *Physica Status Solidi a-Applications and Materials Science*. 2007;204(9):2881-7.
117. Krüger A, Kataoka F, Ozawa M, Fujino T, Suzuki Y, Aleksenskii AE, et al. Unusually tight aggregation in detonation nanodiamond: Identification and disintegration. *Carbon*. 2005;43(8):1722-30.
118. Mochalin VN, Shenderova O, Ho D, Gogotsi Y. The properties and applications of nanodiamonds. *Nature nanotechnology*. 2012;7(1):11-23.
119. Steinmuller-Nethl D, Kloss FR, Najam-Ul-Haq M, Rainer M, Larsson K, Linsmeier C, et al. Strong binding of bioactive BMP-2 to nanocrystalline diamond by physisorption. *Biomaterials*. 2006;27(26):4547-56.
120. Kloss FR, Gassner R, Preiner J, Ebner A, Larsson K, Hachl O, et al. The role of oxygen termination of nanocrystalline diamond on immobilisation of BMP-2 and subsequent bone formation. *Biomaterials*. 2008;29(16):2433-42.
121. Kloss FR, Singh S, Hachl O, Rentenberger J, Auberger T, Kraft A, et al. BMP-2 immobilized on nanocrystalline diamond-coated titanium screws; demonstration of osteoinductive properties in irradiated bone. *Head and Neck*. 2013;35(2):235-41.
122. Moore L, Gatica M, Kim H, Osawa E, Ho D. Multi-protein delivery by nanodiamonds promotes bone formation. *J Dent Res*. 2013;92(11):976-81.
123. Masters KS. Covalent growth factor immobilization strategies for tissue repair and regeneration. *Macromol Biosci*. 2011;11(9):1149-63.
124. Yamachika E, Tsujigiwa H, Shirasu N, Ueno T, Sakata Y, Fukunaga J, et al. Immobilized recombinant human bone morphogenetic protein-2 enhances the phosphorylation of receptor-activated Smads. *J Biomed Mater Res A*. 2009;88(3):599-607.
125. Lee JS, Lee SK, Kim BS, Im GI, Cho KS, Kim CS. Controlled release of BMP-2 using a heparin-conjugated carrier system reduces in vivo adipose tissue formation. *J Biomed Mater Res A*. 2015;103(2):545-54.
126. Visser R, Arrabal PM, Santos-Ruiz L, Fernandez-Barranco R, Becerra J, Cifuentes M. A Collagen-Targeted Biomimetic RGD Peptide to Promote Osteogenesis. *Tissue Eng Part A*. 2014;20(1-2):34-44.
127. Pohl TL, Boergermann JH, Schwaerzer GK, Knaus P, Cavalcanti-Adam EA. Surface immobilization of bone morphogenetic protein 2 via a self-assembled monolayer formation induces cell differentiation. *Acta Biomater*. 2012;8(2):772-80.

128. Yang F, Wang J, Hou J, Guo H, Liu CS. Bone regeneration using cell-mediated responsive degradable PEG-based scaffolds incorporating with rhBMP-2. *Biomaterials*. 2013;34(5):1514-28.
129. Kim HK, Shim WS, Kim SE, Lee KH, Kang E, Kim JH, et al. Injectable In Situ-Forming pH/Thermo-Sensitive Hydrogel for Bone Tissue Engineering. *Tissue Eng Part A*. 2009;15(4):923-33.
130. Quinlan E, Thompson EM, Matsiko A, O'Brien FJ, Lopez-Noriega A. Long-term controlled delivery of rhBMP-2 from collagen-hydroxyapatite scaffolds for superior bone tissue regeneration. *J Controlled Release*. 2015;207:112-9.
131. Kolambkar YM, Boerckel JD, Dupont KM, Bajin M, Huebsch N, Mooney DJ, et al. Spatiotemporal delivery of bone morphogenetic protein enhances functional repair of segmental bone defects. *Bone*. 2011;49(3):485-92.
132. Seo BB, Choi H, Koh JT, Song SC. Sustained BMP-2 delivery and injectable bone regeneration using thermosensitive polymeric nanoparticle hydrogel bearing dual interactions with BMP-2. *J Controlled Release*. 2015;209:67-76.
133. Blackwood KA, Bock N, Dargaville TR, Ann Woodruff M. Scaffolds for Growth Factor Delivery as Applied to Bone Tissue Engineering. *Int J Polym Sci*. 2012;2012:1-25.
134. Haidar ZS, Hamdy RC, Tabrizian M. Delivery of recombinant bone morphogenetic proteins for bone regeneration and repair. Part A: Current challenges in BMP delivery. *Biotechnol Lett*. 2009;31(12):1817-24.
135. Anderson JM, Rodriguez A, Chang DT. Foreign body reaction to biomaterials. *Semin Immunol*. 2008;20(2):86-100.
136. Williams DF. On the mechanisms of biocompatibility. *Biomaterials*. 2008;29(20):2941-53.
137. Morais JM, Papadimitrakopoulos F, Burgess DJ. Biomaterials/tissue interactions: possible solutions to overcome foreign body response. *AAPS J*. 2010;12(2):188-96.
138. Iwasaki A, Medzhitov R. Control of adaptive immunity by the innate immune system. *Nat Immunol*. 2015;16(4):343-53.
139. Badylak SF, Gilbert TW. Immune response to biologic scaffold materials. *Semin Immunol*. 2008;20(2):109-16.
140. Amini AR, Wallace JS, Nukavarapu SP. Short-term and long-term effects of orthopedic biodegradable implants. *J Long Term Eff Med Implants*. 2011;21(2):93-122.
141. Santos SG, Lamghari M, Almeida CR, Oliveira MI, Neves N, Ribeiro AC, et al. Adsorbed fibrinogen leads to improved bone regeneration and correlates with differences in the systemic immune response. *Acta Biomater*. 2013;9(7):7209-17.
142. Luttikhuisen DT, Harmsen MC, Van Luyn MJ. Cellular and molecular dynamics in the foreign body reaction. *Tissue Eng*. 2006;12(7):1955-70.
143. Yahyouche A, Zhidao X, Czernuszka JT, Clover AJ. Macrophage-mediated degradation of crosslinked collagen scaffolds. *Acta Biomater*. 2011;7(1):278-86.
144. Brown BN, Valentin JE, Stewart-Akers AM, McCabe GP, Badylak SF. Macrophage phenotype and remodeling outcomes in response to biologic scaffolds with and without a cellular component. *Biomaterials*. 2009;30(8):1482-91.
145. Pirraco RP, Reis RL, Marques AP. Effect of monocytes/macrophages on the early osteogenic differentiation of hBMSCs. *J Tissue Eng Regen Med*. 2013;7(5):392-400.
146. Higgins DM, Basaraba RJ, Hohnbaum AC, Lee EJ, Grainger DW, Gonzalez-Juarrero M. Localized immunosuppressive environment in the foreign body response to implanted biomaterials. *Am J Pathol*. 2009;175(1):161-70.
147. Wu G, Hunziker EB, Zheng Y, Wismeijer D, Liu Y. Functionalization of deproteinized bovine bone with a coating-incorporated depot of BMP-2 renders the material

- efficiently osteoinductive and suppresses foreign-body reactivity. *Bone*. 2011;49(6):1323-30.
148. Liu WE, Ma ML, Bratlie KM, Dang TT, Langer R, Anderson DG. Real-time in vivo detection of biomaterial-induced reactive oxygen species. *Biomaterials*. 2011;32(7):1796-801.
149. Nair PNR, Schug J. Observations on healing of human tooth extraction sockets implanted with bioabsorbable polylactic-polyglycolic acids (PLGA) copolymer root replicas: A clinical, radiographic, and histologic follow-up report of 8 cases. *Oral Surg Oral Med Oral Pathol Oral Radiol Endod*. 2004;97(5):559-69.
150. Ji W, Yang F, Seyednejad H, Chen Z, Hennink WE, Anderson JM, et al. Biocompatibility and degradation characteristics of PLGA-based electrospun nanofibrous scaffolds with nanoapatite incorporation. *Biomaterials*. 2012;33(28):6604-14.
151. Wu G, Liu Y, Iizuka T, Hunziker EB. The effect of a slow mode of BMP-2 delivery on the inflammatory response provoked by bone-defect-filling polymeric scaffolds. *Biomaterials*. 2010;31(29):7485-93.
152. Schliephake H, Weich HA, Dullin C, Gruber R, Frahse S. Mandibular bone repair by implantation of rhBMP-2 in a slow release carrier of polylactic acid--an experimental study in rats. *Biomaterials*. 2008;29(1):103-10.
153. Ratanavaraporn J, Furuya H, Tabata Y. Local suppression of pro-inflammatory cytokines and the effects in BMP-2-induced bone regeneration. *Biomaterials*. 2012;33(1):304-16.
154. Moizhess TG. Carcinogenesis induced by foreign bodies. *Biochemistry-Moscow*. 2008;73(7):763-75.
155. Hanahan D, Weinberg RA. Hallmarks of cancer: the next generation. *Cell*. 2011;144(5):646-74.
156. Meira LB, Bugni JM, Green SL, Lee CW, Pang B, Borenshtein D, et al. DNA damage induced by chronic inflammation contributes to colon carcinogenesis in mice. *J Clin Invest*. 2008;118(7):2516-25.
157. Tazawa H, Tatemichi M, Sawa T, Gilbert I, Ma N, Hiraku Y, et al. Oxidative and nitrate stress caused by subcutaneous implantation of a foreign body accelerates sarcoma development in Trp53<sup>±</sup> mice. *Carcinogenesis*. 2007;28(1):191-8.
158. Weber A, Strehl A, Springer E, Hansen T, Schad A, Kirkpatrick CJ. Biomaterial-induced sarcomagenesis is not associated with microsatellite instability. *Virchows Arch*. 2009;454(2):195-201.
159. Williams DF. Carcinogenicity of implantable materials: experimental and epidemiological evidence. *Int Urogynecol J*. 2014;25(5):577-80.
160. Nakamura T, Shimizu Y, Okumura N, Matsui T, Hyon SH, Shimamoto T. Tumorigenicity of poly-L-lactide (PLLA) plates compared with medical-grade polyethylene. *J Biomed Mater Res*. 1994;28(1):17-25.
161. Nakamura T, Shimizu Y, Takimoto Y, Tsuda T, Li YH, Kiyotani T, et al. Biodegradation and tumorigenicity of implanted plates made from a copolymer of epsilon-caprolactone and L-lactide in rat. *J Biomed Mater Res*. 1998;42(4):475-84.
162. Kokorina NA, Zakharkin SO, Krebsbach PH, Nussenbaum B. Treatment effects of rhBMP-2 on invasiveness of oral carcinoma cell lines. *Laryngoscope*. 2011;121(9):1876-80.
163. Sand JP, Kokorina NA, Zakharkin SO, Lewis JS, Jr., Nussenbaum B. BMP-2 expression correlates with local failure in head and neck squamous cell carcinoma. *Otolaryngol Head Neck Surg*. 2014;150(2):245-50.

164. Williams DF. The Biomaterials Conundrum in Tissue Engineering. *Tissue Eng Part A*. 2014;20(7-8):1129-31.
165. Williams DF. Regulatory biocompatibility requirements for biomaterials used in regenerative medicine. *J Mater Sci-Mater Med*. 2015;26(2):89
166. ISO 10093-3:2014 Biological evaluation of medical devices - Part 3. Tests for genotoxicity, carcinogenicity and reproductive toxicity. Geneva. *International Organisation for Standardisation*. 2014; 3<sup>rd</sup> edition
167. Gerullis H, Georgas E, Boros M, Klosterhalfen B, Eimer C, Arndt C, et al. Inflammatory Reaction as Determinant of Foreign Body Reaction Is an Early and Susceptible Event after Mesh Implantation. *Biomed Res Int*. 2014;Article ID510807,6 pages
168. Eldesoqi K, Henrich D, El-Kady AM, Arbid MS, Abd El-Hady BM, Marzi I, et al. Safety Evaluation of a Bioglass-Polylactic Acid Composite Scaffold Seeded with Progenitor Cells in a Rat Skull Critical-Size Bone Defect. *PLoS one*. 2014;9(2). e87642
169. Baker DW, Zhou J, Tsai YT, Patty KM, Weng H, Tang EN, et al. Development of optical probes for in vivo imaging of polarized macrophages during foreign body reactions. *Acta Biomater*. 2014;10(7):2945-55.
170. Zhou J, Tsai YT, Weng H, Baker DW, Tang LP. Real time monitoring of biomaterial-mediated inflammatory responses via macrophage-targeting NIR nanoprobes. *Biomaterials*. 2011;32(35):9383-90.
171. Kato S, Akagi T, Sugimura K, Kishida A, Akashi M. Evaluation of biological responses to polymeric biomaterials by RT-PCR analysis IV: study of c-myc, c-fos and p53 mRNA expression. *Biomaterials*. 2000;21(5):521-7.
172. Ward JM. The two-year rodent carcinogenesis bioassay - Will it survive? *J Toxicol Pathol*. 2007;20(1):13-9.
173. Long GG, Morton D, Peters T, Short B, Skydsgaard M. Alternative Mouse Models for Carcinogenicity Assessment: Industry Use and Issues with Pathology Interpretation. *Toxicol Pathol*. 2010;38(1):43-50.
174. Cohen SM. Human carcinogenic risk evaluation: An alternative approach to the two-year rodent bioassay. *Toxicol Sci*. 2004;80(2):225-9.
175. Takanashi S, Hara K, Aoki K, Usui Y, Shimizu M, Haniu H, et al. Carcinogenicity evaluation for the application of carbon nanotubes as biomaterials in rash2 mice. *Sci Rep*. 2012;2:498
176. Kirsch T, Nickel J, Sebald W. BMP-2 antagonists emerge from alterations in the low-affinity binding epitope for receptor BMPR-II. *EMBO J*. 2000;19(13):3314-24.
177. Wei G, Jin Q, Giannobile WV, Ma PX. Nano-fibrous scaffold for controlled delivery of recombinant human PDGF-BB. *J Controlled Release*. 2006;112(1):103-10.
178. Fei ZQ, Hu YY, Wu DC, Wu H, Lu R, Bai JP, et al. Preparation and property of a novel bone graft composite consisting of rhBMP-2 loaded PLGA microspheres and calcium phosphate cement. *J Mater Sci-Mater Med*. 2008;19(3):1109-16.
179. Mustafa K, Wennerberg A, Wroblewski J, Hultenby K, Lopez BS, Arvidson K. Determining optimal surface roughness of TiO<sub>2</sub> blasted titanium implant material for attachment, proliferation and differentiation of cells derived from human mandibular alveolar bone. *Clin Oral Implants Res*. 2001;12(5):515-25.
180. Chang SE, Foster S, Betts D, Marnock WE. DOK, a cell line established from human dysplastic oral mucosa, shows a partially transformed non-malignant phenotype. *Int J Cancer*. 1992;52(6):896-902.
181. Warnakulasuriya S. Global epidemiology of oral and oropharyngeal cancer. *Oral Oncol*. 2009;45(4-5):309-16.

182. Costea DE, Hills A, Osman AH, Thurlow J, Kalna G, Huang X, et al. Identification of two distinct carcinoma-associated fibroblast subtypes with differential tumor-promoting abilities in oral squamous cell carcinoma. *Cancer Res.* 2013;73(13):3888-901.
183. Attard G, Rizzo S, Ledaki I, Clark J, Reid AH, Thompson A, et al. A novel, spontaneously immortalized, human prostate cancer cell line, Bob, offers a unique model for pre-clinical prostate cancer studies. *Prostate.* 2009;69(14):1507-20.
184. Lorens JB, Jang Y, Rossi AB, Payan DG, Bogenberger JM. Optimization of regulated LTR-mediated expression. *Virology.* 2000;272(1):7-15.
185. Dabija-Wolter G, Cimpan MR, Costea DE, Johannessen AC, Sornes S, Neppelberg E, et al. Fusobacterium nucleatum enters normal human oral fibroblasts in vitro. *J Periodontol.* 2009;80(7):1174-83.
186. Lange V, Picotti P, Domon B, Aebersold R. Selected reaction monitoring for quantitative proteomics: a tutorial. *Mol Syst Biol.* 2008;4:222.
187. Robinson NE, Robinson AB. Prediction of protein deamidation rates from primary and three-dimensional structure. *Proc Natl Acad Sci U S A.* 2001;98(8):4367-72.
188. Kroksveen AC, Aasebo E, Vethe H, Van Pesch V, Franciotta D, Teunissen CE, et al. Discovery and initial verification of differentially abundant proteins between multiple sclerosis patients and controls using iTRAQ and SID-SRM. *J Proteomics.* 2013;78:312-25.
189. Poldervaart MT, Gremmels H, van Deventer K, Fledderus JO, Oner FC, Verhaar MC, et al. Prolonged presence of VEGF promotes vascularization in 3D bioprinted scaffolds with defined architecture. *J Controlled Release.* 2014;184:58-66.
190. Hanseler P, Ehrbar M, Kruse A, Fischer E, Schibli R, Ghayor C, et al. Delivery of BMP-2 by two clinically available apatite materials: in vitro and in vivo comparison. *J Biomed Mater Res A.* 2015;103(2):628-38.
191. McCormack E, Bruserud O, Gjertsen BT. Animal models of acute myelogenous leukaemia - development, application and future perspectives. *Leukemia.* 2005;19(5):687-706.
192. Liang X, Osman TA, Sapkota D, Neppelberg E, Lybak S, Liavaag PG, et al. Rapid adherence to collagen IV enriches for tumour initiating cells in oral cancer. *Eur J Cancer.* 2014;50(18):3262-70.
193. Coleman SJ, Watt J, Arumugam P, Solaini L, Carapuca E, Ghallab M, et al. Pancreatic cancer organotypics: High throughput, preclinical models for pharmacological agent evaluation. *World J Gastroenterol : WJG.* 2014;20(26):8471-81.
194. Costea DE, Loro LL, Dimba EA, Vintermyr OK, Johannessen AC. Crucial effects of fibroblasts and keratinocyte growth factor on morphogenesis of reconstituted human oral epithelium. *J Invest Dermatol.* 2003;121(6):1479-86.
195. Varghese F, Bukhari AB, Malhotra R, De A. IHC Profiler: an open source plugin for the quantitative evaluation and automated scoring of immunohistochemistry images of human tissue samples. *PLoS one.* 2014;9(5):e96801.
196. Hsu EL, Ghodasra JH, Ashtekar A, Nickoli MS, Lee SS, Stupp SI, et al. A comparative evaluation of factors influencing osteoinductivity among scaffolds designed for bone regeneration. *Tissue Eng Part A.* 2013;19(15-16):1764-72.
197. Jeon O, Song SJ, Yang HS, Bhang SH, Kang SW, Sung MA, et al. Long-term delivery enhances in vivo osteogenic efficacy of bone morphogenetic protein-2 compared to short-term delivery. *Biochem Biophys Res Commun.* 2008;369(2):774-80.
198. Sharmin F, Adams D, Pensak M, Dukas A, Lieberman J, Khan Y. Biofunctionalizing devitalized bone allografts through polymer-mediated short and long term growth factor delivery. *J Biomed Mater Res A.* 2015.

199. Brown KV, Li B, Guda T, Perrien DS, Guelcher SA, Wenke JC. Improving bone formation in a rat femur segmental defect by controlling bone morphogenetic protein-2 release. *Tissue Eng Part A*. 2011;17(13-14):1735-46.
200. Cho TJ, Gerstenfeld LC, Einhorn TA. Differential temporal expression of members of the transforming growth factor beta superfamily during murine fracture healing. *J Bone Miner Res*. 2002;17(3):513-20.
201. Okubo Y, Bessho K, Fujimura K, Kusumoto K, Ogawa Y, Iizuka T. Expression of bone morphogenetic protein in the course of osteoinduction by recombinant human bone morphogenetic protein-2. *Clin Oral Implants Res*. 2002;13(1):80-5.
202. Fassbender M, Minkwitz S, Strobel C, Schmidmaier G, Wildemann B. Stimulation of bone healing by sustained bone morphogenetic protein 2 (BMP-2) delivery. *Int J Mol Sci*. 2014;15(5):8539-52.
203. Liu T, Wu G, Wismeijer D, Gu Z, Liu Y. Deproteinized bovine bone functionalized with the slow delivery of BMP-2 for the repair of critical-sized bone defects in sheep. *Bone*. 2013;56(1):110-8.
204. Lin CL, Lin CH, Chang HC, Su MC. Protein Attachment on Nanodiamonds. *J Phys Chem A*. 2015;119(28):7704-11.
205. Song Z, Wu C, Sun S, Li H, Wang D, Gong J, et al. Quantitative analysis of factors influencing tissue-engineered bone formation by detecting the expression levels of alkaline phosphatase and bone gamma-carboxylglutamate protein 2. *Exp Ther Med*. 2015;9(4):1097-102.
206. Bi X, You Z, Gao J, Fan X, Wang Y. A functional polyester carrying free hydroxyl groups promotes the mineralization of osteoblast and human mesenchymal stem cell extracellular matrix. *Acta Biomater*. 2014;10(6):2814-23.
207. Kimura Y, Miyazaki N, Hayashi N, Otsuru S, Tamai K, Kaneda Y, et al. Controlled release of bone morphogenetic protein-2 enhances recruitment of osteogenic progenitor cells for de novo generation of bone tissue. *Tissue Eng Part A*. 2010;16(4):1263-70.
208. Liskova J, Babchenko O, Varga M, Kromka A, Hadraba D, Svindrych Z, et al. Osteogenic cell differentiation on H-terminated and O-terminated nanocrystalline diamond films. *Int J Nanomedicine*. 2015;10:869-84.
209. Phillips JE, Petrie TA, Creighton FP, Garcia AJ. Human mesenchymal stem cell differentiation on self-assembled monolayers presenting different surface chemistries. *Acta Biomater*. 2010;6(1):12-20.
210. Bacakova L, Filova E, Parizek M, Ruml T, Svorcik V. Modulation of cell adhesion, proliferation and differentiation on materials designed for body implants. *Biotechnol Adv*. 2011;29(6):739-67.
211. Kloss FR, Steinmuller-Nethl D, Stigler RG, Ennemoser T, Rasse M, Hachl O. In vivo investigation on connective tissue healing to polished surfaces with different surface wettability. *Clin Oral Implants Res*. 2011;22(7):699-705.
212. Man HB, Kim H, Kim HJ, Robinson E, Liu WK, Chow EK, et al. Synthesis of nanodiamond-daunorubicin conjugates to overcome multidrug chemoresistance in leukemia. *Nanomedicine*. 2014;10(2):359-69.
213. Javed A, Afzal F, Bae JS, Gutierrez S, Zaidi K, Pratap J, et al. Specific Residues of RUNX2 Are Obligatory for Formation of BMP2-Induced RUNX2-SMAD Complex to Promote Osteoblast Differentiation. *Cells Tissues Organs*. 2009;189(1-4):133-7.
214. Goldberg K, Krueger A, Meinhardt T, Kroutil W, Mautner B, Liese A. Novel immobilization routes for the covalent binding of an alcohol dehydrogenase from *Rhodococcus ruber* DSM 44541. *Tetrahedron Asymmetry*. 2008;19(10):1171-3.
215. Kashiwagi K, Tsuji T, Shiba K. Directional BMP-2 for functionalization of titanium surfaces. *Biomaterials*. 2009;30(6):1166-75.

216. Wipff PJ, Majd H, Acharya C, Buscemi L, Meister JJ, Hinz B. The covalent attachment of adhesion molecules to silicone membranes for cell stretching applications. *Biomaterials*. 2009;30(9):1781-9.
217. Lee SS, Huang BJ, Kaltz SR, Sur S, Newcomb CJ, Stock SR, et al. Bone regeneration with low dose BMP-2 amplified by biomimetic supramolecular nanofibers within collagen scaffolds. *Biomaterials*. 2013;34(2):452-9.
218. Seeherman HJ, Li XJ, Bouxsein ML, Wozney JM. rhBMP-2 induces transient bone resorption followed by bone formation in a nonhuman primate core-defect model. *J Bone Joint Surg Am*. 2010;92(2):411-26.
219. Zara JN, Siu RK, Zhang X, Shen J, Ngo R, Lee M, et al. High doses of bone morphogenetic protein 2 induce structurally abnormal bone and inflammation in vivo. *Tissue Eng Part A*. 2011;17(9-10):1389-99.
220. Kim HK, Oxendine I, Kamiya N. High-concentration of BMP2 reduces cell proliferation and increases apoptosis via DKK1 and SOST in human primary periosteal cells. *Bone*. 2013;54(1):141-50.
221. Pelaez M, Susin C, Lee J, Fiorini T, Bisch FC, Dixon DR, et al. Effect of rhBMP-2 dose on bone formation/maturation in a rat critical-size calvarial defect model. *J Clin Periodontol*. 2014;41(8):827-36.
222. Lam CX, Hutmacher DW, Schantz JT, Woodruff MA, Teoh SH. Evaluation of polycaprolactone scaffold degradation for 6 months in vitro and in vivo. *J Biomed Mater Res A*. 2009;90(3):906-19.
223. Mountziaris PM, Spicer PP, Kasper FK, Mikos AG. Harnessing and Modulating Inflammation in Strategies for Bone Regeneration. *Tissue Eng Part B Rev*. 2011;17(6):393-402.
224. Bennewitz NL, Babensee JE. The effect of the physical form of poly(lactic-co-glycolic acid) carriers on the humoral immune response to co-delivered antigen. *Biomaterials*. 2005;26(16):2991-9.
225. Nel A, Xia T, Madler L, Li N. Toxic potential of materials at the nanolevel. *Science*. 2006;311(5761):622-7.
226. Jones JA, Chang DT, Meyerson H, Colton E, Kwon IK, Matsuda T, et al. Proteomic analysis and quantification of cytokines and chemokines from biomaterial surface-adherent macrophages and foreign body giant cells. *J Biomed Mater Res A*. 2007;83(3):585-96.
227. Anderson JM, Jones JA. Phenotypic dichotomies in the foreign body reaction. *Biomaterials*. 2007;28(34):5114-20.
228. Collier TO, Anderson JM, Brodbeck WG, Barber T, Healy KE. Inhibition of macrophage development and foreign body giant cell formation by hydrophilic interpenetrating polymer network. *J Biomed Mater Res A*. 2004;69(4):644-50.
229. Brodbeck WG, Patel J, Voskerician G, Christenson E, Shive MS, Nakayama Y, et al. Biomaterial adherent macrophage apoptosis is increased by hydrophilic and anionic substrates in vivo. *Proc Natl Acad Sci U S A*. 2002;99(16):10287-92.
230. Dai XH, Wei Y, Zhang XH, Meng S, Mo XJ, Liu X, et al. Attenuating Immune Response of Macrophage by Enhancing Hydrophilicity of Ti Surface. *J Nanomater*. 2015.
231. Battiston KG, Labow RS, Santerre JP. Protein binding mediation of biomaterial-dependent monocyte activation on a degradable polar hydrophobic ionic polyurethane. *Biomaterials*. 2012;33(33):8316-28.
232. van Buul GM, Villafuertes E, Bos PK, Waarsing JH, Kops N, Narcisi R, et al. Mesenchymal stem cells secrete factors that inhibit inflammatory processes in short-

- term osteoarthritic synovium and cartilage explant culture. *Osteoarthritis Cartilage*. 2012;20(10):1186-96.
233. Bocker W, Docheva D, Prall WC, Egea V, Pappou E, Rossmann O, et al. IKK-2 is required for TNF-alpha-induced invasion and proliferation of human mesenchymal stem cells. *J Mol Med (Berl)*. 2008;86(10):1183-92.
234. Yang X, Ricciardi BF, Hernandez-Soria A, Shi Y, Pleshko Camacho N, Bostrom MP. Callus mineralization and maturation are delayed during fracture healing in interleukin-6 knockout mice. *Bone*. 2007;41(6):928-36.
235. Hutton DL, Kondragunta R, Moore EM, Hung BP, Jia X, Grayson WL. Tumor necrosis factor improves vascularization in osteogenic grafts engineered with human adipose-derived stem/stromal cells. *PLoS one*. 2014;9(9):e107199.
236. Glass GE, Chan JK, Freidin A, Feldmann M, Horwood NJ, Nanchahal J. TNF-alpha promotes fracture repair by augmenting the recruitment and differentiation of muscle-derived stromal cells. *Proc Natl Acad Sci U S A*. 2011;108(4):1585-90.
237. Huang RL, Yuan Y, Tu J, Zou GM, Li Q. Exaggerated inflammatory environment decreases BMP-2/ACS-induced ectopic bone mass in a rat model: implications for clinical use of BMP-2. *Osteoarthritis Cartilage*. 2014;22(8):1186-96.
238. Scott MA, Levi B, Askarinam A, Nguyen A, Rackohn T, Ting K, et al. Brief review of models of ectopic bone formation. *Stem Cells Dev*. 2012;21(5):655-67.
239. Ring A, Langer S, Tilkorn D, Goertz O, Henrich L, Stricker I, et al. Induction of angiogenesis and neovascularization in adjacent tissue of plasma-collagen-coated silicone implants. *Eplasty*. 2010;10.
240. McNally AK, Anderson JM. Phenotypic expression in human monocyte-derived interleukin-4-induced foreign body giant cells and macrophages in vitro: Dependence on material surface properties. *J Biomed Mater Res A*. 2015;103(4):1380-90.
241. Silfversward CJ, Sisask G, Larsson S, Ohlsson C, Frost A, Ljunggren O, et al. Bone formation in interleukin-4 and interleukin-13 depleted mice. *Acta Orthop*. 2008;79(3):410-20.
242. Lind M, Deleuran B, Yssel H, Fink-Eriksen E, Thestrup-Pedersen K. IL-4 and IL-13, but not IL-10, are chemotactic factors for human osteoblasts. *Cytokine*. 1995;7(1):78-82.
243. Finkenzeller G, Hager S, Stark GB. Effects of bone morphogenetic protein 2 on human umbilical vein endothelial cells. *Microvasc Res*. 2012;84(1):81-5.
244. Ozawa M, Inaguma M, Takahashi M, Kataoka F, Krueger A, Osawa E. Preparation and behavior of brownish, clear nanodiamond colloids. *Adv Mater*. 2007;19(9):1201-06.
245. Schrand AM, Huang HJ, Carlson C, Schlager JJ, Osawa E, Hussain SM, et al. Are diamond nanoparticles cytotoxic? *J Phys Chem B*. 2007;111(1):2-7.
246. Thomas V, Halloran BA, Ambalavanan N, Catledge SA, Vohra YK. In vitro studies on the effect of particle size on macrophage responses to nanodiamond wear debris. *Acta Biomater*. 2012;8(5):1939-47.
247. Puzyr AP, Baron AV, Purtov KV, Bortnikov EV, Skobelev NN, Moginaya OA, et al. Nanodiamonds with novel properties: A biological study. *Diam Relat Mat*. 2007;16(12):2124-8.
248. Yuan Y, Chen Y, Liu J-H, Wang H, Liu Y. Biodistribution and fate of nanodiamonds in vivo. *Diam Relat Mat*. 2009;18(1):95-100.
249. Bouard D, Alazard-Dany D, Cosset FL. Viral vectors: from virology to transgene expression. *Br J Pharmacol*. 2009;157(2):153-65.
250. Hadler-Olsen E, Wetting HL, Rikardsen O, Steigen SE, Kanapathippillai P, Grenman R, et al. Stromal impact on tumor growth and lymphangiogenesis in human carcinoma xenografts. *Virchows Arch*. 2010;457(6):677-92.

251. Troy T, Jekic-McMullen D, Sambucetti L, Rice B. Quantitative comparison of the sensitivity of detection of fluorescent and bioluminescent reporters in animal models. *Mol Imaging*. 2004;3(1):9-23.
252. Jarzabek MA, Huszthy PC, Skafnesmo KO, McCormack E, Dicker P, Prehn JH, et al. In vivo bioluminescence imaging validation of a human biopsy-derived orthotopic mouse model of glioblastoma multiforme. *Mol Imaging*. 2013;12(3):161-72.
253. Clark AK, Taubenberger AV, Taylor RA, Niranjana B, Chea ZY, Zotenko E, et al. A bioengineered microenvironment to quantitatively measure the tumorigenic properties of cancer-associated fibroblasts in human prostate cancer. *Biomaterials*. 2013;34(20):4777-85.
254. Black PC, Shetty A, Brown GA, Esparza-Coss E, Metwalli AR, Agarwal PK, et al. Validating bladder cancer xenograft bioluminescence with magnetic resonance imaging: the significance of hypoxia and necrosis. *BJU Int*. 2010;106(11):1799-804.
255. Brutkiewicz S, Mendonca M, Stantz K, Comerford K, Bigsby R, Hutchins G, et al. The expression level of luciferase within tumour cells can alter tumour growth upon in vivo bioluminescence imaging. *Luminescence*. 2007;22(3):221-8.
256. Saur D, Seidler B, Schneider G, Algul H, Beck R, Senekowitsch-Schmidtke R, et al. CXCR4 expression increases liver and lung metastasis in a mouse model of pancreatic cancer. *Gastroenterology*. 2005;129(4):1237-50.
257. Szentirmai O, Baker CH, Lin N, Szucs S, Takahashi M, Kiryu S, et al. Noninvasive bioluminescence imaging of luciferase expressing intracranial U87 xenografts: Correlation with magnetic resonance imaging determined tumor volume and longitudinal use in assessing tumor growth and antiangiogenic treatment effect. *Neurosurgery*. 2006;58(2):365-72.
258. Soares AF, Xavier RL, da Costa Miguel MC, de Souza LB, Pinto LP. Bone morphogenetic protein-2/4 and bone morphogenetic protein receptor type IA expression in metastatic and nonmetastatic oral squamous cell carcinoma. *Am J Otolaryngol*. 2010;31(4):266-71.
259. Raida M, Clement JH, Leek RD, Ameri K, Bicknell R, Niederwieser D, et al. Bone morphogenetic protein 2 (BMP-2) and induction of tumor angiogenesis. *J Cancer Res Clin Oncol*. 2005;131(11):741-50.
260. Yan CL, Grimm WA, Garner WL, Qin L, Travis T, Tan NM, et al. Epithelial to Mesenchymal Transition in Human Skin Wound Healing Is Induced by Tumor Necrosis Factor-alpha through Bone Morphogenetic Protein-2. *Am J Pathol*. 2010;176(5):2247-58.
261. Liu J, Ben QW, Yao WY, Zhang JJ, Chen DF, He XY, et al. BMP2 induces PANC-1 cell invasion by MMP-2 overexpression through ROS and ERK. *Front Biosci (Landmark Ed)*. 2012;17:2541-9.
262. Geng S, Guo Y, Wang Q, Li L, Wang J. Cancer stem-like cells enriched with CD29 and CD44 markers exhibit molecular characteristics with epithelial-mesenchymal transition in squamous cell carcinoma. *Arch Dermatol Res*. 2013;305(1):35-47.
263. Kim BR, Oh SC, Lee DH, Kim JL, Lee SY, Kang MH, et al. BMP-2 induces motility and invasiveness by promoting colon cancer stemness through STAT3 activation. *Tumour Biol*. 2015.
264. Jogi A, Vaapil M, Johansson M, Pahlman S. Cancer cell differentiation heterogeneity and aggressive behavior in solid tumors. *Ups J Med Sci*. 2012;117(2):217-24.
265. Zhang X, Cruz FD, Terry M, Remotti F, Matushansky I. Terminal differentiation and loss of tumorigenicity of human cancers via pluripotency-based reprogramming. *Oncogene*. 2013;32(18):2249-60.

266. Holtzhausen A, Golzio C, How T, Lee YH, Schiemann WP, Katsanis N, et al. Novel bone morphogenetic protein signaling through Smad2 and Smad3 to regulate cancer progression and development. *FASEB J*. 2014;28(3):1248-67.
267. Dwivedi N, Chandra S, Kashyap B, Raj V, Agarwal A. Suprabasal expression of Ki-67 as a marker for the severity of oral epithelial dysplasia and oral squamous cell carcinoma. *Contemp Clin Dent*. 2013;4(1):7-12.
268. Tumuluri V, Thomas GA, Fraser IS. The relationship of proliferating cell density at the invasive tumour front with prognostic and risk factors in human oral squamous cell carcinoma. *J Oral Pathol Med*. 2004;33(4):204-8.
269. Chu HY, Luo HL, Wang HQ, Chen XN, Li P, Bai Y, et al. Silencing BMP-2 expression inhibits A549 and H460 cell proliferation and migration. *Diagn Pathol*. 2014;9:123.
270. Hsu MY, Rovinsky S, Penmatcha S, Herlyn M, Muirhead D. Bone morphogenetic proteins in melanoma: angel or devil? *Cancer Metastasis Rev*. 2005;24(2):251-63.
271. Singh A, Morris RJ. The Yin and Yang of bone morphogenetic proteins in cancer. *Cytokine Growth Factor Rev*. 2010;21(4):299-313.
272. Jin H, Pi J, Huang X, Huang F, Shao W, Li S, et al. BMP2 promotes migration and invasion of breast cancer cells via cytoskeletal reorganization and adhesion decrease: an AFM investigation. *Appl Microbiol Biotechnol*. 2012;93(4):1715-23.
273. Fei ZH, Yao CY, Yang XL, Huang XE, Ma SL. Serum BMP-2 up-regulation as an indicator of poor survival in advanced non-small cell lung cancer patients. *Asian Pac J Cancer Prev*. 2013;14(9):5293-9.
274. Zhang Y, Chen X, Qiao M, Zhang BQ, Wang N, Zhang Z, et al. Bone morphogenetic protein 2 inhibits the proliferation and growth of human colorectal cancer cells. *Oncol Rep*. 2014;32(3):1013-20.
275. Zhang J, Ge Y, Sun L, Cao J, Wu Q, Guo L, et al. Effect of bone morphogenetic protein-2 on proliferation and apoptosis of gastric cancer cells. *Int J Med Sci*. 2012;9(2):184-92.
276. Jin Y, Tipoe GL, Liong EC, Lau TY, Fung PC, Leung KM. Overexpression of BMP-2/4, -5 and BMP-1A associated with malignancy of oral epithelium. *Oral Oncol*. 2001;37(3):225-33.
277. Gao Q, Tong W, Luria JS, Wang Z, Nussenbaum B, Krebsbach PH. Effects of bone morphogenetic protein-2 on proliferation and angiogenesis in oral squamous cell carcinoma. *Int J Oral Maxillofac Surg*. 2010;39(3):266-71.
278. Elinav E, Nowarski R, Thaiss CA, Hu B, Jin CC, Flavell RA. Inflammation-induced cancer: crosstalk between tumours, immune cells and microorganisms. *Nat Rev Cancer*. 2013;13(11):759-71.
279. Braakhuis BJM, Bloemena E, Leemans CR, Brakenhoff RH. Molecular analysis of surgical margins in head and neck cancer: More than a marginal issue. *Oral Oncol*. 2010;46(7):485-91.
280. Tabor MP, Brakenhoff RH, Ruijter-Schippers HJ, Kummer JA, Leemans CR, Braakhuis BJM. Genetically altered fields as origin of locally recurrent head and neck cancer: A retrospective study. *Clin Cancer Res*. 2004;10(11):3607-13.
281. Kirkpatrick CJ, Alves A, Kohler H, Kriegsmann J, Bittinger F, Otto M, et al. Biomaterial-induced sarcoma - A novel model to study preneoplastic change. *Am J Pathol*. 2000;156(4):1455-67.
282. Geuze RE, Prins HJ, Oner FC, van der Helm YJ, Schuijff LS, Martens AC, et al. Luciferase labeling for multipotent stromal cell tracking in spinal fusion versus ectopic bone tissue engineering in mice and rats. *Tissue Eng Part A*. 2010;16(11):3343-51.

## **ORIGINAL PAPERS**

**PAPER I**

**Release and bioactivity of bone morphogenetic protein-2 are affected by scaffold binding techniques *in vitro* and *in vivo***

**Suliman S**, Xing Z, Wu X, Xue Y, Pedersen TO, Sun Y, Døskeland AP, Nickel J, Waag T, Lygre H, Finne-Wistrand A, Steinmüller-Nethl D, Krueger A, Mustafa K.

*J Control Release.* 2015;197:148–157.





## Release and bioactivity of bone morphogenetic protein-2 are affected by scaffold binding techniques *in vitro* and *in vivo*

Salwa Suliman <sup>a,\*</sup>, Zhe Xing <sup>a,1</sup>, Xujun Wu <sup>b</sup>, Ying Xue <sup>a</sup>, Torbjorn O. Pedersen <sup>a</sup>, Yang Sun <sup>c</sup>, Anne P. Døskeland <sup>d</sup>, Joachim Nickel <sup>e,f</sup>, Thilo Waag <sup>i</sup>, Henning Lygre <sup>g</sup>, Anna Finne-Wistrand <sup>c</sup>, Doris Steinmüller-Nethl <sup>h</sup>, Anke Krueger <sup>i</sup>, Kamal Mustafa <sup>a,\*</sup>

<sup>a</sup> Department of Clinical Dentistry, Center for Clinical Dental Research, University of Bergen, Norway

<sup>b</sup> Department of Cranio-Maxillofacial and Oral Surgery, Medical University of Innsbruck, Innsbruck, Austria

<sup>c</sup> Department of Fibre and Polymer Technology, Royal Institute of Technology, KTH, Stockholm, Sweden

<sup>d</sup> Department of Biomedicine, University of Bergen, Norway

<sup>e</sup> Chair Tissue Engineering and Regenerative Medicine, University Hospital of Würzburg, Germany

<sup>f</sup> Fraunhofer Project Group Regenerative Technologies in Oncology, Würzburg, Germany

<sup>g</sup> Department of Clinical Science, University of Bergen, Bergen, Norway

<sup>h</sup> DiaCoating GmbH, Innsbruck, Austria

<sup>i</sup> Institute of Organic Chemistry, University of Würzburg, Würzburg, Germany

### ARTICLE INFO

#### Article history:

Received 27 June 2014

Accepted 3 November 2014

Available online 10 November 2014

#### Chemical compounds studied in this article:

L-lactide (PubChem CID: 107983)

Caprolactone (PubChem CID 10401)

Benzoquinone (PubChem CID: 4650)

#### Keywords:

Drug delivery

Functionalization

Growth factor

Nanodiamond

Copolymer scaffold

Tissue engineering

### ABSTRACT

A low dose of 1  $\mu$ g rhBMP-2 was immobilised by four different functionalising techniques on recently developed poly(L-lactide)-co-( $\epsilon$ -caprolactone) [(poly(LLA-co-CL)] scaffolds. It was either (i) physisorbed on unmodified scaffolds [PHY], (ii) physisorbed onto scaffolds modified with nanodiamond particles [nDP-PHY], (iii) covalently linked onto nDPs that were used to modify the scaffolds [nDP-COV] or (iv) encapsulated in microspheres distributed on the scaffolds [MICS]. Release kinetics of BMP-2 from the different scaffolds was quantified using targeted mass spectrometry for up to 70 days. PHY scaffolds had an initial burst of release while MICS showed a gradual and sustained increase in release. In contrast, NDP-PHY and NDP-COV scaffolds showed no significant release, although NDP-PHY scaffolds maintained bioactivity of BMP-2. Human mesenchymal stem cells cultured *in vitro* showed upregulated BMP-2 and osteocalcin gene expression at both week 1 and week 3 in the MICS and NDP-PHY scaffold groups. These groups also demonstrated the highest BMP-2 extracellular protein levels as assessed by ELISA, and mineralization confirmed by Alizarin red. Cells grown on the PHY scaffolds *in vitro* expressed collagen type 1 alpha 2 early but the scaffold could not sustain rhBMP-2 release to express mineralization. After 4 weeks post-implantation using a rat mandible critical-sized defect model, micro-CT and Masson trichrome results showed accelerated bone regeneration in the PHY, NDP-PHY and MICS groups. The results demonstrate that PHY scaffolds may not be desirable for clinical use, since similar osteogenic potential was not seen under both *in vitro* and *in vivo* conditions, in contrast to NDP-PHY and MICS groups, where continuous low doses of BMP-2 induced satisfactory bone regeneration in both conditions. The NDP-PHY scaffolds used here in critical-sized bone defects for the first time appear to have promise compared to growth factors adsorbed onto a polymer alone and the short distance effect prevents adverse systemic side effects.

© 2014 The Authors. Published by Elsevier B.V. This is an open access article under the CC BY-NC-ND license (<http://creativecommons.org/licenses/by-nc-nd/3.0/>).

### 1. Introduction

Reconstruction of critical-sized bone defects continues to be a challenge. The limitations of current treatment methods [1] highlight

the importance of introducing a potent bone substitute or a scaffold that can induce bone healing by unlocking the body's own powers of self-repair; not only should the substrate be osteo-inductive, it must also act as a delivery system for the regenerative cues necessary [2]. The osteo-inductive capacity of the FDA approved recombinant human bone morphogenetic protein (rhBMP-2) in bone and cartilage formation has been confirmed in preclinical models [3] and evaluated in clinical trials [4]. It has usually been delivered in bolus injections with supra-physiological doses to attain a therapeutic effect, leading to severe side effects ranging from heterotopic bone to oedema or high morbidity in cases of spinal fusion [5]. The

\* Corresponding authors at: Department of Clinical Dentistry, Center for Clinical Dental Research, Faculty of Medicine and Dentistry, University of Bergen, 5009 Bergen, Norway. Tel.: +47 55586356; fax: +47 55586568.

E-mail addresses: [salwa.suliman@iko.uib.no](mailto:salwa.suliman@iko.uib.no) (S. Suliman), [kamal.mustafa@iko.uib.no](mailto:kamal.mustafa@iko.uib.no) (K. Mustafa).

<sup>1</sup> Contributed equally.

high doses of rhBMP-2 chosen were used to compensate for short half-life *in vivo* (1–4 h) [6,7].

Many studies have pursued the design of different carriers delivering BMP-2 including implant coatings or organic and inorganic matrices [8–10]. Control over its bioactivity and spatial–temporal presence is essential for a beneficial effect but has been difficult to achieve [1]. To improve the unsatisfactory outcomes resulting from bolus delivery of BMP-2, attempts have been made to develop biomaterial carriers that maintain a sufficient concentration at the application site to stimulate the normal physiological mechanism required for bone regeneration [11]. Adsorption to collagen sponges and soaking of collagen sponges and hydrogels in BMP-2 are the most commonly used potential carrier approaches due to their high binding capacities and successful induction of trabecular bone volume in critical defects of the canine has been reported [12]. Recent reports using FDA approved polymers, such as poly(lactide-co-glycolide) (PLGA) and polycaprolactone (PCL) have looked at functionalising with BMP-2 [13] due to the affinity of rhBMP-2 for molecules such as heparin or RGD peptides [14]. Covalent immobilisation of BMP-2 to biomaterials modified with heparin, plasma treatment, UV light or disulphide bonds [15,16] has also been examined in attempts to improve the stability and increase retention in regeneration sites by reducing the release of BMP-2 and sustaining its activity.

The introduction of micro- and nano-structured materials has been shown to increase the surface area of scaffolds, allowing for numerous non-covalent interactions between the scaffold surface and protein [17]. Protein encapsulation within microspheres is a potent tool to protect its biological activity and enable sustained release over longer periods [18]. PLGA has generated great interest as a copolymer for microsphere fabrication due to its biocompatibility as well as the ability to tailor its *in vivo* lifetime [11]. This can be achieved by varying the polymer molecular weight, composition, microsphere size and distribution. Several studies have shown that the rate of release depends on the microsphere size, therefore by mixing particles with different sizes one can obtain a degree of control over release [19]. This control of the release profile of growth factors results in optimised concentrations for growth, making it suitable for experimental designs lasting for a long term.

Surface coatings with diamonds at the nano-level gained significance in the medical field after it was shown to demonstrate chemical stability, and to enhance mechanical properties and biocompatibility [20]. In recent years, research has focused on nano-topographic surface modifications aiming to allow for numerous non-covalent interactions between the surface and protein, resulting in adsorbed protein layers which in turn increase cellular adhesion and durability of biomedical implants [21,22], improving various biological applications including delivery of growth factors [23,24]. Previous work showed enhanced cellular response through coating with nanocrystalline diamond (NCD) films [25]. NCD modified titanium dental implant surfaces with terminal oxygen groups that interacted strongly with rhBMP-2 allowing the physisorption of BMP-2. This was demonstrated by greatly enhanced osseointegration [26]. Nanodiamond particles (nDPs) provided enhanced surface properties enhancing bone formation [27,28], encouraging further studies of binding growth factors onto nDP to evaluate their bioactivity.

Long-term delivery of BMP-2 in mini pig models proved enhancement of *in vivo* osteogenic efficacy of the protein compared to short-term delivery [29], while burst release has shown significance in an ectopic bone-forming model using transplanted hydrogels [30] rather than in long-term osteogenic activity. It is, however, difficult to compare these approaches due to the variety in animal models, doses and delivery vehicles used, although collectively, they have resulted in understanding how to design an optimum delivery system. Therefore, since the release of BMP-2 and its effect on the tissues depend on the carrier, method of immobilisation and subsequent mode of delivery, the release kinetics and osteoinductive capacity of different loading approaches need further evaluation.

Degradable poly(L-lactide-co-ε-caprolactone) [Poly(LLA-co-CL)], an aliphatic polyester, copolymer of L-lactide and ε-caprolactone has been extensively studied as a scaffold for bone regeneration [31,32] proving its biocompatibility and osteoconductivity. Mechanical and surface properties can be modified [33] to enhance the regenerative potential, and functionalisation of these scaffolds with nDP to improve cellular response and subsequent bone formation has been reported [28].

In an effort to further improve these scaffolds, the aim of the current study was to study the effect of rhBMP-2 in low amount (1 µg) immobilised on poly (LLA-co-CL) scaffolds utilising four different methods. The release kinetics of rhBMP-2 from the different methods was first quantified *in vitro* and bioactivity evaluated on human mesenchymal stem cells (hMSCs) and then the osteogenic effect of these different methods was further compared *in vivo*.

## 2. Materials and methods

### 2.1. Poly(LLA-co-CL) scaffold fabrication (CL scaffold)

Scaffolds were fabricated as previously described [31]. Scaffolds were punched out in two different dimensions for *in vitro* and *in vivo* experiments (*in vitro*: 12 mm diameter and 1.3 mm thickness) and (*in vivo*: 6 mm diameter and 2.5 mm thickness).

### 2.2. Scaffold functionalisation and BMP-2 immobilisation techniques

#### 2.2.1. BMP-2 production

BMP-2 cDNA was prepared corresponding to residues 283–396 of the mature protein plus an N-terminal MA extension. The BMP-2 protein was expressed in *Escherichia coli* (*E. coli*), isolated from inclusion bodies, renatured and purified as previously described [34]. One microgram of BMP-2 was used per scaffold for each type of functionalisation for *in vitro* with hMSC and *in vivo* experiments.

#### 2.2.2. Physisorbed BMP-2 (PHY scaffold)

BMP-2 was physisorbed onto unmodified poly(LLA-co-CL) scaffolds as follows: scaffolds were placed on a sterilised hydrophobic surface (M Barrier Film, Parafilm®) and 1 µg of BMP-2/50 µl phosphate buffered saline (PBS) was dropped in two increments of 25 µl each onto the surface of the scaffold. The first aliquot was allowed to adsorb under humid shaking conditions for 30 min, after which the second aliquot was added and left for 30 min before the scaffold was used for *in vitro* or *in vivo* experiments.

#### 2.2.3. Colloidal nDP production

Acid purified detonation diamond (Gansu Lingyun Corp. Lanzhou, China) was subjected to attrition milling using a method previously described [35] achieving a narrow size distribution at ~5 nm particle diameter (measured by dynamic light scattering in water) and low agglomeration of the diamond particles.

#### 2.2.4. Scaffolds modified with nDP and physisorbed with BMP-2 (nDP-PHY scaffold)

Scaffolds were modified with the nDP solution (2% (w/v), i.e. 20 mg/ml) by a vacuum technique: 0.5 ml nDP solution and one scaffold were put in a glass beaker and perfused in vacuum. The vacuum chamber was evacuated down to the pressure where the nDP–water–solution changes into the vapour phase and the nDP burst into the scaffold surface. This cycle was repeated 10 times. After the modification, the nDP modified scaffolds were rinsed with distilled water and dried in vacuum for 8 h. Brunauer–Emmett–Teller (BET) method using Argon at 87 K according to DIN ISO 9277 was performed to quantify the amount of nDP on the porous scaffold and the concentration of nDP was determined to be 14 mg in 1 g scaffold material. To physisorb the BMP-2, the modified scaffolds were treated with aforementioned protocol for PHY.

### 2.2.5. nDP functionalisation with BMP-2 (nDP-COV scaffold)

To functionalise nDP with benzoquinone, 189 mg of mechanically de-agglomerated nDP was suspended in 20 ml of PBS (pH 8) and 150 mg of benzoquinone (1.38 mmol) was added (all from VWR International, Radnor, PA, US). After stirring for 24 h at room temperature (RT) the reaction mixture was centrifuged and the nDP was washed with PBS (pH 7.4) and deionized water. Then nDP scaffolds were functionalised with BMP-2 by suspending 20 mg of benzoquinone-functionalised nDP in 15 ml of PBS buffer (pH 6). After adding 10 µg BMP-2 the reaction mixture was stirred for 24 h at RT. The nDP was centrifuged and then the supernatant was checked for residual BMP-2 and then discarded. The precipitate was washed with PBS (pH 7.4) and deionized water. The scaffolds were then modified with the functionalised nDP according to the procedure described in Section 2.2.4.

### 2.2.6. Microsphere preparation and scaffold modification (MICS scaffold)

BMP-2-loaded PLGA5050 (Purac Biochem, Gorinchem, Netherlands) microspheres were fabricated using a previously described water-in-oil-in-water double emulsion solvent extraction technique [11,36]. Briefly, 1 ml of a 50 µg/ml BMP-2 solution was emulsified in a solution of 15% (w/v) PLGA5050 in 5 ml of dichloromethane using a probe ultrasonicator (Branson sonifier cell disruptor 200, USA). The mixture was then immediately re-emulsified for 60 s in 10 ml of a 1% w/v aqueous poly(vinyl alcohol) (PVA, 87–89 mol% hydrolysed, Mw = 13,000–23,000) solution to create the double emulsion. The product was then added to 100 ml of a 0.5% w/v aqueous PVA solution and 100 ml of a 2% w/v aqueous isopropanol solution and stirred for 2 h. The microspheres were centrifuged, washed 5 times and vacuum dried into a free flowing powder (Braun Biotech International SpeedVac Concentrator SVC 10H Savant, USA). BMP-2 loaded microspheres were incorporated into the porous poly(LLA-co-CL) scaffold using a seeding technique described previously [37] with slight modifications. Depending on the amount of BMP-2 for loading, dry microspheres were dispersed in 100 µl ethanol using an ultrasonic bath (VWR International). Fifty microlitres of the microsphere suspension was placed onto both sides of the scaffold and dried overnight under vacuum.

The loading efficiency of the microspheres was determined using a solvent-extraction technique [38]. Approximately 20 mg of microparticles was dissolved in 1 ml of dichloromethane for 6 h at 37 °C. The entrapped rhBMP-2 was extracted from the organic phase to the aqueous phase by incubation with 5 ml of PBS for an additional 24 h. The concentration of rhBMP-2 was analysed by a commercially available human BMP-2 enzyme-linked immunosorbent assay (ELISA) (RnD Systems, Minneapolis, Minnesota, USA). The average loading efficiency was 0.04%. This optimization method was performed three times. Accordingly the amount of microspheres needed to contain exactly 1 µg of BMP-2 from loading efficiency is calculated, i.e. 2.5 mg microparticles contains 1 µg, each optimisation added 2.5 mg to the scaffold.

### 2.3. In vitro BMP-2 release kinetics

Scaffolds were immersed in 1 ml of PBS in glass test tubes (Duran®, Wertheim, Germany) and incubated in a shaking water bath (Julabo®, SW22, Germany) at 37 °C. Half of the supernatant was collected and replaced with fresh PBS at predetermined time points up to 70 days.

### 2.4. Sample preparation for selected reaction monitoring (SRM) analysis

rhBMP-2 (residues 283–396) expressed in *E. coli* was purchased (RELIATech GmbH, Wolfenbüttel, Germany). Four peptides derived from the 26 kDa protein by trypsinisation were tested for SRM analysis. Only one peptide NYQDMVVEGCGCR representative of BMP-2 revealed good transitions and was therefore selected for relative quantification of the protein. A stable isotope-labelled internal standard (SIS)

corresponding to that signature peptide was purchased in AQUA QuantPro quality (Thermo Fisher Scientific, Waltham, MA, USA). The C-terminal arginine for the SIS was labelled with <sup>13</sup>C and <sup>15</sup>N resulting in a mass difference of 10 Da to the corresponding non-labelled peptide. In addition, cysteine was carbamidomethylated and methionine was oxidized. The chemically synthesised modified peptides were reported to be stable by the manufacturer. The peptide was optimised by direct infusion on a Q-Trap 5500 (AB SCIEX, MA, USA). Twenty five femtomole of SIS peptide NYQDMVVEGCGCR was spiked into samples containing unknown amounts of BMP-2 in low-binding tubes (LoBind, Eppendorf). The mixture was lyophilised (Centrivap® Centrifugal, USA) prior to in-solution protein digestion according to the protocol described previously (<http://www.uib.no/file-archive/in-solution-protein-digestion.pdf>). Prior to liquid chromatography SRM-mass spectrometry (LC SRM-MS) analysis, the mixtures of reduced and alkylated tryptic peptides were desalted using reverse phase Oasis® HLBµElution Plate 30 µm (Waters, Milford, MA, USA) as described previously [39]. The eluted peptides were dried in a speed vacuum drier and finally suspended in 8 µl of 1% FA and 2% ACN. In order to oxidize all methionine residues, H<sub>2</sub>O<sub>2</sub> was added in a final concentration of 0.5%, and the samples were incubated for 30 min at 30 °C. The experiment was performed in triplicate. For each measurement, slightly different SRM methods were used and improved progressively to measure the release with addition of heavy peptide. The data shown in Fig. 1 were obtained with the most optimised SRM method, considered the most robust and representative of the conclusion derived from all measurements performed.

### 2.5. SRM analysis

LC SRM-MS analysis was performed on a Q-Trap 5500 coupled to a Dionex Ultimate system (Thermo Scientific, MA, USA) as previously described [39]. The protein digest was dissolved in 2% ACN, 0.1% FA and loaded into the instrument. For quantification of the signature peptide from BMP-2, all y transitions with significant intensity were used and a mean of the ratio values calculated to obtain ratio Light/Heavy (L/H). The Q1 values for the light peptide were 802.319, that for the SIS heavy labelled peptide 807.32. The collision energy used for SRM analysis was 45.5 eV. The raw data files generated were processed using Skyline (MacCoss Lab Software version 2.5).

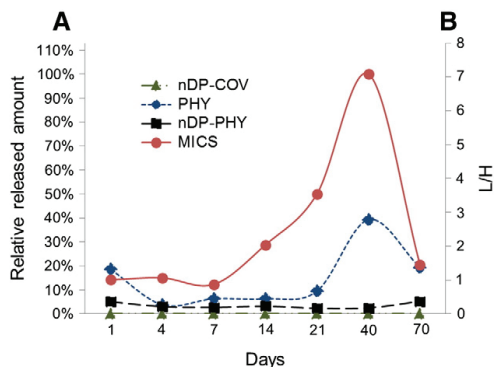


Fig. 1. Release kinetics of BMP-2 measured by SRM. (Axis-A) Relative amount released where 100% value corresponds to the highest value observed for the total amount of BMP-2 measured at a specific time point. (Axis-B) Release over time of rhBMP-2 from the different scaffolds expressed by the ratio (L/H) between endogenous light (L) and heavy synthetic (H) peptide spiked-in our sample measured by SRM. The figure is a representative of the data from the most optimised SRM method obtained from triplicate measurements.

## 2.6. Cell maintenance and seeding

Primary hMSCs (StemCell™ Technologies, Vancouver, BC, Canada) were expanded in MSCGM™ complete medium (Lonza, Basel, Switzerland) following the manufacturer's instructions. Flow cytometry used to assess the cells' purity showed that >90% of cells expressed CD29, CD44, CD105, and CD166 and that they lacked expression of CD14, CD34, and CD45. Morphology of the hMSCs was assessed by a light microscope (Nikon TS100, Tokyo, Japan). Cells used in the experiments were from passages 3 to 6. The cells were seeded onto the scaffolds at a density of  $2 \times 10^5$  per scaffold and allowed to distribute better by a plate shaker (MixMate® Eppendorf, Hamburg, Germany) for 5 min before incubation at 37 °C and 5% CO<sub>2</sub> [40]. Once the cells reached 80–90% confluence the medium was replaced with osteogenic medium (MSCGM™ complete medium plus 50 µg/ml ascorbic acid,  $10^{-8}$  M dexamethasone, and 3.5 mM β-glycerophosphate) and changed every fourth day. All cultures were performed in triplicate and the experiments were repeated three times.

Human osteoblast-like cells (HOB) were used as a positive control for the *in vitro* mineralization staining (Alizarin red S) (Section 2.10). They were isolated from routine surgical samples from patients being treated at the Section for Oral and Maxillofacial Surgery, Department of Clinical Dentistry, University of Bergen and Haukeland University Hospital. The procedure was approved by the Ethics Committee at the University of Bergen. The protocol for isolation and expansion has been previously described [41].

## 2.7. Scanning electron microscope (SEM) analysis

Attachment and spreading of hMSC on scaffolds at 1 and 3 days after seeding were analysed by SEM (Jeol JSM 7400F, Tokyo, Japan), voltage of 10 kV as previously described [40].

## 2.8. Genes expressed by cultured hMSC *in vitro*

Total RNA was isolated from *in vitro* cultures at week 1 and week 3 using a Tissue RNA isolation kit (Maxwell®, Promega, Madison, WI, USA), and reverse transcribed according to the manufacturer's instructions using the High capacity cDNA Reverse Transcription Kit (Applied Biosystems®, Carlsbad, CA, USA). Real-time reverse transcription-polymerase chain reaction (RT-PCR) was performed as previously described [40]. Taqman® gene expression assays (Applied Biosystems®) were used to detect mRNA levels of glyceraldehyde-3-phosphate dehydrogenase (GAPDH), Antigen KI-67 (Ki-67), Runt-related transcription factor 2 (Runx2), BMP-2 receptor 1A (BMPRIA), BMP-2 receptor 2 (BMPRII), Alkaline phosphatase (ALP), Collagen type 1 alpha 2 (Col1α2), Bone morphogenetic protein-2 (BMP-2) and Osteocalcin (OC). The data were analysed with a comparative C<sub>T</sub> method and GAPDH served as endogenous control. Unmodified scaffold (CL) at week 1 was the reference.

## 2.9. Enzyme-linked immunosorbent assay

The culture medium was collected at week 1 and week 3. Human BMP-2 ELISA Development Kit (900-M255, Peprotech, Rocky Hill, NJ, US) was used to measure extracellular and intracellular BMP-2 following the manufacturers' instructions. To measure the intracellular production of BMP-2, the scaffolds with cells from both time points were washed with PBS before incubation at 4 °C on a shaker for 20 min with 175 µl RIPA buffer (Thermo Scientific), 1 × Halt™ Protease Inhibitor Cocktail and 1 × Halt™ Phosphatase Inhibitor Cocktail (Thermo Scientific). This was followed by sonication for 5 min and then centrifugation for 20 min at 16,000 g at 4 °C. The extracted protein was collected and measured using a bicinchoninic acid assay

(BCA) (Pierce BCA Protein Assay Kit, Thermo Scientific) following the manufacturer's instructions.

## 2.10. *In vitro* mineralization

The cell/scaffold constructs were harvested at week 1 of culture, washed thrice in PBS and fixed for 10 min in 4% paraformaldehyde (PFA) (Merck & Co, White House Station, NJ, USA). Alizarin red S staining was performed to determine matrix mineralization. Two percent of alizarin red S powder (Sigma Aldrich) was dissolved in distilled water and pH was adjusted to 4.2 with 0.5% ammonium hydroxide. Constructs were stained for 20 min and imaged with a Nikon TS100 microscope. HOB cells cultured on CL scaffolds for 1 week were used as a positive control.

## 2.11. Animal model of mandibular defects

Male Sprague–Dawley rats (300–350 g) were anaesthetised with isoflurane (IsobaVet®; Schering-Plough, Kenilworth, NJ, USA) combined with O<sub>2</sub> using a custom-made platform and mask. A 1 cm incision was made along the lower border of the mandible and after retracting the muscles a round-shaped bone defect (5 mm diameter) was created in the mandibular angle region. A trephine bur (Komet Medical, Lemgo, Germany) was used. The defect was filled with a scaffold (n = 8 for each experimental group). The muscles were repositioned and the skin closed with resorbable sutures (Vicryl Rapide 4-0; Ethicon, Somerville, NJ, USA). Animals were euthanised with an overdose of CO<sub>2</sub> after 2 and 4 weeks. Mandibles were dissected and the samples were stored in RNAlater (Invitrogen, Carlsbad, CA, USA) for RT-PCR, micro computed tomography (micro-CT) and histological analyses.

## 2.12. Gene expressions *in vivo*

Total RNA was isolated from *in vivo* scaffolds at 2 weeks. Taqman® gene expression assays (Applied Biosystems™, USA) were used to detect mRNA levels of GAPDH, ALP, OC, Runx2, Col1α2, BMP-2, Bone morphogenetic protein-4 (BMP-4), Tartrate-resistant acid phosphatase (TRAP) and Cathepsin K (CTSK). The data were analysed with a comparative C<sub>T</sub> method and GAPDH served as endogenous control. CL served as reference.

## 2.13. Micro-CT analysis

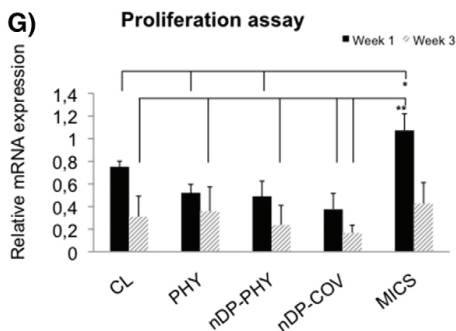
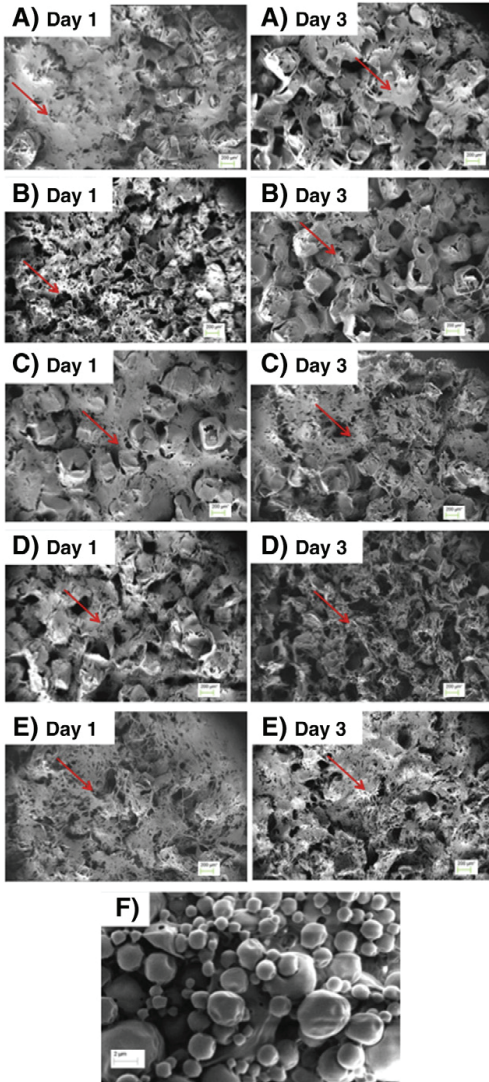
The amount of bone formation within the defects was examined using micro-CT (micro-CT 40, Scanco Medical AG, Bruettisellen, Switzerland) with 19 µm isotropic voxel size and 70 kV, 43 µA tube current, 380 ms exposure time, and 1000 projections [42]. Three-dimensional isosurface rendering and images were constructed with the software provided by Scanco Medical and measurements included the ratio of new bone volume relative to the tissue volume (BV/TV).

## 2.14. Histological evaluation

Specimens for histological examination were processed as previously described [43]. Sections were then stained with Masson's trichrome to confirm the osteoid-like tissue and images were made with an inverted microscope (Nikon Ti, Tokyo, Japan) using the software NIS-Elements AR 4.10.

## 2.15. Statistical analysis

The average values were analysed using SPSS Statistics 21.0 (IBM, Armonk, NY, US). The data were expressed as mean ± standard deviation (SD). Data were tested for variance homogeneity and normal distribution and One-way ANOVA were followed by a multiple-



comparison Tukey test. Analysis of the *in vivo* experiment data was performed with the Kruskal–Wallis test. Differences between the means were considered statistically significant when  $p < 0.05$ .

### 3. Results

#### 3.1. *In vitro* kinetics of BMP-2 release

The release of BMP-2 was monitored through identification of signature peptide NYQDMoxVVEGCcamGCCamR as analysed by SRM. The amount of a signature peptide (L, endogenous peptide) for BMP-2 is related to a known amount of internal standard (H, heavy synthetic peptide) spiked-in our sample, and the ratio (L/H) is used as an index for the amount of BMP-2 released (Fig. 1). The figure is a representative of the data from the most optimised SRM method obtained from triplicate measurements.

In the first 24 h, the PHY scaffolds had an initial burst of release. There was a steady release from the MICS scaffolds starting from 24 h while the nDP-COV scaffold group showed no release. MICS scaffolds showed a gradual increase in release from day 7 on, with the greatest release being found between days 21 and 40. In comparison to the MICS scaffolds, the PHY scaffolds showed a smaller increase in release between days 21 and 40, while the nDP-PHY scaffolds showed a maintained level.

#### 3.2. hMSC attachment and proliferation

SEM images at day 1 and day 3 of culture show the spreading and attachment of hMSC on the different scaffolds. Significantly more cells on the MICS modified group were proliferating on day 7 compared to the other scaffold groups (Fig. 2 G).

#### 3.3. BMP-2 signalling and hMSC differentiation

Similar results were seen between the groups (Fig. 3) for expression of the two main receptors of BMP-2 signalling (BMPRIA and BMPRII). Results showed the highest expression of receptor significantly from the MICS at 3 weeks ( $p = 0.033$ ,  $p = 0.029$ ). At week 1 the nDP-PHY group showed higher but not statistically significant expression compared with the PHY group, while at week 3 the PHY group showed a higher trend, coinciding with the release profile during that period, which was again not statistically significant. A tendency was seen for an increase in the master transcription factor Runx2 in all groups at week 3 compared to week 1 (Fig. 3). Col1 $\alpha$ 2 was upregulated in all groups at week 3 compared to week 1 except in the nDP-COV group, where it was downregulated. In all the other groups, ALP was upregulated at week 3 with nDP-PHY showing the highest tendency (Fig. 3). MICS and nDP-PHY showed the highest BMP-2 expression at both early and late time points (Fig. 3), although this was only significant in the MICS group at week 3. OC was significantly upregulated at week 3 in the MICS group followed by the nDP-PHY group, compared with the other groups.

#### 3.4. *In vitro* endogenous BMP-2 protein expression

The medium was collected at week 1 and week 3 to determine the extracellular release of endogenous BMP-2 from hMSC. The BMP-2 ELISA kit used is sensitive to natural and mammalian-expressed BMP-

**Fig. 2** Attachment and proliferation of hMSC cultured on the different scaffolds. SEM images at days 1 and 3 showing attachment of hMSCs (red arrows) (A) CL, (B) PHY, (C) nDP-PHY, (D) nDP-COV and (E) MICS. Scale bar = 200  $\mu$ m. (F) Higher magnification of MICS scaffold without cells showing the increased surface area resulting from the microspheres. Scale bar = 2  $\mu$ m. (G) The proliferative activity of the hMSC seeded onto the different scaffolds evaluated in terms of mRNA expression of the proliferative marker (Ki67) (\* $p < 0.05$ , \*\* $p < 0.001$ ).

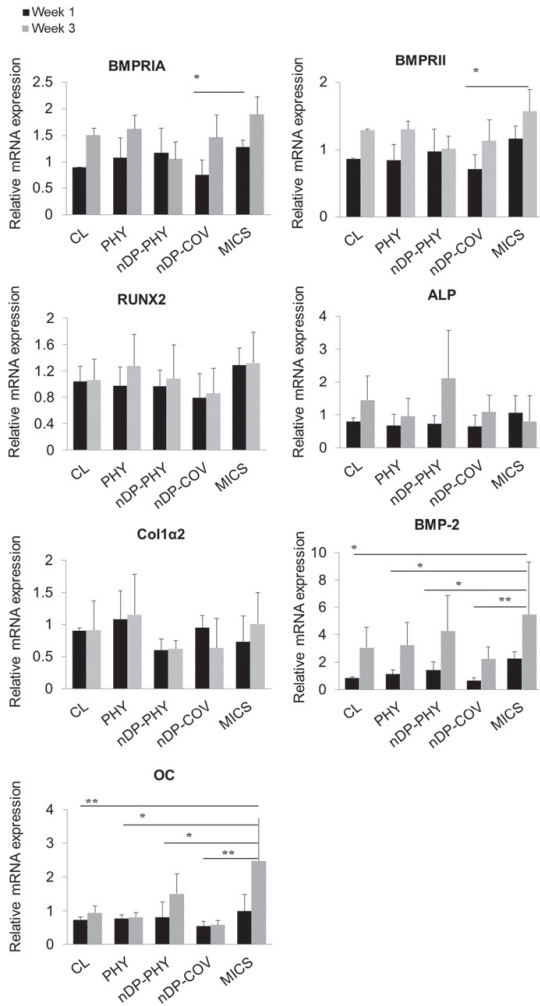


**Fig. 3.** Relative mRNA expression from hMSC cultured *in vitro* after week 1 and week 3. Relative mRNA levels of BMP-2 signalling receptors, transcription factor and osteogenic markers (\* $p < 0.05$ , \*\* $p < 0.001$ ).

2 and does not recognize *E. coli*-expressed rhBMP-2. The levels detected here were therefore protein originating solely from hMSC. Extracellular endogenous BMP-2 showed the lowest expressions in the CL and nDP-COV groups, with minor differences between time points. The highest expression was seen from the MICS group at early and late time points and nDP-PHY at week 1 (Fig. 4A). Intracellular BMP-2 showed the highest levels in the MICS group at both time points and lowest in the nDP-PHY group (Fig. 4B). None were significant.

### 3.5. Alizarin red staining for *in vitro* mineralization

Staining revealed surface mineralization. Most groups showed variable reddish extracellular matrices while vast extracellular darker spots could be observed in the MICS and nDP-PHY group scaffolds as evidence of calcium deposits in the matrix (Fig. 5).

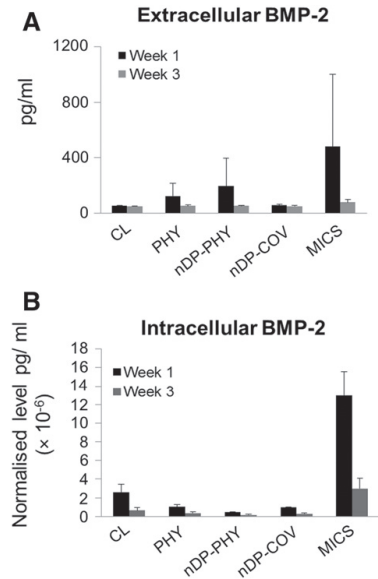


**Fig. 4.** *In vitro* endogenous BMP-2 protein expression by ELISA at week 1 and week 3. (A) for extracellular concentration of BMP-2 secreted in medium and (B) intracellular BMP-2.

### 3.6. Gene expressions from *in vivo* experiments

*In vivo* RT-PCR results showed coherence in several genes with the expressions *in vitro*. The transcription marker Runx2 showed the highest expression on the MICS scaffolds, although not significant. Significant upregulation of the early osteogenic marker ALP was expressed on MICS while COL1 was higher from the PHY scaffolds. OC was upregulated most on MICS scaffolds, followed by expression on nDP-PHY scaffolds, consistent with the *in vitro* results indicating deposition of bone matrix and mineralization. MICS scaffolds also demonstrated significant upregulation of the osteoclast markers TRAP and CTSK at 2 weeks.

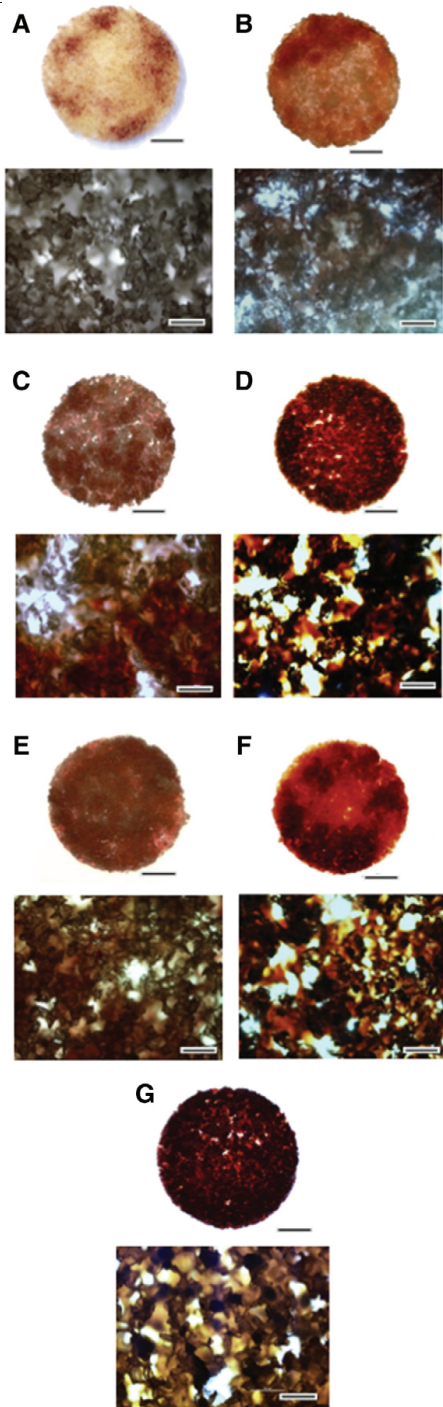
### 3.7. De novo bone formation

Morphometric results with micro-CT show that most of the treated groups had increased bone volume inside the defined defect area compared to the empty group. Bone volume recover was greatest in the PHY and MICS groups at 4 weeks, and that both were significant in comparison to the nDP-COV scaffold group (Fig. 7A). They were followed by nDP-PHY.

Masson's trichrome staining was carried out to identify the osteoid-like tissue and collagen enriched areas in the defects. In the empty group (Fig. 7B) it was predominantly soft tissues growing around and into the defect. The scaffold architecture was highly preserved in the CL and nDP-COV groups compared with other 3 functionalised scaffold groups. Most of the pores of the CL scaffolds were filled with loose fibrous connective tissue without much evidence of osteoid tissue formation. Histological results were in line with the micro-CT analysis showing mostly osteoid formation among the pores of the scaffolds in PHY, nDP-PHY and MICS at an early time point of 4 weeks (Fig. 7D, E and G).

## 4. Discussion

We evaluated the *in vitro* and *in vivo* efficacy of four different modes of rh-BMP-2 delivery utilising a low dose of 1  $\mu$ g.



*In vitro* rhBMP-2 release from scaffolds was evaluated with targeted quantification using SRM and an absolute quantification method (AQUA). The SIS peptide was chemically identical to the native peptide with respect to retention time, ionization efficiency, and fragmentation characteristics. Its mass unit was higher and could therefore be distinguished from the native counterpart during MS analysis permitting the detection of very low concentrations [44]. In the PHY scaffold most of the BMP-2 was located superficially with weak bonds causing the initial burst release. A second increase in release from PHY was seen at a time point when the scaffold is beginning to degrade. This hypothesis is supported by the degradation profile from the same scaffold analysed by *in vitro* hydrolysis where forty days showed to be a sufficient time for significant reduction of its molecular weight contributing to increased degradation [45].

In contrast, the release of BMP-2 from MICS scaffolds was different. Several factors explain this difference, such as the microsphere size and its rate of degradation, which controlled the BMP-2 diffusion in a steadily increased fashion retaining the BMP-2 for an extended time. OC was highly expressed in cells grown on MICS at week 1 ( $p < 0.05$ ) and week 3 *in vitro* and at 2 weeks *in vivo*, implying increased mineralization in comparison to that seen on PHY scaffolds. This demonstrates how long-term sustained delivery of BMP-2 enhances its osteogenic efficacy at the same dose compared to short-term delivery [46]. Differences in the initial burst release of BMP-2 from PHY and nDP-PHY scaffolds could be attributed to the lower amount of protein being only weakly bound to the scaffold in the case of nDP-PHY. No burst release was encountered as in PHY because the interaction of proteins with nDPs is known to be rather strong [47]. Also previous reports where spectroscopic and theoretical investigations were carried out, showed a strong binding of BMP-2 with NCD surfaces [25], supporting the contention that nDP could express similar properties [27]. The nDP modification of copolymer scaffolds has been shown to increase its hydrophilicity [28], facilitating stronger physisorption of rhBMP-2. An overview of different O-termination techniques facilitating surface attachment of organic groups has been reported [21]. The overall binding strength of the noncovalent interaction is governed by a multitude of individual interactions. Several forces were reported to contribute to the overall binding on NCD, such as van der Waals forces, H-bonds and electrostatic interactions. Although the release kinetics were not remarkably different between nDP-PHY and nDP-COV scaffolds, it is clear from our results that the bioactivity of rhBMP-2 was conserved on nDP-PHY scaffolds. Studies suggest that slightly acidic environments stimulate the release of proteins loaded noncovalently on nDP modified surfaces [24], a condition that was absent in our PBS buffer set-up. Body fluids aid degradation of carriers and release of BMP-2 in a variable manner, which is why comparison to the present *in vivo* results is important.

The burst release and degradation of the scaffolds might be accentuated *in vivo* [45], explaining why PHY might show higher trends of early markers such as Runx2 and COL1 *in vivo*, although the difference was not significant. Several factors play a role in bone regeneration *in vivo* [48], which could have assisted the PHY to form mineralized tissue *in vivo* but not *in vitro*. The *in vivo* experiments had different time points from the *in vitro*, bringing another variable to the effect of the release kinetics of the various scaffolds. At 2 weeks *in vivo*, the release profile showed a relatively higher release from MICS, which continued to increase, compared to PHY, and thus had a significant effect on the

**Fig. 5** 3D mineralization *in vitro* visualised with Alizarin red S staining. Macroscopic images (round) and increased magnifications ( $\times 4$ ) images of (A) unseeded CL scaffold, (B) cultured hMSC for 1 week on CL scaffold (C) on PHY, (D) on nDP-PHY, (E) on nDP-COV, (F) on MICS, and (G) HOB cells on CL scaffold (positive control). Scale bar = 500  $\mu\text{m}$ . 3D mineralization *in vitro* visualised with Alizarin red S staining. Macroscopic images (round) and increased magnifications ( $\times 4$ ) images of (A) unseeded CL scaffold, (B) cultured hMSC for 1 week on CL scaffold (C) on PHY, (D) on nDP-PHY, (E) on nDP-COV, (F) on MICS, and (G) HOB cells on CL scaffold (positive control). Scale bar = 500  $\mu\text{m}$ .

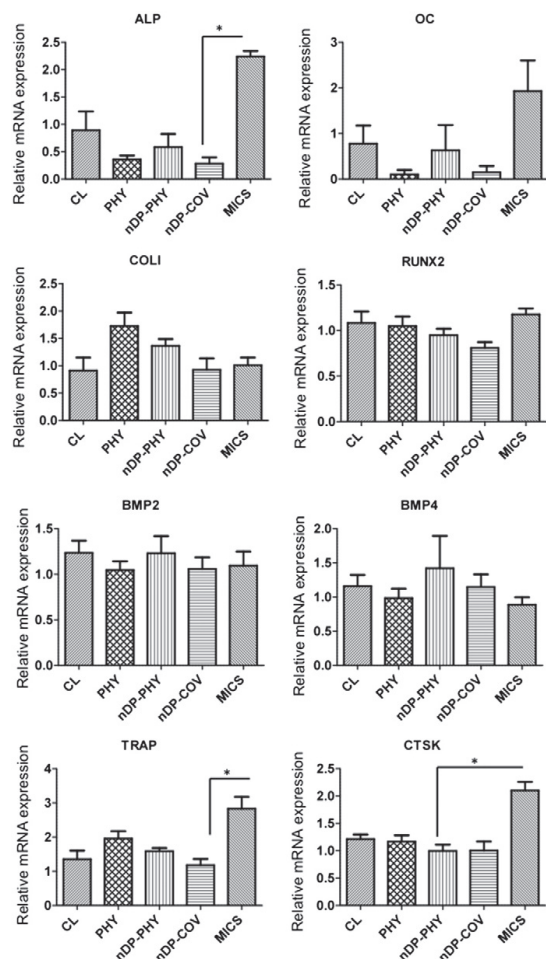


**Fig. 6.** Relative mRNA expression *in vivo* after week 2. Expression of BMP-2 transcription, osteogenic genes and remodelling markers by RT-PCR from animals samples after 2 weeks in place (\* $p < 0.05$ ).

osteogenic marker, ALP. The second cross-sectional analysis *in vivo* was at four weeks which corresponds to between 21 days and 40 days of *in vitro* release kinetics. PHY and MICS showed the significantly higher bone regeneration and nDP-PHY came later, perhaps suggesting the effects of sustained release in low doses from the latter group as seen in the release curve (Fig. 1). Longer-term evaluation *in vivo* is required to fully assess the quality and architecture of new bone.

The *in vitro* results in the present study demonstrated lower ALP expression by cells grown onto MICS scaffolds than on nDP-PHY, with cells from the MICS group still significantly highly proliferative as seen by Ki67 expression at week 1, possibly related to the increased surface area from the microspheres. It has been reported that osteosarcoma cells cultured on NCD implant surfaces showed increased ALP activity in less than 2 weeks of culture [25]. *In vivo*, a significantly higher expression of mRNA ALP was demonstrated from MICS scaffolds indicating bone induction. ALP expression tended to be higher in cells on nDP-PHY scaffolds than on PHY scaffolds both *in vitro* and *in vivo*, although not significantly so, highlighting the effect of nanoparticles

on enhancing the osteoinduction of copolymer scaffolds. A slight upsurge in the BMP-2 kinetic release after almost 40 days in nDP-PHY is believed to be due to the degrading polymer, but in this case the rhBMP-2 is still bound to nDP and bioactive in levels to increase osteogenic differentiation when compared with PHY scaffold. This was confirmed by Alizarin red staining in the nDP-PHY and MICS scaffold groups.

The nDP-COV group showed no release of BMP-2 during the 70 days of incubation and also showed lesser osteogenic potential both *in vitro* and *in vivo*. This demonstrates the high stability of the covalent immobilization of the protein on the diamond surface. The loss of the BMP-2 functionality indicates that the protein is most likely deformed during the binding onto the diamond surface by both the covalent linker and additional, non-covalent interactions. Similar results have been reported previously for the covalent immobilization of other proteins such as enzymes [49]. This brings to our notice the necessity of improving the method for covalently bonding the rhBMP-2 to the nDP without affecting the bioactivity of rhBMP-2. Furthermore, we take into consideration that the *in vitro* design of 3 weeks was not suitable for the nDP-COV group; additional degradation of the scaffold is required to release rhBMP-2. This was evidenced by the observation of limited osteoid tissue around the nDP areas at 4 weeks *in vivo* (Fig. 7F).

BMP-2 exerts a bipolar effect depending on its concentration: osteoprogenitor cells are recruited and differentiated at low doses, whereas osteoclasts are transiently activated at high doses [50]. This was reflected by the *in vivo* expression of TRAP and CTSK, (Fig. 6), both highly expressed by osteoclasts. They were significantly highly expressed in the MICS scaffold group after 2 weeks; *in vivo* this release could be amplified due to environments favourable to erosion of the microspheres. Recent reports [51] have underlined the importance of decreasing the dose of BMP-2 to the lowest level that is compatible with the desired effect of bone formation. BMP-2 is expressed from days 1 to 21 during bone healing [48], hence for delivering BMP-2 for bone regeneration, the ideal carrier would provide sustained release over a period of at least three weeks. Following injury, BMP-2 is released locally into the defect site from the surrounding matrix [48], consistent with the increased BMP-2 levels *in vivo* seen here in all groups, although this increase was not statistically significant. Also consistent with trends seen here, BMP-2 expression is upregulated in differentiating osteoprogenitor cells and maintained for about 21 days [52]. At week 3 *in vitro*, the highest expression was seen in the MICS ( $p < 0.05$ ) and followed by nDP-PHY at both time points. A similar trend in the extracellular protein levels of BMP-2 was shown by ELISA. Comparing the gene and protein expressions of BMP-2 between PHY and nDP-PHY highlights the valuable effect of nDP functionalisation. BMP-2 is an extracellular signalling molecule which is washed out rapidly, thus the protein level of extra- and intra-cellular BMP-2 was reduced at week 3 in all groups [53]. Small amounts induce cellular responses *in vitro*; however exogenously delivered BMP-2 requires ultra-physiological doses for humans compared to animals to overcome the rapid wash out.

It is important to note that *in vitro* statistical relevance was seen in mRNA expressions of the potent osteogenic markers BMP-2 and OC *in vitro*, hence our discussion and subsequent conclusions are based on this finding. Significance *in vivo* was only demonstrated for ALP mRNA from MICS scaffold compared to other osteogenic markers. However, microCT and histological evaluations disclosed a confirmative dimension supporting the interpretations and conclusions related to the osteogenic potential of these scaffolds. The nDP-PHY and MICS scaffolds have strong potential for future applications due to their controlled release of growth factors. Furthermore, the data demonstrated that the protein on nDP-PHY was bioactive with comparable efficacy despite being strongly bound to the carrier (scaffolds), indicating a short distance effect on the local surrounding tissues.

In the clinical trials, high doses of not less than 1 mg BMPs per ml have been used and the complications of this dose have been discussed [54]. However, it is difficult to establish a correlation from animals to humans due to different bone healing mechanisms [55]. Interestingly,

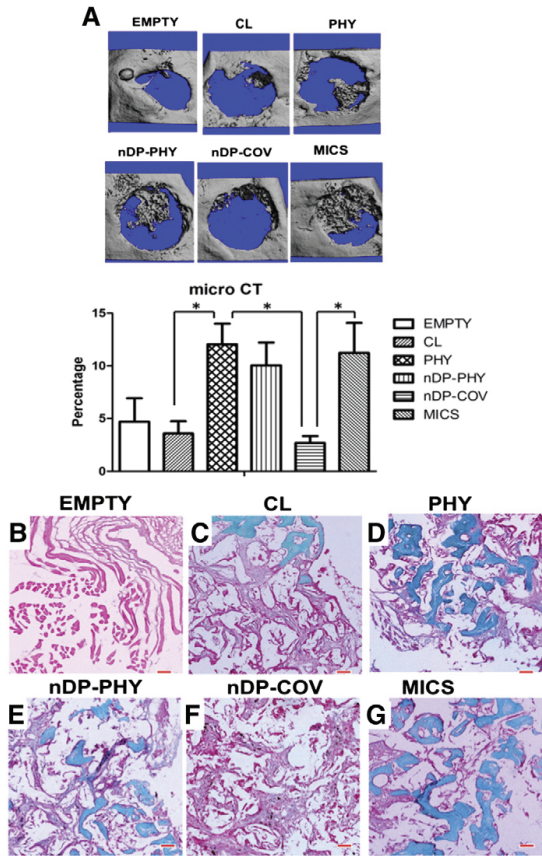


**Fig. 7.** *De novo* bone formation after 4 weeks post-implantation. (A) Micro-CT analysis showing different bone formation volumes inside the region of the defect at 4 weeks ( $p < 0.05$ ). (B–G) Masson trichrome staining of defects implanted with different scaffolds at 4 weeks post-implantation. The bluish green colour indicated osteoid-like tissue and collagen-rich areas. Scale bar = 100 μm.

in our study a low dose of only 1 μg was sufficient to induce *de novo* bone. Very few experiments using comparably low doses *in vivo* have been reported. Researchers used carrier minerals, which might have a confounding osteoinductive effect [56] or including osteoprogenitor cells in the construct [57]. A recent study using collagen sponges in critical sized defects in rat calvaria [58] concluded that rhBMP-2 accelerates local bone formation once reaching an osteoinductive dose threshold at 1.25–2.5 μg in their model, which is not load bearing. Previous reports also proved that non-glycosylated BMP-2 which is produced via bacterial expression systems is less soluble. Despite it having lower biological activity and release *in vitro* compared to glycosylated BMP-2, it significantly increased bone formation at low dosages [59].

Taken together, we conclude from our results that low doses of BMP-2 are found to be bioactive for bone regeneration. Obtaining bone after just 4 weeks *in vivo* suggests accelerated bone regeneration in the PHY, nDP-PHY and MICS groups. Physisorption onto nDP modified copolymer scaffolds is a material reported for the first time in critical sized bone defects and appears to hold great promise compared to growth factors adsorbed solely onto a polymer.

## Acknowledgements

The research leading to these results has received funding by the European Union's Seventh Framework Programme under grant agreement number 242175-VascuBone. The MS work was carried out at the Proteomics Unit at UiB (PROBE) and the authors acknowledge Prof. Frode Berven, Proteomics Unit at the University of Bergen and Dr. Frank Kloss, Medical University of Innsbruck, Austria for the scientific discussions during the design of the experiments. The authors thank Dr. Michele Cottler-Fox, University of Arkansas for Medical Sciences, Little Rock, USA for English revision and constructive criticism of the manuscript.

## References

- [1] K. Lee, E.A. Silva, D.J. Mooney, Growth factor delivery-based tissue engineering: general approaches and a review of recent developments, *J. R. Soc. Interface*, *R. Soc.* 8 (2011) 153–170.
- [2] J.E. Schroeder, R. Moseiff, Tissue engineering approaches for bone repair: concepts and evidence, *Injury* 42 (2011) 609–613.
- [3] Q. Zhang, Q.F. He, T.H. Zhang, X.L. Yu, Q. Liu, F.L. Deng, Improvement in the delivery system of bone morphogenetic protein-2: a new approach to promote bone formation, *Biomed. Mater.* 7 (2012) 045002.
- [4] S. Gowender, C. Csimma, H.K. Genant, A. Valentin-Opran, Y. Amit, R. Arbel, H. Aro, D. Atar, M. Bishay, M.G. Borner, P. Chiron, P. Choong, J. Cinats, B. Courtenay, R. Feibel, B. Geulette, C. Gravel, N. Haas, M. Raschke, E. Hammacher, D. van der Velde, P. Hardy, M. Holt, C. Josten, R.L. Ketterli, B. Lindeque, G. Lob, H. Mathevon, G. McCoy, D. Marsh, R. Miller, E. Munting, S. Oevert, L. Nordstletten, A. Patel, A. Pohl, W. Rennie, P. Reynders, P.M. Rommens, J. Rondia, W.C. Rossouw, P.J. Daneel, S. Ruff, A. Ruter, S. Santavirta, T.A. Schildhauer, C. Gekle, R. Schnettler, D. Segal, H. Seiler, R.B. Snowdowne, J. Stapert, G. Taglang, R. Verdonk, L. Vogels, A. Weckbach, A. Wentzensen, T. Wisniewski, B.M.P.E.i.S.I.T.T.S. Group, Recombinant human bone morphogenetic protein-2 for treatment of open tibial fractures: a prospective, controlled, randomized study of four hundred and fifty patients, *J. Bone Joint Surg.* 84-A (2002) 2123–2134.
- [5] L.B. Shields, G.H. Raque, S.D. Glassman, M. Campbell, T. Vitaz, J. Harring, C.B. Shields, Adverse effects associated with high-dose recombinant human bone morphogenetic protein-2 use in anterior cervical spine fusion, *Spine* 31 (2006) 542–547.
- [6] A.C. Carreira, F.H. Lujdic, E. Halcsik, R.D. Navarro, M.C. Sogayar, J.M. Granjeiro, Bone morphogenetic proteins: facts, challenges, and future perspectives, *J. Dent. Res.* 93 (2014) 335–345.
- [7] J.P. Issa, M.V. Bentley, M.M. Iyomasa, W. Sebald, R.F. De Albuquerque, Sustained release carriers used to delivery bone morphogenetic proteins in the bone healing process, *Anat. Histol. Embryol.* 37 (2008) 181–187.
- [8] T.H. Kim, Y.P. Yun, Y.E. Park, S.H. Lee, W. Yong, J. Kundu, J.W. Jung, J.H. Shim, D.W. Cho, S.E. Kim, H.R. Song, *In vitro* and *in vivo* evaluation of bone formation using solid freeform fabrication-based bone morphogenetic protein-2 releasing PCL/PLGA scaffolds, *Biomed. Mater.* 9 (2014) 025008.
- [9] E.L. Hsu, J.H. Ghodadra, A. Ashtekar, M.S. Nickolis, S.S. Lee, S.I. Stupp, W.K. Hsu, A comparative evaluation of factors influencing osteoinductivity among scaffolds designed for bone regeneration, *Tissue Eng. A* 19 (2013) 1764–1772.
- [10] G. Wu, Y. Liu, T. Izuka, E.B. Hunziker, The effect of a slow mode of BMP-2 delivery on the inflammatory response provoked by bone-defect-filling polymeric scaffolds, *Biomaterials* 31 (2010) 7485–7493.
- [11] D.H. Kempen, L. Lu, T.E. Hefferan, L.B. Creemers, A. Maran, K.L. Classic, W.J. Dhert, M.J. Yaszemski, Retention of *in vitro* and *in vivo* BMP-2 bioactivities in sustained delivery vehicles for bone tissue engineering, *Biomaterials* 29 (2008) 3245–3252.
- [12] S. Asamura, Y. Mochizuki, M. Yamamoto, Y. Tabata, N. Isogai, Bone regeneration using a bone morphogenetic protein-2 saturated slow-release gelatin hydrogel sheet: evaluation in a canine orbital floor fracture model, *Ann. Plast. Surg.* 64 (2010) 496–502.
- [13] S. Srouji, D. Ben-David, R. Lotan, E. Livne, R. Avrahami, E. Zussman, Slow-release human recombinant bone morphogenetic protein-2 embedded within electrospun scaffolds for regeneration of bone defect: *in vitro* and *in vivo* evaluation, *Tissue Eng. A* 17 (2011) 269–277.
- [14] A. Shekaran, A.J. Garcia, Extracellular matrix-mimetic adhesive biomaterials for bone repair, *J. Biomed. Mater. Res. A* 96 (2011) 261–272.
- [15] F. Yang, J. Wang, J. Hou, H. Guo, C. Liu, Bone regeneration using cell-mediated responsive degradable PEG-based scaffolds incorporating with rhBMP-2, *Biomaterials* 34 (2013) 1514–1528.
- [16] H. Zhang, F. Migneco, C.Y. Lin, S.J. Hollister, Chemically-conjugated bone morphogenetic protein-2 on three-dimensional polycaprolactone scaffolds stimulates osteogenic activity in bone marrow stromal cells, *Tissue Eng. A* 16 (2010) 3441–3448.
- [17] T.S. Tsapikouni, Y.F. Missirlis, Protein-material interactions: from micro-to-nano scale, *Sci. Eng. B Adv. Funct. Solid-State Mater.* 152 (2008) 2–7.
- [18] S. Freiberg, X.X. Zhu, Polymer microspheres for controlled drug release, *Int. J. Pharm.* 282 (2004) 1–18.
- [19] C. Nugraha, M. Bora, S.S. Venkatraman, Release retardation of model protein on polyelectrolyte-coated PLGA nano- and microparticles, *PLoS One* 9 (2014) e92393.

- [20] F.R. Kloss, M. Najam-Ul-Haq, M. Rainer, R. Gassner, G. Lepperdinger, C.W. Huck, G. Bonn, F. Klausner, X. Liu, N. Memmel, E. Bertel, J.A. Garrido, D. Steinmuller-Nethl, Nanocrystalline diamond—an excellent platform for life science applications, *J. Nanosci. Nanotechnol.* 7 (2007) 4581–4587.
- [21] A. Krueger, D. Lang, Functionality is key: recent progress in the surface modification of nanodiamond, *Adv. Funct. Mater.* 22 (2012) 890–906.
- [22] M. Mansoorianfar, M.A. Shokrgozar, M. Mehrjoo, E. Tamjid, A. Simchi, Nanodiamonds for surface engineering of orthopedic implants: enhanced biocompatibility in human osteosarcoma cell culture, *Diam. Relat. Mater.* 40 (2013) 107–114.
- [23] V.N. Mochalin, A. Pentecost, X.M. Li, I. Neitzel, M. Nelson, C.Y. Wei, T. He, F. Guo, Y. Gogotsi, Adsorption of drugs on nanodiamond: toward development of a drug delivery platform, *Mol. Pharm.* 10 (2013) 3728–3735.
- [24] L. Moore, M. Gatica, H. Kim, E. Osawa, D. Ho, Multi-protein delivery by nanodiamonds promotes bone formation, *J. Dent. Res.* 92 (2013) 976–981.
- [25] D. Steinmuller-Nethl, F.R. Kloss, M. Najam-Ul-Haq, M. Rainer, K. Larsson, C. Linsmeier, G. Kohler, C. Fehrer, G. Lepperdinger, X. Liu, N. Memmel, E. Bertel, C.W. Huck, R. Gassner, G. Bonn, Strong binding of bioactive BMP-2 to nanocrystalline diamond by physisorption, *Biomaterials* 27 (2006) 4547–4556.
- [26] F.R. Kloss, R. Gassner, J. Preiner, A. Ebner, K. Larsson, O. Hachl, T. Tuli, M. Rasse, D. Moser, K. Laimer, E.A. Nickel, G. Laschober, R. Brunauer, G. Klima, P. Hinterdorfer, D. Steinmuller-Nethl, G. Lepperdinger, The role of oxygen termination of nanocrystalline diamond on immobilisation of BMP-2 and subsequent bone formation, *Biomaterials* 29 (2008) 2433–2442.
- [27] A. Krueger, New carbon materials: biological applications of functionalized nanodiamond materials, *Chemistry* 14 (2008) 1382–1390.
- [28] Z. Xing, T.O. Pedersen, X. Wu, Y. Xue, Y. Sun, A. Finne-Wistrand, F.R. Kloss, T. Waag, A. Krueger, D. Steinmuller-Nethl, K. Mustafa, Biological effects of functionalizing copolymer scaffolds with nanodiamond particles, *Tissue Eng. A* 19 (2013) 1783–1791.
- [29] E.B. Hunziker, L. Enggist, A. Kuffer, D. Buser, Y. Liu, Osseointegration: the slow delivery of BMP-2 enhances osteoinductivity, *Bone* 51 (2012) 98–106.
- [30] G. Bhakta, B. Rai, Z.X. Lim, J.H. Hui, G.S. Stein, A.J. van Wijnen, V. Nurcombe, G.D. Prestwich, S.M. Cool, Hyaluronic acid-based hydrogels functionalized with heparin that support controlled release of bioactive BMP-2, *Biomaterials* 33 (2012) 6113–6122.
- [31] S. Danmark, A. Finne-Wistrand, M. Wendel, K. Arvidson, A.C. Albertsson, K. Mustafa, Osteogenic differentiation by rat bone marrow stromal cells on customized biodegradable polymer scaffolds, *J. Bioact. Compat. Polym.* 25 (2010) 207–223.
- [32] S.B. Idris, S. Danmark, A. Finne-Wistrand, K. Arvidson, A.C. Albertsson, A.I. Bolstad, K. Mustafa, Biocompatibility of polyester scaffolds with fibroblasts and osteoblast-like cells for bone tissue engineering, *J. Bioact. Compat. Polym.* 25 (2010) 567–583.
- [33] U. Edlund, S. Danmark, A.C. Albertsson, A strategy for the covalent functionalization of resorbable polymers with heparin and osteoinductive growth factor, *Biomacromolecules* 9 (2008) 901–905.
- [34] T. Kirsch, J. Nickel, W. Sebald, BMP-2 antagonists emerge from alterations in the low-affinity binding epitope for receptor BMPR-II, *EMBO J.* 19 (2000) 3314–3324.
- [35] A. Krüger, F. Kataoka, M. Ozawa, T. Fujino, Y. Suzuki, A.E. Aleksenskii, A.Y. Vul', E. Osawa, Unusually tight aggregation in detonation nanodiamond: identification and disintegration, *Carbon* 43 (2005) 1722–1730.
- [36] Y. Yang, G. Tang, H. Zhang, Y. Zhao, X. Yuan, Y. Fan, M. Wang, Controlled release of BSA by microsphere-incorporated PLGA scaffolds under cyclic loading, *Mater. Sci. Eng. C* 31 (2011) 350–356.
- [37] G. Wei, Q. Jin, W.V. Giannobile, P.X. Ma, Nano-fibrous scaffold for controlled delivery of recombinant human PDGF-BB, *J. Control. Release* 112 (2006) 103–110.
- [38] Z.Q. Fei, Y.Y. Hu, D.C. Wu, H. Wu, R. Lu, J.P. Bai, H.X. Song, Preparation and property of a novel bone graft composite consisting of rhBMP-2 loaded PLGA microspheres and calcium phosphate cement, *J. Mater. Sci. Mater. Med.* 19 (2008) 1109–1116.
- [39] A.C. Krokvsveen, E. Aasebo, H. Vethe, V. Van Pesch, D. Franciotta, C.E. Teunissen, R.J. Ulvik, C. Vedeler, K.M. Myhr, H. Barsnes, F.S. Berven, Discovery and initial verification of differentially abundant proteins between multiple sclerosis patients and controls using iTRAQ and SID-SRM, *J. Proteome* 78 (2013) 312–325.
- [40] Z. Xing, Y. Xue, S. Danmark, A. Finne-Wistrand, K. Arvidson, S. Hellem, Z.Q. Yang, K. Mustafa, Comparison of short-run cell seeding methods for poly(L-lactide-co-1,5-dioxepan-2-one) scaffold intended for bone tissue engineering, *Int. J. Artif. Organs* 34 (2011) 432–441.
- [41] K. Mustafa, A. Wennerberg, J. Wroblewski, K. Hulthen, B.S. Lopez, K. Arvidson, Determining optimal surface roughness of TiO2 blasted titanium implant material for attachment, proliferation and differentiation of cells derived from human mandibular alveolar bone, *Clin. Oral Implants. Res.* 12 (2001) 515–525.
- [42] J. Schnabl, R. Glueckert, G. Feuchtnr, W. Recheis, T. Potrusil, V. Kuhn, A. Wolf-Magele, H. Riechelmann, G.M. Springl, Sheep as a large animal model for middle and inner ear implantable hearing devices: a feasibility study in cadavers, *Otol. Neurotol.* 33 (2012) 481–489.
- [43] Z. Xing, Y. Xue, S. Danmark, K. Schander, S. Ostvold, K. Arvidson, S. Hellem, A. Finne-Wistrand, A.C. Albertsson, K. Mustafa, Effect of endothelial cells on bone regeneration using poly(L-lactide-co-1,5-dioxepan-2-one) scaffolds, *J. Biomed. Mater. Res.* A 96 (2011) 349–357.
- [44] S.A. Gerber, J. Rush, O. Stemman, M.W. Kirschner, S.P. Gygi, Absolute quantification of proteins and phosphoproteins from cell lysates by tandem MS, *Proc. Natl. Acad. Sci. U. S. A.* 100 (2003) 6940–6945.
- [45] S. Danmark, A. Finne-Wistrand, K. Schander, M. Hakkarainen, K. Arvidson, K. Mustafa, A.C. Albertsson, *In vitro* and *in vivo* degradation profile of aliphatic polyesters subjected to electron beam sterilization, *Acta Biomater.* 7 (2011) 2035–2046.
- [46] O. Jeon, S.J. Song, H.S. Yang, S.H. Bhang, S.W. Kang, M.A. Sung, J.H. Lee, B.S. Kim, Long-term delivery enhances *in vivo* osteogenic efficacy of bone morphogenetic protein-2 compared to short-term delivery, *Biochem. Biophys. Res. Commun.* 369 (2008) 774–780.
- [47] J. Mona, C.J. Kuo, E. Peregudentseva, A.V. Priezhev, C.L. Cheng, Adsorption of human blood plasma on nanodiamond and its influence on activated partial thromboplastin time, *Diam. Relat. Mater.* 39 (2013) 73–77.
- [48] M. Mehta, K. Schmidt-Bleek, G.N. Duda, D.J. Mooney, Biomaterial delivery of morphogens to mimic the natural healing cascade in bone, *Adv. Drug Deliv. Rev.* 64 (2012) 1257–1276.
- [49] K. Goldberg, A. Krueger, T. Meinhardt, W. Kroutil, B. Mautner, A. Liese, Novel immobilization routes for the covalent binding of an alcohol dehydrogenase from *Rhodococcus ruber* DSM 44541, *Tetrahedron Asymmetry* 19 (2008) 1171–1173.
- [50] M. Okamoto, J. Murai, H. Yoshikawa, N. Tsumaki, Bone morphogenetic proteins in bone stimulate osteoclasts and osteoblasts during bone development, *J. Bone Miner. Res. Off. J. Am. Soc. Bone Miner. Res.* 21 (2006) 1022–1033.
- [51] S. Granholm, P. Henn, C. Lindholm, U.H. Lerner, Osteoclast progenitor cells present in significant amounts in mouse calvarial osteoblast isolations and osteoclastogenesis increased by BMP-2, *Bone* 52 (2013) 83–92.
- [52] Z. Huang, E.R. Nelson, R.L. Smith, S.B. Goodman, The sequential expression profiles of growth factors from osteoprogenitors [correction of osteoprogenitors] to osteoblasts *in vitro*, *Tissue Eng.* 13 (2007) 2311–2320.
- [53] E. Birmingham, G.L. Niebur, P.E. McHugh, G. Shaw, F.P. Barry, L.M. McNamara, Osteogenic differentiation of mesenchymal stem cells is regulated by osteocyte and osteoblast cells in a simplified bone niche, *Eur. Cells Mater.* 23 (2012) 13–27.
- [54] M.C. Simmonds, J.V.E. Brown, M.K. Heirs, J.P.T. Higgins, R.J. Mannion, M.A. Rodgers, L.A. Stewart, Safety and effectiveness of recombinant human bone morphogenetic protein-2 for spinal fusion: a meta-analysis of individual-participant data, *Ann. Intern. Med.* 158 (2013) 877–+.
- [55] V.E. Santo, M.E. Gomes, J.F. Mano, R.L. Reis, Controlled release strategies for bone, cartilage, and osteochondral engineering—Part II: challenges on the evolution from single to multiple bioactive factor delivery, *Tissue Eng. B Rev.* 19 (2013) 327–352.
- [56] Y. Liu, K. de Groot, E.B. Hunziker, BMP-2 liberated from biomimetic implant coatings induces and sustains direct ossification in an ectopic rat model, *Bone* 36 (2005) 745–757.
- [57] S. Jo, S. Kim, T.H. Cho, E. Shin, S.J. Hwang, I. Noh, Effects of recombinant human bone morphogenetic protein-2 and human bone marrow-derived stromal cells on *in vivo* bone regeneration of chitosan-poly(ethylene oxide) hydrogel, *J. Biomed. Mater. Res.* A 101 (2013) 892–901.
- [58] M. Pelaez, C. Susin, J. Lee, T. Fiorini, F.C. Bischof, D.R. Dixon, J.C. McPherson, A.N. Buxton III, U.M. Wikesjo, Effect of rhBMP-2 dose on bone formation/maturation in a rat critical-size calvarial defect model, *J. Clin. Periodontol.* 41 (2014) 827–836.
- [59] F.C.J. van de Watering, J. van den Beuken, S.P. van der Woning, A. Briest, A. Eek, H. Qureshi, L. Winnubst, O.C. Boerman, J.A. Jansen, Non-glycosylated BMP-2 can induce ectopic bone formation at lower concentrations compared to glycosylated BMP-2, *J. Control. Release* 159 (2012) 69–77.

## PAPER III

### **Establishment of a bioluminescence model for microenvironmentally induced oral carcinogenesis with implications for screening bioengineered scaffolds**

**Suliman S.** Parajuli H, Sun Y, Johannessen AC, Finne–Wistrand A, McCormack E, Mustafa K, Costea DE.

*Head and Neck.* 2015 doi: 10.1002/hed.24187(Epub ahead of print)



# Establishment of a bioluminescence model for microenvironmentally induced oral carcinogenesis with implications for screening bioengineered scaffolds

Salwa Suliman, BDS,<sup>1,2,3</sup> Himalaya Parajuli, BDS,<sup>2,3</sup> Yang Sun, PhD,<sup>4</sup> Anne Christine Johannessen, PhD,<sup>2,5,6</sup> Anna Finne-Wistrand, PhD,<sup>4</sup> Emmet McCormack, PhD,<sup>7,8</sup> Kamal Mustafa, PhD,<sup>1</sup> Daniela Elena Costea, PhD<sup>2,5,6\*</sup>

<sup>1</sup>Department of Clinical Dentistry, Centre for Clinical Dental Research, University of Bergen, Bergen, Norway, <sup>2</sup>Gade Laboratory for Pathology, Department of Clinical Medicine, University of Bergen, Bergen, Norway, <sup>3</sup>Centre for International Health, Department of Global Public Health and Primary Care, University of Bergen, Bergen, Norway, <sup>4</sup>Department of Fibre and Polymer Technology, KTH Royal Institute of Technology, Stockholm, Sweden, <sup>5</sup>Centre for Cancer Biomarkers, Department of Clinical Medicine, University of Bergen, Bergen, Norway, <sup>6</sup>Department of Pathology, Haukeland University Hospital, Bergen, Norway, <sup>7</sup>Department of Clinical Science, University of Bergen, Bergen, Norway, <sup>8</sup>Department of Medicine, Haematology Section, Haukeland University Hospital, Bergen, Norway.

Accepted 3 July 2015

Published online 00 Month 2015 in Wiley Online Library (wileyonlinelibrary.com). DOI 10.1002/hed.24187

**ABSTRACT:** *Background.* Microenvironmental cues play a major role in head and neck cancer. Biodegradable scaffolds used for bone regeneration might also act as stimulative cues for head and neck cancer. The purpose of this study was to establish an experimental model for precise and noninvasive evaluation of tumorigenic potential of microenvironmental cues in head and neck cancer.

*Methods.* Bioluminescence was chosen to image tumor formation. Early neoplastic oral keratinocyte (DOK) cells were luciferase-transduced (DOK<sup>Luc</sup>), then tested in nonobese diabetic severe combined immunodeficient IL2r $\gamma$  null mice either orthotopically (tongue) or subcutaneously for their potential as "screening sensors" for diverse microenvironmental cues.

*Results.* Tumors formed after inoculation of DOK<sup>Luc</sup> were monitored easier by bioluminescence, and bioluminescence was more sensitive in detecting differences between various microenvironmental cues when compared to manual measurements. Development of tumors from DOK<sup>Luc</sup> grown on scaffolds was also successfully monitored noninvasively by bioluminescence.

*Conclusion.* The model presented here is a noninvasive and sensitive model for monitoring the impact of various microenvironmental cues on head and neck cancer in vivo. © 2015 The Authors Head & Neck Published by Wiley Periodicals, Inc. *Head Neck* 00: 000–000, 2015

**KEY WORDS:** cancer, microenvironment, bioluminescence, tissue engineering, scaffold

## INTRODUCTION

Recent evidence implicates environmental cues as key factors in cancer progression.<sup>1</sup> Among the important determinants is the surrounding stroma, including fibroblasts, endothelial cells, infiltrating immune cells, and extracellular matrix components.<sup>2,3</sup> The scaffolds used in tissue engineering as provisional matrices for cell proliferation and extracellular matrix deposition can also act as microenvironmental cues. The surrounding tissues might react toward these by foreign body reactions or even tumor formation,<sup>4</sup> and long-term subcutaneous implants of nonabsorbable or slowly degrading materials were shown to be tumorigenic.<sup>5,6</sup> Thus, there is a great concern that certain biomaterials may be potential initiators of

malignancies, and the size and surface roughness of certain biomaterials were already suggested to influence tumor formation.<sup>7</sup> To date, at the regulatory level, the basic approach for biomaterials' safety is defined in the International Organization for Standardization 10993.<sup>8,9</sup> These tests start with an initial safety evaluation targeting leachable for cytotoxicity. Genotoxicity and evaluation of mRNA levels of proto-oncogenes and tumor suppressor genes<sup>10</sup> from mammalian or bacterial cells exposed to the biomaterials has also been used as methods for safety check.<sup>11</sup> Current carcinogenicity tests determine the tumorigenic potential of materials and/or their extracts from either single or multiple exposures or contacts over a period of the major portion of the life span of the test animal or transgenic mice.<sup>12</sup> Long-term, conventional 2-year rodent bioassays are often not feasible, with questionable relevance also because of limitations associated with species extrapolation.<sup>13,14</sup> Finding a relevant animal model for every kind of human cancer is impractical, but preclinical animal xenograft tumor models, particularly heterotopic (subcutaneous), have proven useful especially in identifying cytotoxic agents.<sup>15–18</sup> On the other hand, although more technically demanding, the orthotopic xenograft models simulate the same local microenvironment and thus offer the advantage of less complicated translation to the clinical setting.<sup>19</sup>

Scaffolds used for bone regeneration in the oral and maxillofacial area might come in contact with the oral

\*Corresponding author: D. E. Costea, Department of Clinical Medicine and Department of Clinical Dentistry, University of Bergen, 5009 Bergen, Norway. E-mail: daniela.costea@k1.uib.no

Contract grant sponsor: This work was funded by VascuBone project, EU FP7; no. 242175 and Bergen Medical Research Foundation (grant no. 20/2009), The Norwegian Cancer Research Association (grant no. 515970/2011), Norwegian Cancer Society (grant no. 732200), and Helse Vest (grant nos. 911902/2013, 911884, and 911789).

This is an open access article under the terms of the Creative Commons Attribution-NonCommercial-NoDerivs License, which permits use and distribution in any medium, provided the original work is properly cited, the use is non-commercial and no modifications or adaptations are made.

epithelium. Because over 90% of head and neck cancers are, as most of the human malignancies, of epithelial origin,<sup>20,21</sup> there is a need to study the potentially carcinogenic effect of degradable bioengineered scaffolds on oral epithelial cells. To study oral and head and neck carcinogenesis, both orthotopic and heterotopic (subcutaneous) models were previously developed by use of malignant cells derived from established oral or head and neck cancer.<sup>22</sup> In this study, we chose to develop a xenotransplantation model by use of an early neoplastic oral keratinocyte (DOK) cell line derived from early neoplastic oral mucosa.<sup>23</sup> These cells were found to be partly transformed but nontumorigenic in nude mice, and were described as having potential as “screening recipients” for carcinogens *in vitro*.<sup>23</sup>

Different *in vivo* optical imaging modalities have been tested in various tumor models.<sup>24–26</sup> However, there is a need for a noninvasive head and neck cancer model with the ability to detect possible tumorigenic effects of various microenvironmental cues, including implanted scaffolds. Bioluminescent imaging is a well-established method in preclinical investigation of the complexity of cancers<sup>27–29</sup> including head and neck cancer,<sup>30,31</sup> but for a screening of the potential to fully transform and generate malignant tumors from the early neoplastic cells, the application of bioluminescence would offer a novel noninvasive approach. In carcinogenicity testing of biomaterials, controls of a comparable form and shape should be included. However, in the presented system, the use of appropriate controls is not necessary because the inclusion of a positive environment with the use of carcinoma-associated fibroblasts (CAFs) has been developed. The noninvasive *in vivo* visualization for several weeks also provides additional unique advantages over the aforementioned established carcinogenicity testing systems.

To achieve real-time bioluminescence in this study, DOK cells were first transduced to contain the firefly luciferase. They were then tested *in vivo* in NSG mice for their potential as “screening sensors” for diverse microenvironmental cues, such as various types of head and neck CAFs and copolymer scaffolds intended for tissue engineering. The biodegradable poly L-lactide-co-ε-caprolactone (poly[LLA-co-CL]), an aliphatic polyester copolymer of L-lactic acid and ε-caprolactone, has been extensively studied at our laboratory as a scaffold for bone regeneration proving its biocompatibility and osteoconductivity,<sup>8,32</sup> and, hence, was chosen for developing this model.

## MATERIALS AND METHODS

### Cell choice and maintenance

The DOK cell line was purchased from The European Collection of Cell Cultures (Salisbury, Wiltshire, UK).<sup>23</sup> They were maintained in Dulbecco’s modified Eagle’s medium (DMEM) supplemented with 10% fetal calf serum (FCS; Invitrogen, Waltham, MA), 20 μg/mL L-glutamine, 5 μg/mL hydrocortisone (all from Sigma, St. Louis, MO).

CAFs ( $n = 3$ ; CAF1, CAF15\_13, and CAF15\_23) were isolated from histologically confirmed head and neck squamous cell carcinoma, after receiving informed consent.

They were maintained in FAD medium: DMEM/Ham’s F12 1:3 mixture, 1% L-glutamine, 0.4 μg/mL hydrocortisone, 50 μg/mL ascorbic acid, 10 ng/mL epidermal growth factor, 5 μg/mL insulin, and 20 μg/mL transferrin and linoleic acid (all from Sigma) with 10% FCS.

### Luciferase transduction of early neoplastic oral keratinocytes

**Virus production.** DOK wild type (DOK<sup>WT</sup>) cells were transduced with a tTA, L192 construct (expressing luciferase).<sup>33</sup> Infectious retroviral vector particles were produced in Phoenix A cells (LG Standards AB, Borås, Sweden) cultured in DMEM, supplemented with 10% FCS, 1% penicillin-streptomycin, and 1% glutamine. When 70% to 80% was confluent, 8 μL of 50 mM chloroquine (Sigma) was added. Four micrograms of DNA construct (tTA, L192) was mixed with 128 μL of 2M calcium chloride (CaCl<sub>2</sub>) and sterile ddH<sub>2</sub>O to a total volume of 1 mL plus 1 mL of 2×HEPES-buffered (Sigma) and transferred onto each plate. After 12-hour incubation, the medium was replaced by a fresh medium and by DOK’s medium after 24 hours.

### Infection and selection of luciferase-transduced early neoplastic oral keratinocyte

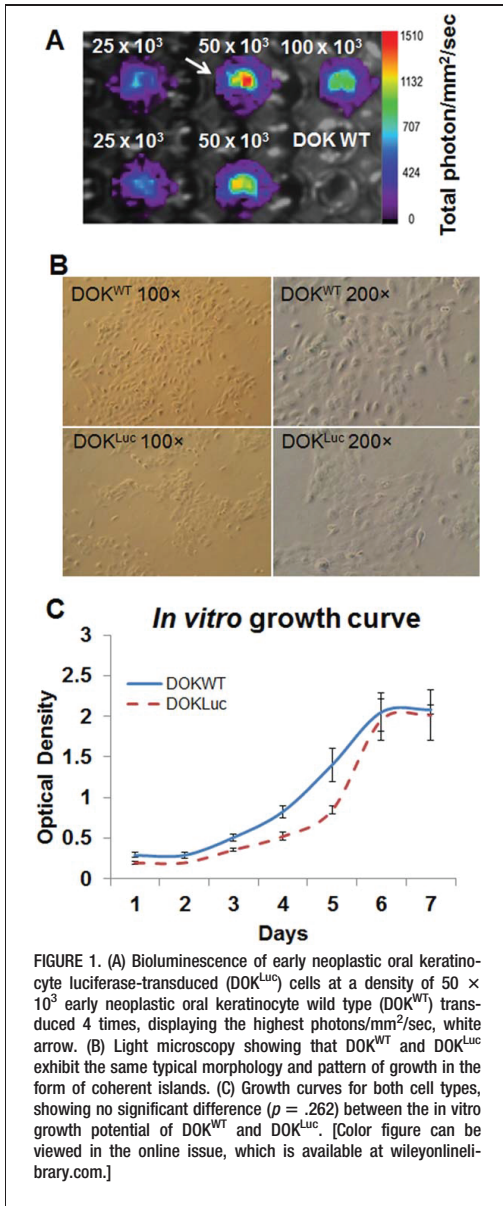
The virus supernatant was collected, filtered, and gene transfer enhanced with protamine sulfate (5 μg/mL). DOK<sup>WT</sup> were seeded at 3 different seeding densities (25 × 10<sup>3</sup>; 50 × 10<sup>3</sup>; and 100 × 10<sup>3</sup> cells/well) in a 6-well plate and centrifuged at 1200 g for 90 minutes. The virus supernatant was replaced with the DOK medium 24 hours postinfection. Successfully infected DOK cells were selected by puromycin (1 μg/mL; Sigma). To obtain a cell-clone with a stable, high expression of luciferase, transduced DOK cells were sorted using fluorescence-activated cell sorter (FACS Aria SORP, BD Biosciences, San Jose, CA).

### Selection of highly bioluminescent early neoplastic oral keratinocyte luciferase-transduced cells

Approximately 1 × 10<sup>6</sup> cells of each group in 100 μL DOK medium were transferred to 96-well plate with 1 well containing 100 μL of DOK medium only for background autofluorescence. Luciferin, (1.6 g/L of D-luciferin; Biosynth AG, Staad, Switzerland) was added 10 minutes before imaging in the Time-Domain Small Molecular Imager Optix MX3 (ART; GE Healthcare, Little Chalfont, UK). Using the OptiView acquisition software (ART Advanced Research Technologies, Quebec, Canada), the region of interest was chosen and plates were scanned with the scan step 1.0 mm and integration time 0.1 seconds.

### Assessment of cell morphology and proliferation

Both cell types, DOK<sup>WT</sup> and early neoplastic oral keratinocyte luciferase-transduced (DOK<sup>LUC</sup>), were cultured at passages (45–48) and their morphology was compared under a light microscope (Nikon TS100; Nikon, Tokyo, Japan). The growth rate was analyzed using a colorimetric assay based on methylthiazol tetrazolium (Sigma) and measured at 570 nm using a microplate reader (BMG LABTECH, GmbH, Ortenberg, Germany).



### Assessment of tumorigenicity in vivo

Both DOK<sup>WT</sup> and DOK<sup>Luc</sup> cells were cultured and allowed to reach their log phase before they were trypsinized and suspended in 50  $\mu$ L of growth factor-reduced matrigel (BD Biosciences). The cells were inoculated at 2 different densities, low ( $1 \times 10^3$ ) and high ( $1 \times 10^5$ ), at 2 different locations, the tongue and subcutaneously in the back of 8 to 10 weeks old male nonobese diabetic severe combined immunodeficient IL2r<sup>mut</sup> mice (NSG)

(University of Bergen - originally a generous gift from Prof. Leonard D. Shultz, Jackson Laboratories, Bar Harbor, ME;  $n = 24$ , 6 mice for each group). Weekly for 6 weeks, tumor volumes for both cell types were manually assessed by digital caliper, using the formula [length  $\times$  (width<sup>2</sup>)/2]. In the group inoculated with DOK<sup>Luc</sup>, tumor development was also measured weekly by bioluminescence. We euthanized the mice after 45 days and harvested tissues for histology.

### Orthotopic tongue xenograft mouse model for early neoplastic oral keratinocyte + carcinoma-associated fibroblast co-inoculations

To create a positive tumor formation control,  $1 \times 10^3$  DOK<sup>WT</sup> were suspended with  $1 \times 10^5$  CAFs (CAF1) in 50  $\mu$ L matrigel and inoculated in the tongue of NSG mice ( $n = 12$ ; 6 mice for each group). Tumors were measured manually up to 45 days.

To assess the sensitivity of bioluminescence to differentiate between tumors formed by different strains of CAFs, DOK<sup>Luc</sup> in a density of  $1 \times 10^3$  were co-inoculated in combination with  $1 \times 10^5$  of 2 different strains of CAFs (CAF15\_13 and CAF15\_23) in the tongue. The total number of animals was 24 with at least 6 for each group. The development of the tumors in this group was followed up manually and evaluated weekly by bioluminescence.

### Preparation of cell-seeded poly L-lactide-co- $\epsilon$ -caprolactone scaffolds for ectopic subcutaneous scaffold xenograft

The copolymer poly(LLA-co-CL) was polymerized from  $\epsilon$ -caprolactone (Sigma-Aldrich, Germany) and LLA (Boehringer, Ingelheim, Germany) by ring-opening polymerization, as previously described.<sup>32</sup> The average molecular weight of the purified copolymer was 100,000 and polydispersity index 1.3 determined by Size Exclusion Chromatography (Polymer Laboratories, Shropshire, UK). The copolymer was composed of 75 mol % LLA and 25 mol % caprolactone, confirmed by <sup>1</sup>H-NMR (Bruker Avance 400, Billerica, MA). The porous scaffolds were prepared by solvent casting particulate leaching<sup>32</sup> and a disc-shaped scaffold (diameter approximately 6 mm, thickness approximately 1.3 mm) was formed with >83% porosities. Porosities were calculated by a Micro-CT (Sky Scan 1172 scanner, Kontich, Belgium) using 40 kV and 2.4 micron voxel and 3D analysis was carried using the software CT-Analyzer version 1.13 (Bruker).

The scaffolds were pre-wet with DOK medium and left for 2 to 3 hours before being then seeded with cells, DOK<sup>Luc</sup> alone or DOK<sup>Luc</sup> + CAFs (CAF1). Three different densities of DOK were used ( $1 \times 10^3$ ,  $1 \times 10^5$ , and  $1 \times 10^9$ ); the density of CAFs was fixed to  $1 \times 10^5$ . Plates were vortexed (Eppendorf, Hamburg, Germany) and the cells were allowed to attach overnight before scaffolds were xenotransplanted in 8 to 10-week-old NSG mice.

The mice were anesthetized with Isoflurane (Isoba VetTM; Schering Plough, Kenilworth, NJ) before 2 incisions (1 cm) were made on their back. One incision was

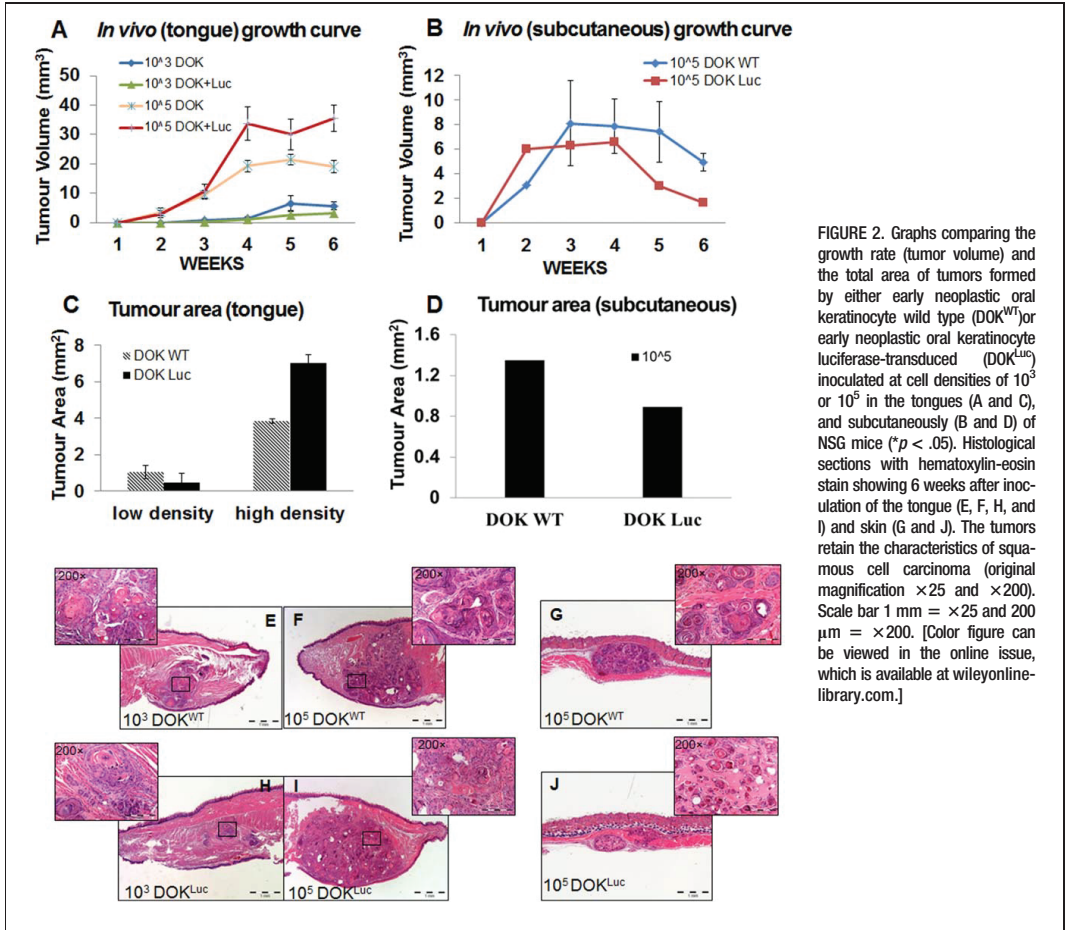


FIGURE 2. Graphs comparing the growth rate (tumor volume) and the total area of tumors formed by either early neoplastic oral keratinocyte wild type (DOK<sup>WT</sup>) or early neoplastic oral keratinocyte luciferase-transduced (DOK<sup>Luc</sup>) inoculated at cell densities of 10<sup>3</sup> or 10<sup>5</sup> in the tongues (A and C), and subcutaneously (B and D) of NSG mice (\**p* < .05). Histological sections with hematoxylin-eosin stain showing 6 weeks after inoculation of the tongue (E, F, H, and I) and skin (G and J). The tumors retain the characteristics of squamous cell carcinoma (original magnification  $\times 25$  and  $\times 200$ ). Scale bar 1 mm =  $\times 25$  and 200  $\mu$ m =  $\times 200$ . [Color figure can be viewed in the online issue, which is available at [wileyonlinelibrary.com](http://wileyonlinelibrary.com).]

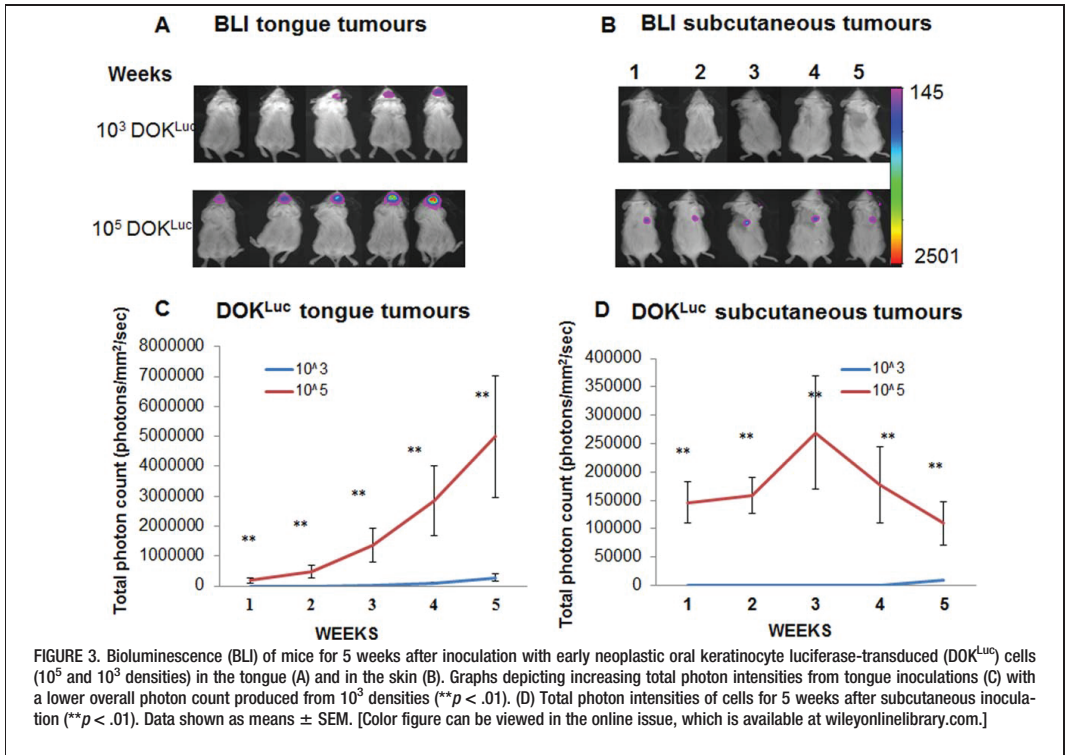
made between the upper limbs and another between the lower limbs, providing sufficient space for implantation of scaffolds and to avoid bioluminescence bleeding. Two scaffolds were implanted into each mouse, 1 scaffold with DOK<sup>Luc</sup> alone and the other with DOK<sup>Luc</sup> + CAFs. The different densities were distributed among all mice (*n* = 6). Wounds were closed with Histoacryl tissue adhesive (B. Braun Surgical AS, Melsungen, Germany). At 12 weeks, the animals were euthanized with CO<sub>2</sub> overdose and scaffolds processed for histology.

### Optical bioluminescence imaging

Mice were depilated and scanned after intraperitoneal delivery of 150 mg/kg of D-luciferin. Animals were maintained under 1% gas anesthesia during scanning. Images were captured using In Vivo MS FX PRO (Carestream Health, Rochester, NY) and analyzed using Carestream MI SE version 5.0.6.20, 1 exposure of 90-second duration.

### Histology and immunohistochemistry

Samples were fixed in 4% paraformaldehyde before embedding in paraffin. Sections of 3 to 4  $\mu$ m were stained with hematoxylin-eosin (Sigma). For p53 immunostaining, paraffin sections were deparaffinized and rehydrated. Epitope retrieval was performed by heating the sections in citrate buffer pH 6.0 in a microwave. Endogenous enzyme activity and unspecific binding were blocked using peroxidase block (DAKO, Golstrup, Denmark) and 10% normal goat serum (DAKO) for 5 minutes and 30 minutes, respectively, at room temperature. As primary antibody, p53 with a monoclonal specific antibody (DO-7 clone, DAKO) 1:50 was incubated for 1 hour at room temperature. For negative controls, samples were treated with antibody diluents alone. The bound reaction was visualized using 3, 3'-diaminobenzidine tetra hydrochloride (DAB, DAKO). Double staining with vimentin (DAKO) 1:1000 was carried out using a double stain kit (Envision G2 double stain system; DAKO), in accord with the manufacturer's instructions. Tumor areas were



calculated from areas of interest in hematoxylin-eosin sections using Olympus DP Soft 5.0 software (Munster, Germany).

### Ethics statement

The ethical approval for patients with head and neck squamous cell carcinoma samples was obtained from the Regional Committees for Medical and Health Research Ethics (REK NO. 2010/48) and lesions were collected following ethical approval and written informed consent of the patients. All animal experiments were approved by the Norwegian Animal Research Authority and conducted in strict accordance with the European Convention for the Protection of Vertebrates used for Scientific Purposes (FOTS no. 20134643/20123961). All procedures were performed under isoflurane gas anesthesia, and all efforts were made to minimize suffering.

### Statistical analysis

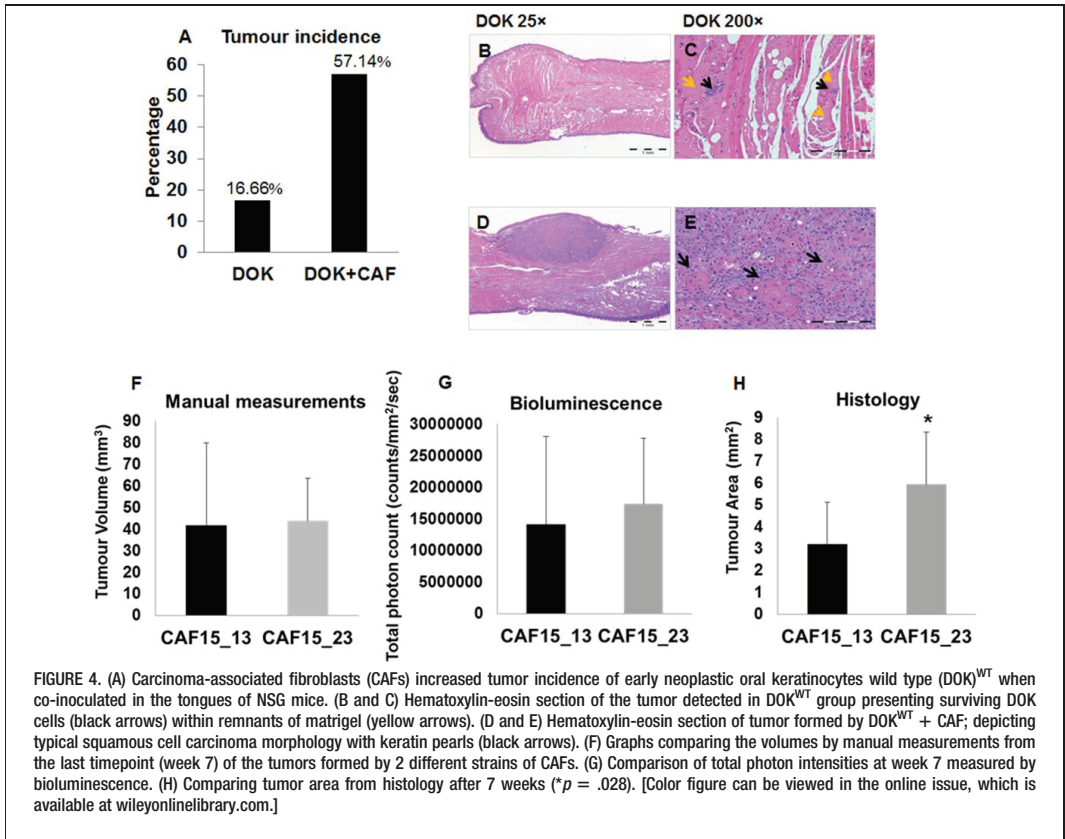
Average values were analyzed by IBM SPSS Statistics 21.0 (SPSS, Chicago, IL) and the data expressed as mean ± SEM. Paired *t* test or the independent Mann–Whitney *U* tests were used to compare differences between the tumors formed. Spearman's correlation was used to correlate the manual tumor measurements and histological measurements with corresponding bioluminescence signals. Differences were considered statistically significant when *p* < .05.

## RESULTS

### Successful transduction of early neoplastic oral keratinocyte with luciferase containing vector generated a new cell line

The bioluminescence signal recorded for DOK<sup>Luc</sup> cells cultured *in vitro* for 2 to 3 weeks posttransduction showed that the seeding density of  $50 \times 10^3$  displayed the highest photons/mm<sup>2</sup>/sec (Figure 1A, white arrow). Cells derived following this protocol were expanded and used for further *in vivo* experiments. Light microscopy showed that DOK<sup>WT</sup> and DOK<sup>Luc</sup> had typical epithelial morphology and similar patterns of growth in the form of coherent islands. No signs of epithelial-to-mesenchymal transition could be observed in either (Figure 1B). The growth curve was comparable for the 2 cell types (*p* = .262), indicating that transduction with luciferase did not alter the *in vitro* growth potential of these cells (Figure 1C).

The *in vivo* tumorigenic potential of DOK cells before and after transduction with luciferase expressing gene was evaluated after DOK<sup>WT</sup> and DOK<sup>Luc</sup> were inoculated in the tongue and also subcutaneously in NSG mice at low ( $1 \times 10^3$ ) and high ( $1 \times 10^5$ ) density. At the high inoculation density, visible tumors were detected with the same incidence after 2 weeks, at both sites, for both DOK<sup>WT</sup> and DOK<sup>Luc</sup>. At the low density, tumors formed only in the tongue, and after 4 weeks, with the same incidence for



DOK<sup>WT</sup> and DOK<sup>Luc</sup>. There was no statistical significance between the volume of the tumors formed in both tongue and subcutaneously by DOK<sup>WT</sup> and DOK<sup>Luc</sup> at all time-points (Figures 2A and 2B). The histological area of the tumors derived from DOK<sup>WT</sup> and DOK<sup>Luc</sup> at low density in the tongue (Figure 2C) and at high density subcutaneously (Figure 2D) did not show any statistical significant difference. The only statistical significant difference was found for the tongue tumors formed at higher inoculation density by DOK<sup>Luc</sup> than tumors formed by DOK<sup>WT</sup> (*p* < .05; Figure 2C). Tumor xenografts generated from DOK<sup>WT</sup> (Figures 2E–2G) showed the same histological picture as DOK<sup>Luc</sup> xenografts (Figures 2H–2J), with epithelial islands of atypical epithelial cells in the host stroma and keratin pearls.

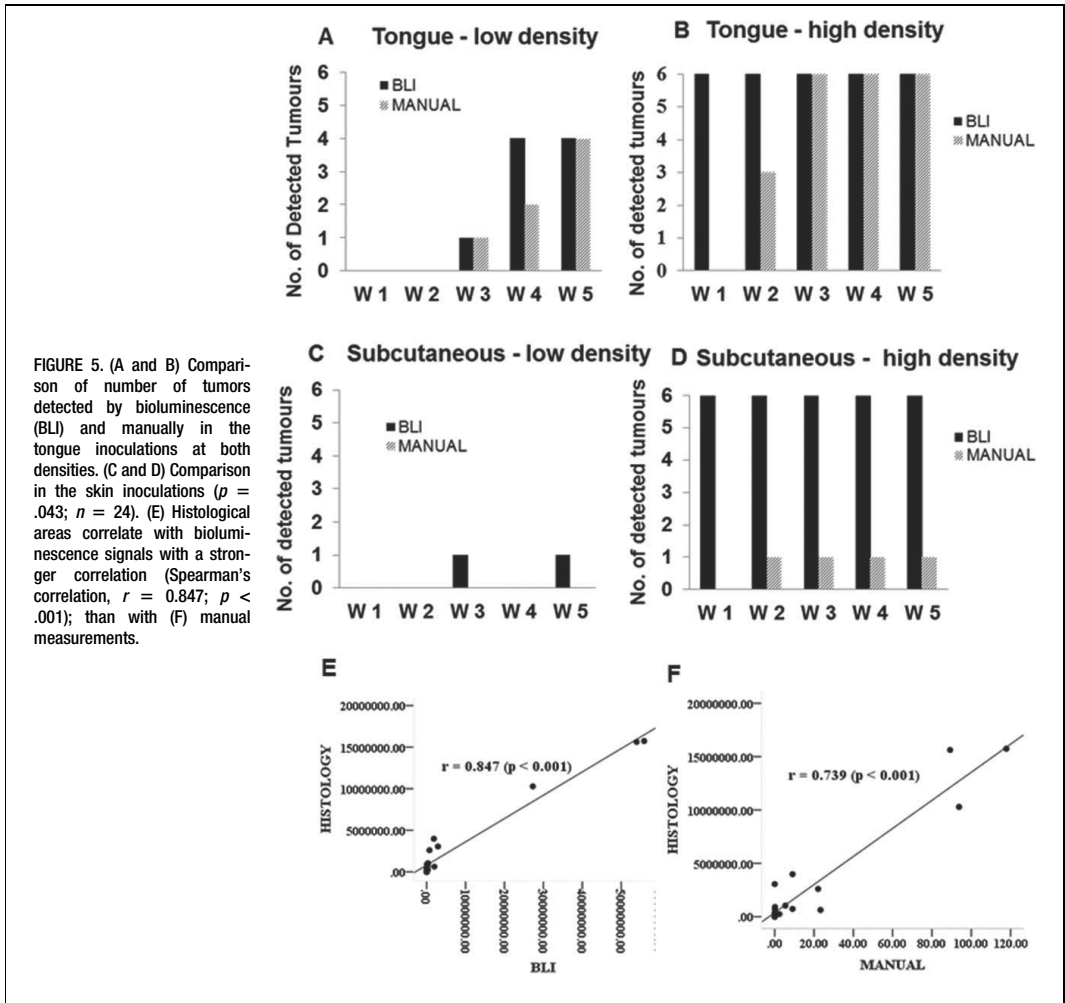
#### Development of tumors formed after inoculation of early neoplastic oral keratinocyte luciferase transduced cells was easily monitored by bioluminescence

Luciferase activity increased with time after both tongue and subcutaneous inoculations for both inoculation densities (Figures 3A and 3B). The bioluminescence signal was significantly higher for the inoculations of DOK<sup>Luc</sup> at higher inoculation density at both tongue and subcutaneous locations (Figures 3C and 3D), at all time-

points, correlating well with the tumor growth curve as assessed by the manual measurements.

#### Both early neoplastic oral keratinocyte wild type and early neoplastic oral keratinocyte luciferase-transduced were responsive to carcinoma-associated fibroblast-derived microenvironmental cues and bioluminescence was more sensitive than manual measurement in detecting differences between various types of microenvironmental cues

Co-inoculating DOK<sup>WT</sup> with 10<sup>5</sup> CAFs in the tongues of NSG mice increased tumor incidence from 16.66% to 57.14% (Figure 4A). Histological sections of the tumors formed by DOK<sup>WT</sup> + CAF showed typical squamous cell carcinoma histology with invasive epithelial islands growing in the host stroma and keratin pearl formation (Figures 4D and 4E). The only 1 tumor formed by the DOK<sup>WT</sup> alone, which was detected manually, was found histologically to be surviving DOK<sup>WT</sup> cells within remnants of undissolved matrigel (Figures 4B and 4C). When 2 different types of fibroblasts (CAF15\_13 and CAF15\_23) were tested for their stimulative support for the in vivo growth of DOK<sup>Luc</sup>, bioluminescence seemed to be more sensitive than the manual



measurement in detecting differences in the tumor growth of xenografts (Figures 4F and 4G), although the difference was not statistically significant. This difference was also observed by histological area calculations after 7 weeks, this time with statistical significance ( $p = .028$ ; Figure 4H).

### Both bioluminescence and manual measurement showed high correlation with histological area of the tumors, but tumor formation was detected earlier by bioluminescence

Bioluminescence consistently disclosed a higher number of tumors throughout all 5 weeks of monitoring compared to visible tumors measured manually by calipers (Figures 5A–5D). Both the tumor volume as quantified by caliper (manual) measurements and the bioluminescence signal from the corresponding tumor at the last timepoint showed a positive

correlation with the tumor area quantified from histological sections (considered to be the “golden standard”). A stronger significant correlation ( $r = 0.846$ ;  $p < .001$ ) was found between the histological tumor area and bioluminescence signals than between the histological tumor area and the manual measurement ( $r = 0.739$ ;  $p < .001$ ; Figures 5E and 5F).

### Development of tumors from early neoplastic oral keratinocyte luciferase-transduced grown on poly L-lactide-co-ε-caprolactone scaffolds under different microenvironmental cues was successfully monitored noninvasively by bioluminescence

$DOK^{Luc}$  were cultured on poly(LLA-co-CL) scaffolds at 3 different densities with or without CAFs. Total photon count from bioluminescence showed significantly higher bioluminescence intensity of scaffolds

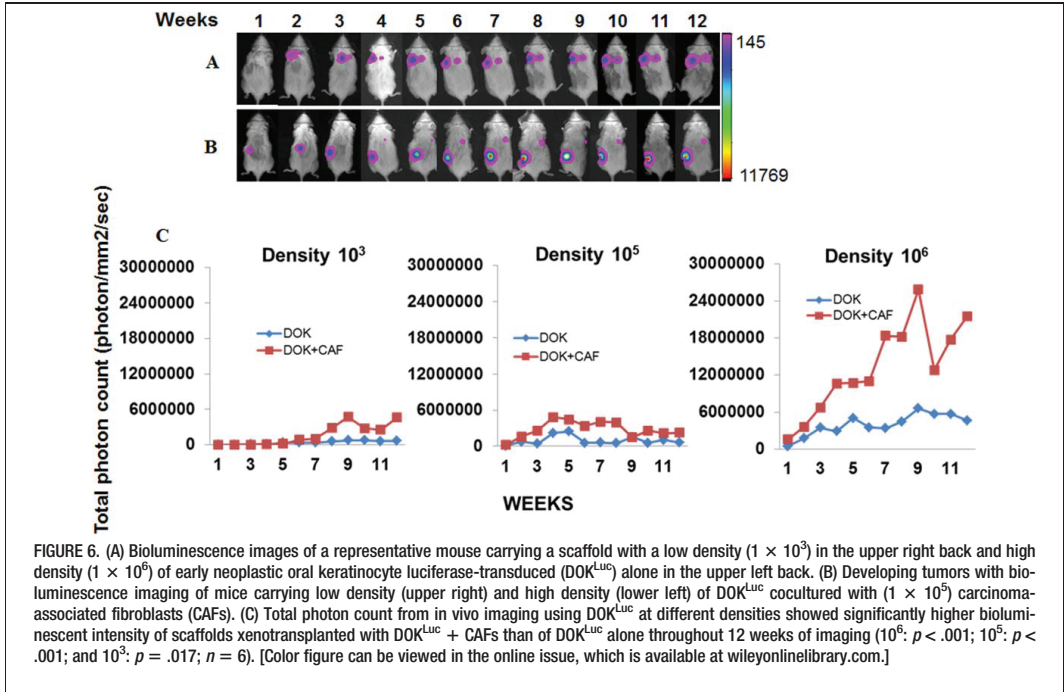


FIGURE 6. (A) Bioluminescence images of a representative mouse carrying a scaffold with a low density ( $1 \times 10^3$ ) in the upper right back and high density ( $1 \times 10^6$ ) of early neoplastic oral keratinocyte luciferase-transduced (DOK<sup>Luc</sup>) alone in the upper left back. (B) Developing tumors with bioluminescence imaging of mice carrying low density (upper right) and high density (lower left) of DOK<sup>Luc</sup> cocultured with ( $1 \times 10^5$ ) carcinoma-associated fibroblasts (CAFs). (C) Total photon count from *in vivo* imaging using DOK<sup>Luc</sup> at different densities showed significantly higher bioluminescent intensity of scaffolds xenotransplanted with DOK<sup>Luc</sup> + CAFs than of DOK<sup>Luc</sup> alone throughout 12 weeks of imaging ( $10^6$ :  $p < .001$ ;  $10^5$ :  $p < .001$ ; and  $10^3$ :  $p = .017$ ;  $n = 6$ ). [Color figure can be viewed in the online issue, which is available at [wileyonlinelibrary.com](http://wileyonlinelibrary.com).]

xenotransplanted with DOK<sup>Luc</sup> + CAFs than of DOK<sup>Luc</sup> alone at all densities, just above the threshold 1 week after xenotransplantation and throughout the 12 weeks of *in vivo* imaging ( $10^6$ :  $p < .001$ ;  $10^5$ :  $p < .001$ ;  $10^3$ :  $p = .017$ ; Figure 6C). In the scaffolds xenotransplanted with DOK<sup>Luc</sup> alone, no tumors were formed outside the scaffolds and the bioluminescence signal stayed within the same range throughout the 12 weeks of imaging (Figure 6A). In contrast, the bioluminescence intensity of scaffolds cocultured with CAFs increased with time (Figure 6B), indicating an increase in tumor growth over time, and this was confirmed by histology. After 12 weeks, histological analysis of xenotransplants of scaffolds with DOK<sup>Luc</sup> cells alone showed the presence of few atypical epithelial cells, limited to the scaffold area (Figures 7A, 7B, 7F, and 7G). Around the remnants of the scaffolds, scattered giant cells of mouse origin were observed (Figure 7K, blue arrow). The origin of the epithelial cells was confirmed by immunostaining using an antibody against human p53, recognizing only p53 mutated human cells, DOK. In contrast, the histology of xenografts of DOK<sup>Luc</sup> + CAFs scaffolds showed squamous epithelial tumor nests (confirmed by p53 positive staining; Figures 7C, 7D, 7I, and 7J), with many of the islands retaining differentiation and containing keratin pearls, growing within and outside the scaffold area, invading the surrounding connective tissue and musculature, thus displaying the characteristic hallmarks of head and neck carcinoma. Few fibroblasts were observed in the xenotransplants even after 12 weeks of growth *in vivo* in mice (Figure 7K, black arrow). Figure 7E shows

the pronounced macroscopic differences observed during harvesting of the scaffolds.

## DISCUSSION

This study describes the development of a noninvasive, *in vivo* model for testing the tumorigenic potential of various microenvironmental cues, including scaffolds intended for use in tissue engineering. Numerous studies<sup>34</sup> support the concept that carcinogenesis, including head and neck cancer, is a multistep process involving a pre-malignant phase of long-term accumulated chromosomal alterations.<sup>35</sup> The use of normal cells in tumor models is time-consuming, if not irrelevant, because it is well-known that the transformation of human cells is a long process, involving at least 5 to 7 mutagenic events, which are difficult to achieve in an experimental setting.<sup>20,36</sup> For the present model, the DOK cell line, exhibiting early neoplastic epithelial dysplastic features was selected as a "screening sensor."<sup>23</sup> To facilitate the noninvasive visualization of these cells after xenotransplantation, they were transduced with luciferase gene, successfully generating a new cell line, DOK<sup>Luc</sup>. The *in vitro* growth and behavioral characteristics of the transfected cells were comparable to those of the parent cells. To evaluate their behavior *in vivo*, both cell lines (DOK<sup>WT</sup> and DOK<sup>Luc</sup>) were xenotransplanted alone at low and high densities, both orthotopically, in the tongue, and ectopically, on the back of NSG mice. With a single exception for the tumor size when injected in the tongue at high density, DOK<sup>WT</sup> and DOK<sup>Luc</sup> showed a comparable *in vivo* behavior as well.

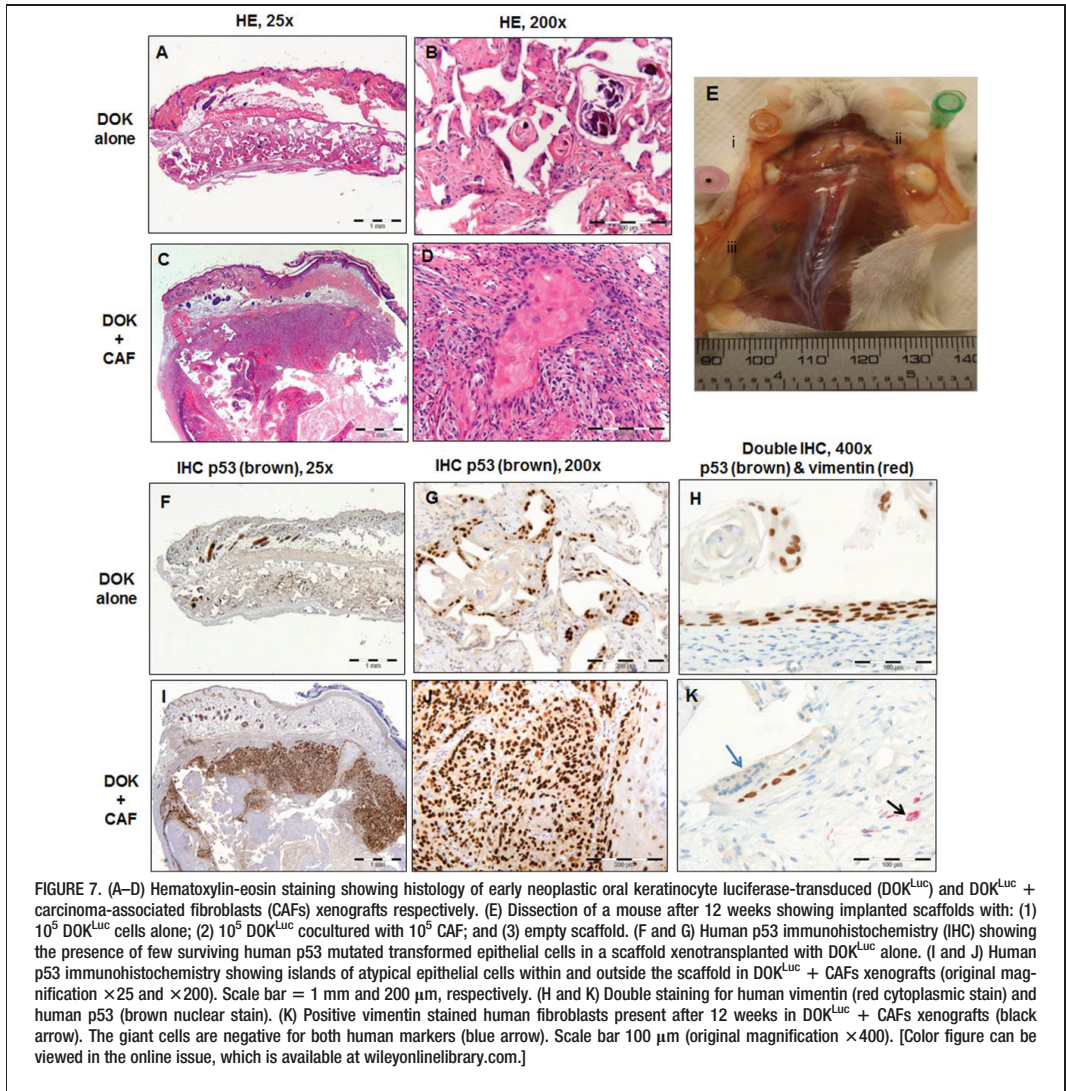


**FIGURE 7.** (A–D) Hematoxylin-eosin staining showing histology of early neoplastic oral keratinocyte luciferase-transduced ( $\text{DOK}^{\text{Luc}}$ ) and  $\text{DOK}^{\text{Luc}}$  + carcinoma-associated fibroblasts (CAFs) xenografts respectively. (E) Dissection of a mouse after 12 weeks showing implanted scaffolds with: (1)  $10^5$   $\text{DOK}^{\text{Luc}}$  cells alone; (2)  $10^5$   $\text{DOK}^{\text{Luc}}$  cocultured with  $10^5$  CAF; and (3) empty scaffold. (F and G) Human p53 immunohistochemistry (IHC) showing the presence of few surviving human p53 mutated transformed epithelial cells in a scaffold xenotransplanted with  $\text{DOK}^{\text{Luc}}$  alone. (I and J) Human p53 immunohistochemistry showing islands of atypical epithelial cells within and outside the scaffold in  $\text{DOK}^{\text{Luc}}$  + CAFs xenografts (original magnification  $\times 25$  and  $\times 200$ ). Scale bar = 1 mm and 200  $\mu\text{m}$ , respectively. (H and K) Double staining for human vimentin (red cytoplasmic stain) and human p53 (brown nuclear stain). (K) Positive vimentin stained human fibroblasts present after 12 weeks in  $\text{DOK}^{\text{Luc}}$  + CAFs xenografts (black arrow). The giant cells are negative for both human markers (blue arrow). Scale bar 100  $\mu\text{m}$  (original magnification  $\times 400$ ). [Color figure can be viewed in the online issue, which is available at [wileyonlinelibrary.com](http://wileyonlinelibrary.com).]

This indicates that the DOK cell line retained a high degree of stability after transfection, although it carried a complex karyotype and multiple mutations, including p53 mutations. In accordance with previous oral carcinogenesis animal studies, the incidence and size of subcutaneous tumors in the present study was lower than those of tongue tumors.<sup>16</sup> This could be related to a greater stimulation of lymphangiogenesis in the tongue area<sup>16</sup> or simply because of the fact that orthotopic models allow cells to grow better in their original environment.

When  $\text{DOK}^{\text{WT}}$  cells were co-inoculated with CAFs in the tongue, the incidence of tumor formation increased by more than 40% compared with tumors formed by  $\text{DOK}^{\text{WT}}$  alone. This further highlights the important role of the

microenvironmental cues in tumor initiation and early growth, supporting previous studies.<sup>37,38</sup> The tumor detected by manual measurements formed by  $\text{DOK}^{\text{WT}}$  was proven later on, histologically, to contain mainly remnants of matrigel, which might have given the mass that could be measurable by the caliper, and only few islands of nonproliferative DOK cells. This illustrates one of the drawbacks of the manual measurements that can be avoided by the use of other methods, such as bioluminescence.

In this study, bioluminescence detected more than 50% of the total number of tumors formed in the tongue by  $\text{DOK}^{\text{Luc}}$  from the first week; much earlier than tumor detection with caliper measurements. In the skin tumors,

6 of 7 were visible by bioluminescence from the first week. One of the tumors was from low density inoculations, which were too small for detection by manual measurements, but it was later confirmed histologically. The total number of tumors detected by bioluminescence was significantly greater than manual detection ( $p = .043$ ), and in concordance with the histological findings, indicating higher sensitivity for early detection using the bioluminescence method.

The measurements from the last timepoint of tumor growth assessment period showed higher bioluminescence signals from tumors with CAF15\_23 than those with CAF15\_13; this difference was not detected by the manual measurements. Histological evaluation confirmed statistically bigger tumors formed by DOK<sup>Luc</sup> co-injected with the CAF15\_23, a difference that was not indicated by the manual measurements. This brings further indications for the greater sensitivity of the bioluminescence method compared to the manual method that might carry subjective evaluations (eg, inflammation, tongue pull, position of the mouse, and lesion margins).

Degradable copolymer scaffolds were used to further optimize and validate the model for use in screening tests for tumorigenesis of various microenvironmental cues from biomaterials. The manual monitoring of tumors at early stages was impossible because the tumors initially developed within the scaffold. However, this was not an impediment for bioluminescence. The correlation between bioluminescence signals and the golden standard method of histological examination was higher, confirming the method is more sensitive than manual measurements. Therefore, bioluminescence was further used solely to monitor the scaffolds when developing the model.

A challenge for using the bioluminescence method would be monitoring of bigger tumors. We monitored a drop in intensity for a tumor developed from very high seeding density of DOK<sup>Luc</sup> + CAFs xenografts ( $1 \times 10^6$ ). We interpreted that to be an underestimation of the real bioluminescence signal from the cells because that tumor was later found to be cystic. Cystic content or necrosis that can occur in large or late stage tumors might reduce the production of light because of decreased proliferation or hypoxia.<sup>27,39</sup> Therefore, we recommend inoculating fewer cells per area of scaffold in order to circumvent these limitations and monitor tumor formation for longer period of times, as required in carcinogenesis studies. Although the use of such immunodeficient models greatly aids the development of “humanized” models of cancer using biomaterials,<sup>25</sup> it does come with the caveat of no innate host immunity. Whereas this limitation prevents the current study of role of the immune system in tumor prevention in such models or the use of immunotherapeutic interventions, steps have been made to circumvent such constraints. Recent efforts have demonstrated that introduction of distinct human immune components are possible in mice xenografted with cancer cell lines,<sup>40</sup> suggesting that further evolution of the NSG mice system may yet render models to study human immune reactions in cancer.

Our model provides an abridged alternative to the years spent in rodent models to get tumors from biomaterials implanted solely in animals and foreign body tumorigene-

sis has several stages, with specific sequences of preneoplastic characteristics.<sup>12,41</sup> The processing time is reduced because of the ability of screening several animals simultaneously, which makes it cheaper compared to other high throughput imaging methods used in the field, such as MRI.

## CONCLUSIONS

The model generated and validated in this study is a sensitive and reliable model for monitoring microenvironmentally induced carcinogenesis providing early, consistent surveillance of tumor development associated with implantation of scaffolds for tissue engineering.

## Acknowledgments

The authors thank Dr. Joan Bevenius-Carrick, Dr. Andrew Davis, and Prof. Mustafa Nur Elhuda for English revision and constructive criticism of the manuscript. We are grateful to Tereza Osdal (University of Bergen) for assistance with cell transduction, Gunnvor Øjordsbakken (Gade Laboratory for Pathology) for support with histology, and Mihaela Popa (KinN Therapeutics AS, Bergen) for bioluminescence imaging training. The bioluminescence imaging was performed at the Molecular Imaging Centre (MIC), University of Bergen.

## REFERENCES

- De Wever O, Mareel M. Role of tissue stroma in cancer cell invasion. *J Pathol* 2003;200:429–447.
- Kalluri R, Zeisberg M. Fibroblasts in cancer. *Nat Rev Cancer* 2006;6:392–401.
- Mantovani A, Allavena P, Sica A, Balkwill F. Cancer-related inflammation. *Nature* 2008;454:436–444.
- Anderson JM, Rodriguez A, Chang DT. Foreign body reaction to biomaterials. *Semin Immunol* 2008;20:86–100.
- Nakamura T, Shimizu Y, Okumura N, Matsui T, Hyon SH, Shimamoto T. Tumorigenicity of poly-L-lactide (PLLA) plates compared with medical-grade polyethylene. *J Biomed Mater Res* 1994;28:17–25.
- Nakamura T, Shimizu Y, Takimoto Y, et al. Biodegradation and tumorigenicity of implanted plates made from a copolymer of epsilon-caprolactone and L-lactide in rat. *J Biomed Mater Res* 1998;42:475–484.
- Kirkpatrick CJ, Alves A, Köhler H, et al. Biomaterial-induced sarcoma: a novel model to study preneoplastic change. *Am J Pathol* 2000;156:1455–1467.
- Idris SB, Dänmark S, Finne-Wistrand A, et al. Biocompatibility of polyester scaffolds with fibroblasts and osteoblast-like cells for bone tissue engineering. *J Bioact Compat Polym* 2010;25:567–583.
- ISO/EN ID. Biological evaluation of medical devices—part 5. Test for cytotoxicity: in vitro methods. Geneva, Switzerland: International Organisation of Standardisation; 1992.
- Kato S, Akagi T, Sugimura K, Kishida A, Akashi M. Evaluation of biological responses to polymeric biomaterials by RT-PCR analysis IV: study of c-myc, c-fos and p53 mRNA expression. *Biomaterials* 2000;21:521–527.
- Carraway J, Ghosh C. The challenge to global acceptance of part 3 of ISO 10993. *Med Device Technol* 2006;17:16–18.
- Takanashi S, Hara K, Aoki K, et al. Carcinogenicity evaluation for the application of carbon nanotubes as biomaterials in rasH2 mice. *Sci Rep* 2012;2:498.
- Cohen SM. Human carcinogenic risk evaluation: an alternative approach to the two-year rodent bioassay. *Toxicol Sci* 2004;80:225–229.
- Ward JM. The two-year rodent carcinogenesis bioassay – Will it survive? *J Toxicol Pathol* 2007;20:13–19.
- Ahmed SU, Zair M, Chen K, et al. Generation of subcutaneous and intrahepatic human hepatocellular carcinoma xenografts in immunodeficient mice. *J Vis Exp* 2013;79:e50544.
- Hadler-Olsen E, Wetting HL, Rikardsen O, et al. Stromal impact on tumor growth and lymphangiogenesis in human carcinoma xenografts. *Virchows Arch* 2010;457:677–692.
- Ruggeri BA, Camp F, Miknyoczki S. Animal models of disease: pre-clinical animal models of cancer and their applications and utility in drug discovery. *Biochem Pharmacol* 2013;87:150–161.
- Sano D, Myers JN. Xenograft models of head and neck cancers. *Head Neck Oncol* 2009;1:32.

19. Bibby MC. Orthotopic models of cancer for preclinical drug evaluation: advantages and disadvantages. *Eur J Cancer* 2004;40:852–857.
20. Debnath J, Brugge JS. Modelling glandular epithelial cancers in three-dimensional cultures. *Nat Rev Cancer* 2005;5:675–688.
21. Warnakulasuriya S. Global epidemiology of oral and oropharyngeal cancer. *Oral Oncol* 2009;45:309–316.
22. Yang K, Zhao N, Zhao D, Chen D, Li Y. The drug efficacy and adverse reactions in a mouse model of oral squamous cell carcinoma treated with oxaliplatin at different time points during a day. *Drug Des Devel Ther* 2013;7:511–517.
23. Chang SE, Foster S, Betts D, Marnock WE. DOK, a cell line established from human dysplastic oral mucosa, shows a partially transformed non-malignant phenotype. *Int J Cancer* 1992;52:896–902.
24. Khemthongcharoen N, Jolivot R, Rattanavarin S, Piyawattanametha W. Advances in imaging probes and optical microendoscopic imaging techniques for early in vivo cancer assessment. *Adv Drug Deliv Rev* 2013;74:53–74.
25. Lee J, Li M, Milwid J, et al. Implantable microenvironments to attract hematopoietic stem/cancer cells. *Natl Acad Sci U S A* 2012;109:19638–19643.
26. McCormack E, Silden E, West RM, et al. Nitroreductase, a near-infrared reporter platform for in vivo time-domain optical imaging of metastatic cancer. *Cancer Res* 2013;73:1276–1286.
27. Jarzabek MA, Huszthy PC, Skaftnesmo KO, et al. In vivo bioluminescence imaging validation of a human biopsy-derived orthotopic mouse model of glioblastoma multiforme. *Mol Imaging Biol* 2013;12:161–172.
28. Kotopoulis S, Delalande A, Popa M, et al. Sonoporation-enhanced chemotherapy significantly reduces primary tumour burden in an orthotopic pancreatic cancer xenograft. *Mol Imaging Biol* 2014;16:53–62.
29. Zinn KR, Chaudhuri TR, Szafran AA, et al. Noninvasive bioluminescence imaging in small animals. *ILAR J* 2008;49:103–115.
30. Pinsky MS, Song W, Dong Z, et al. Activation of iCaspase-9 in neovessels inhibits oral tumor progression. *J Dent Res* 2006;85:436–441.
31. Warner KA, Miyazawa M, Cordeiro MM, et al. Endothelial cells enhance tumor cell invasion through a crosstalk mediated by CXCL chemokine signaling. *Neoplasia* 2008;10:131–139.
32. Dänmark S, Finne-Wistrand A, Wendel M, Arvidsson K, Albertsson A-C, Mustafa K. Osteogenic differentiation by rat bone marrow stromal cells on customized biodegradable polymer scaffolds. *Bioact Compat Polym* 2010;25:207–223.
33. McCormack E, Haaland I, Venås G, et al. Synergistic induction of p53 mediated apoptosis by valproic acid and nutlin-3 in acute myeloid leukemia. *Leukemia* 2012;26:910–917.
34. Hanahan D, Weinberg RA. Hallmarks of cancer: the next generation. *Cell* 2011;144:646–674.
35. Vineis P, Schatzkin A, Potter JD. Models of carcinogenesis: an overview. *Carcinogenesis* 2010;31:1703–1709.
36. Leemans CR, Braakhuis BJ, Brakenhoff RH. The molecular biology of head and neck cancer. *Nat Rev Cancer* 2011;11:9–22.
37. Clark AK, Taubenberger AV, Taylor RA, et al. A bioengineered microenvironment to quantitatively measure the tumorigenic properties of cancer-associated fibroblasts in human prostate cancer. *Biomaterials* 2013;34:4777–4785.
38. Costea DE, Hills A, Osman AH, et al. Identification of two distinct carcinoma-associated fibroblast subtypes with differential tumor-promoting abilities in oral squamous cell carcinoma. *Cancer Res* 2013;73:3888–3901.
39. Black PC, Shetty A, Brown GA, et al. Validating bladder cancer xenograft bioluminescence with magnetic resonance imaging: the significance of hypoxia and necrosis. *BJU Int* 2010;106:1799–1804.
40. McCormack E, Adams KJ, Hassan NJ, et al. Bi-specific TCR-anti CD3 redirected T-cell targeting of NY-ESO-1- and LAGE-1-positive tumors. *Cancer Immunol Immunother* 2013;62:773–785.
41. Moizhess TG. Carcinogenesis induced by foreign bodies. *Biochemistry (Mosc)* 2008;73:763–775.